Smart Polymers & Hydrogels

Dumb and Dumber ~ Smart and Ordinary

Dumb Dumber

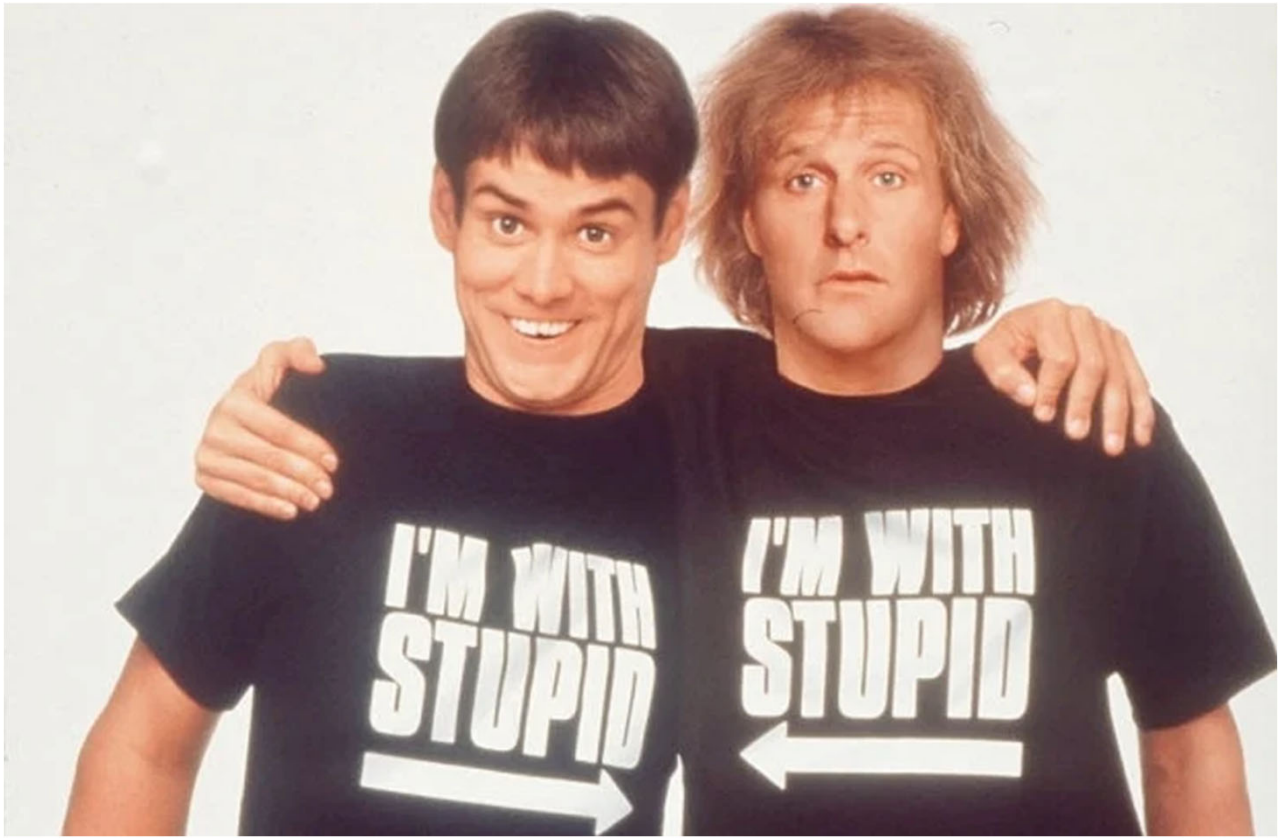

Smart Ordinary

Smart vs. Intelligent

Smart pavement compared with ordinary pavement

Ordinary Polymers & Hydrogels

Polymers

Precipitation ⟷ Dissolution

Contraction ⟷ Expansion

Hydrogels

Shrinking ⟷ Swelling

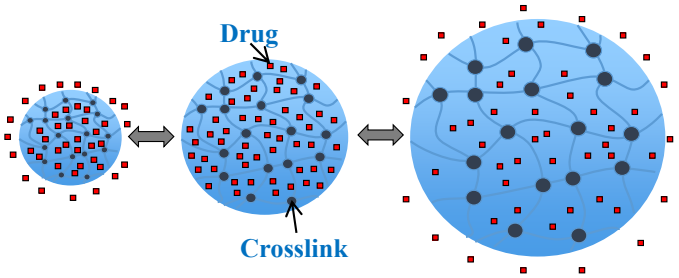

Precipitation

Shrunken state
- Squeezing
- Trapping

Dilution

Swollen state
- Opening
- Absorbing

Smart Polymers & Hydrogels

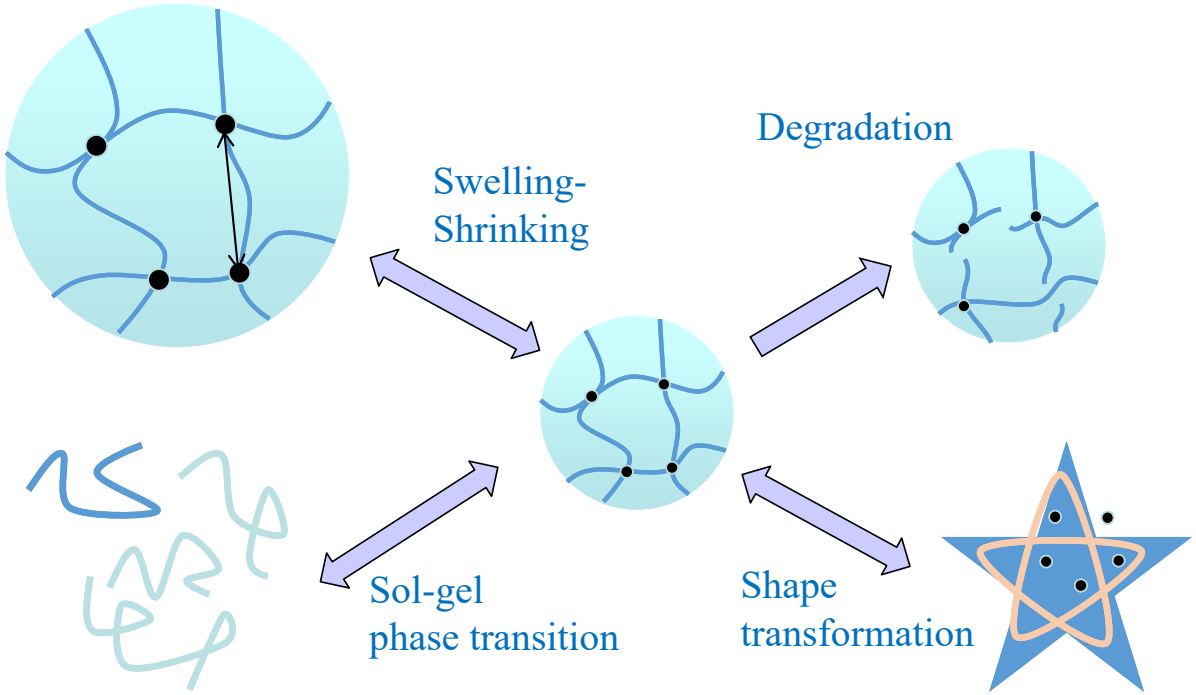

Respond to minute changes in environmental conditions by large and sharp changes in physicochemical properties

(Intelligent, Environment-sensitive, Stimulus-responsive)

Ordinary Polymers & Hydrogels

Polymers

Precipitation ⟷ Dissolution

Contraction ⟷ Expansion

Hydrogels

Shrinking ⟷ Swelling

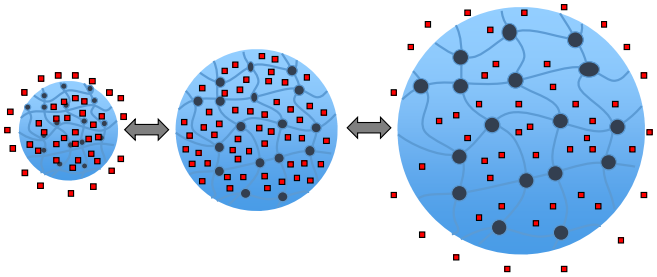

Polymers and hydrogels that undergo changes in physicochemical properties without external factors.

Adjunctive Hemostats

https://www.jnjmedtech.com/en-US/product/surgicel-original-absorbable-hemostat

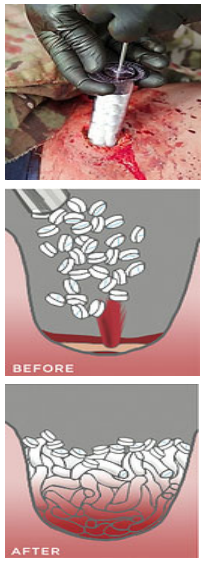

Wound Care

Severe puncture wounds can be life-threatening if first aid is delayed. Oregon-based company RevMedx has developed a new medical product that can staunch bleeding, and is particularly useful for wounds to the shoulder and pelvis, where tourniquets are ineffective. The XStat injects compressed sponges that have been treated with blood clotting and antimicrobial agents. The pellets expand to 10 times their original size and exert pressure to stop the bleeding. In animal studies, the XSTAT reduced blood loss and increased survival rates. The company hopes the device will become FDA-approved this year for military and medical applications.

https://www.revmedx.com/xstat/

Smart Polymers & Hydrogels

Polymers and hydrogels that undergo changes in physicochemical properties by external factors, commonly known as environmental stimuli.

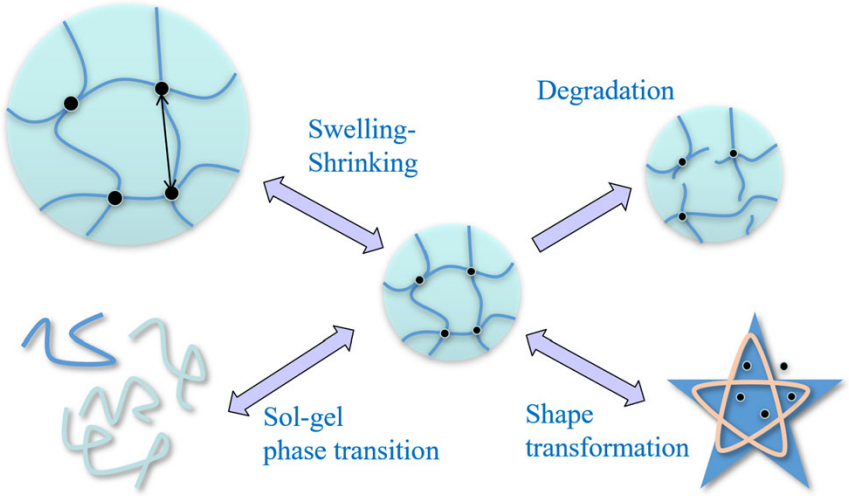

Respond to minute changes in environmental conditions by large and sharp changes in physicochemical properties

(Intelligent, Environment-sensitive, Stimulus-responsive)

Environmental Stimuli

Physical

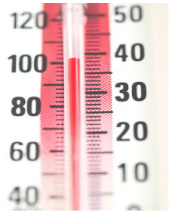
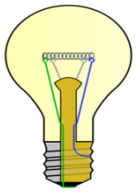

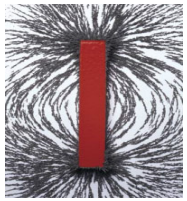


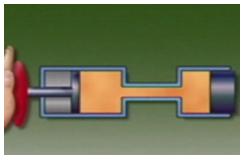

Stimuli

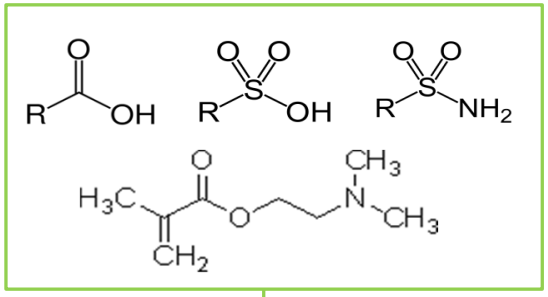

Biological

Chemical

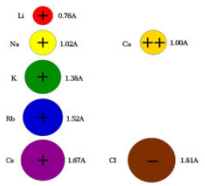
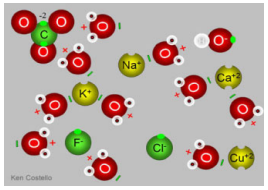

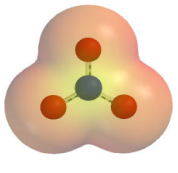

Smart Polymers & Hydrogel

Prof. You Han Bae, University of Utah

Drug Delivery

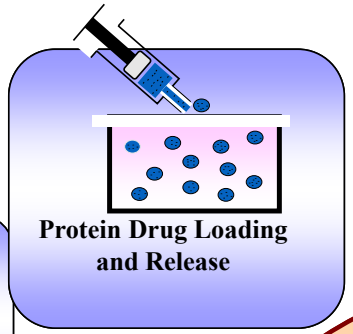

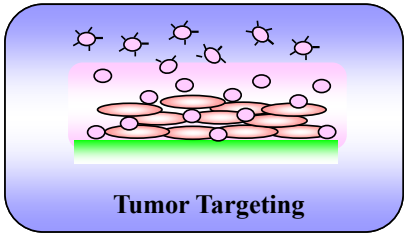

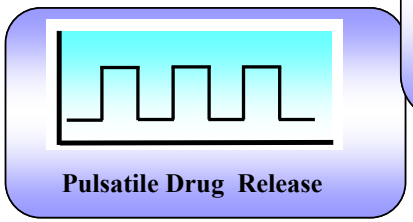

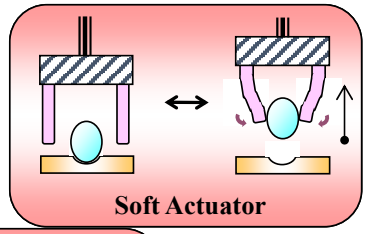

Bioseparation

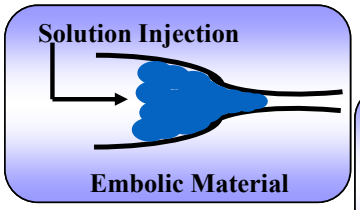

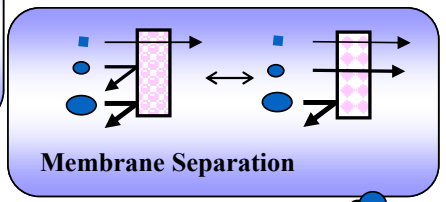

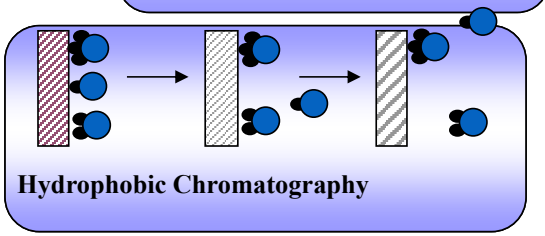

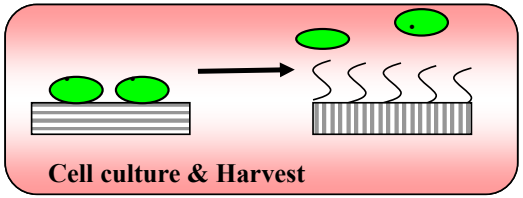

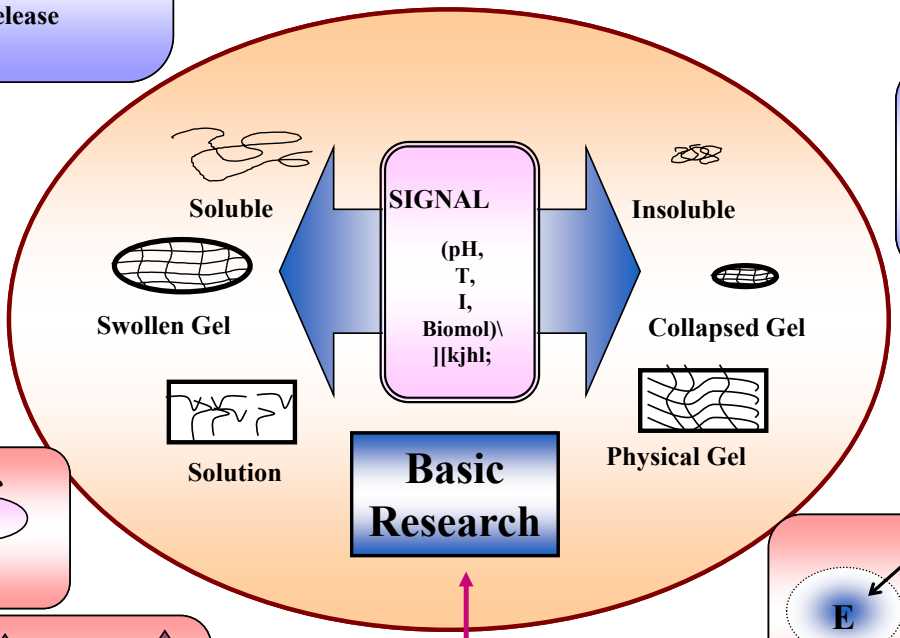

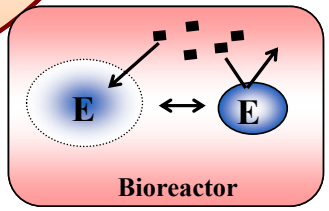

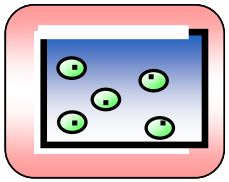

Biosensor

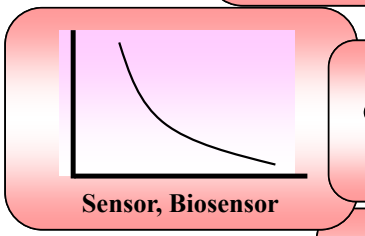

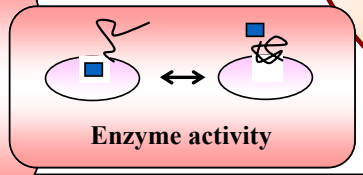

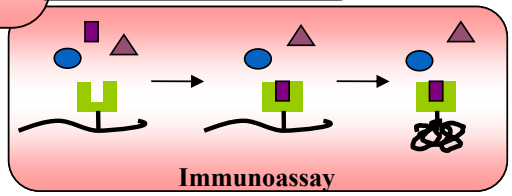

Applied
Research

Tissue Engineering

Pressure- & Temperature-Sensitive Materials

https://www.youtube.com/watch?v=ULa60DWu66U

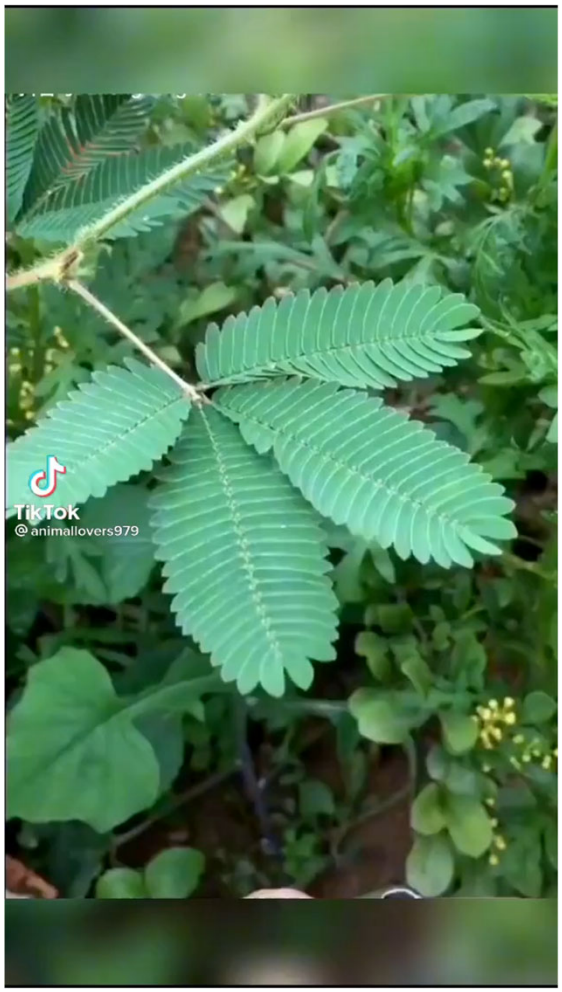

Temperature-Sensitive Systems

Temperature-Sensitive Polymers & Hydrogels

Positive Thermosensitivity

as T ↑ Solubility/Swelling ↑

Negative Thermosensitivity

as T ↑ Solubility/Swelling ↓

Covalent bond: ~ 5 eV ($\approx 0.8 \times 10^{-18}$ J)

Secondary interaction forces: ~ 0.1 eV

Thermal fluctuation energy: ~ 0.03 eV ($\approx$ 1 kT)

Competition between the two forces
(H-bonding & Hydrophobic interaction)

Temperature-dependent interactions

as T ↑ Hydrogen-bonding ↓

as T ↑ Hydrophobic interaction ↑

Hydrophobic interactions

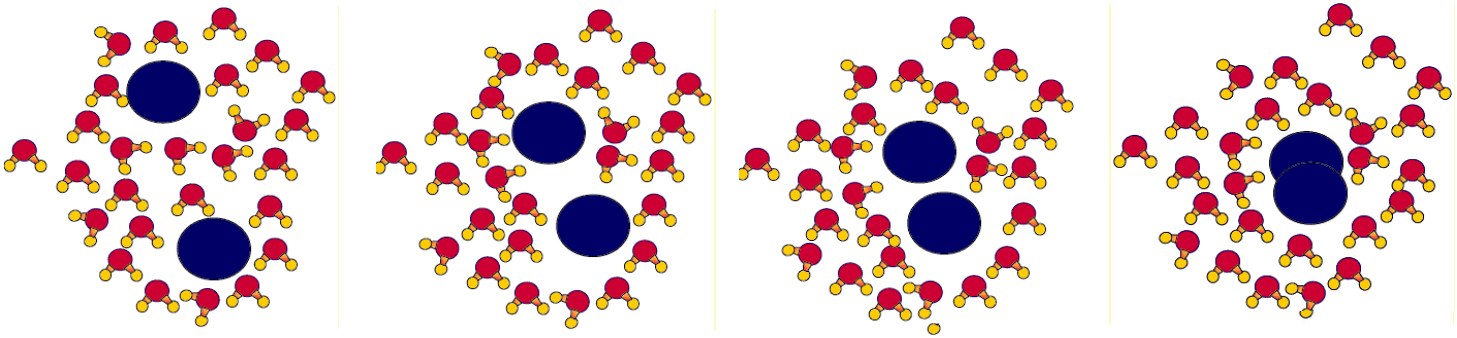

The chemical structure of PNIPAAm.

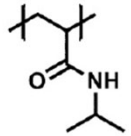

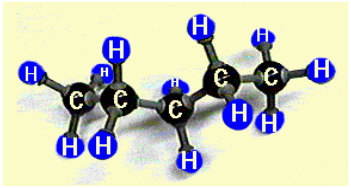

Hydrocarbons: Lipophilic hydrocarbon-like groups in solutes.

A droplet of water forms a spherical shape to minimize contact with the hydrophobic leaf.
http://en.wikipedia.org/wiki/Hydrophobic_effect

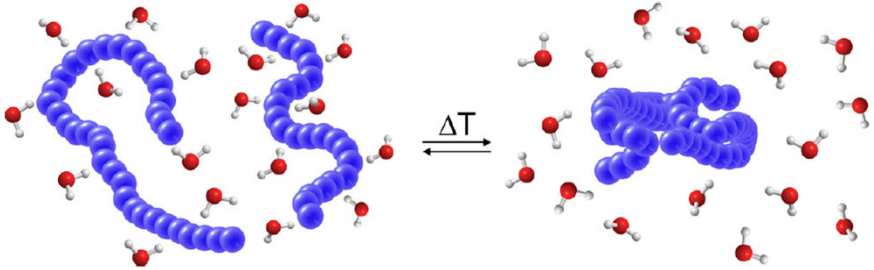

Fig. 1. Schematic representation of a polymer phase transition in aqueous solution from a completely dissolved homogeneous state to a two-phase demixed system comprising a high polymer concentration phase and a low polymer concentration aqueous phase. Even though the collapsed polymer chains in the high concentrated phase are still partially hydrated, these water molecules are not shown in the picture for simplicity. The scheme shows an LCST transition if $\Delta T > 0$ and an UCST if $\Delta T < 0$.

http://academic.brooklyn.cuny.edu/biology/bio4fv/page/hydropho.htm

Vancoillie 2014, Thermoresponsive poly(oligo ethylene glycol acrylates)

Temperature-Sensitive Polymers & Hydrogels

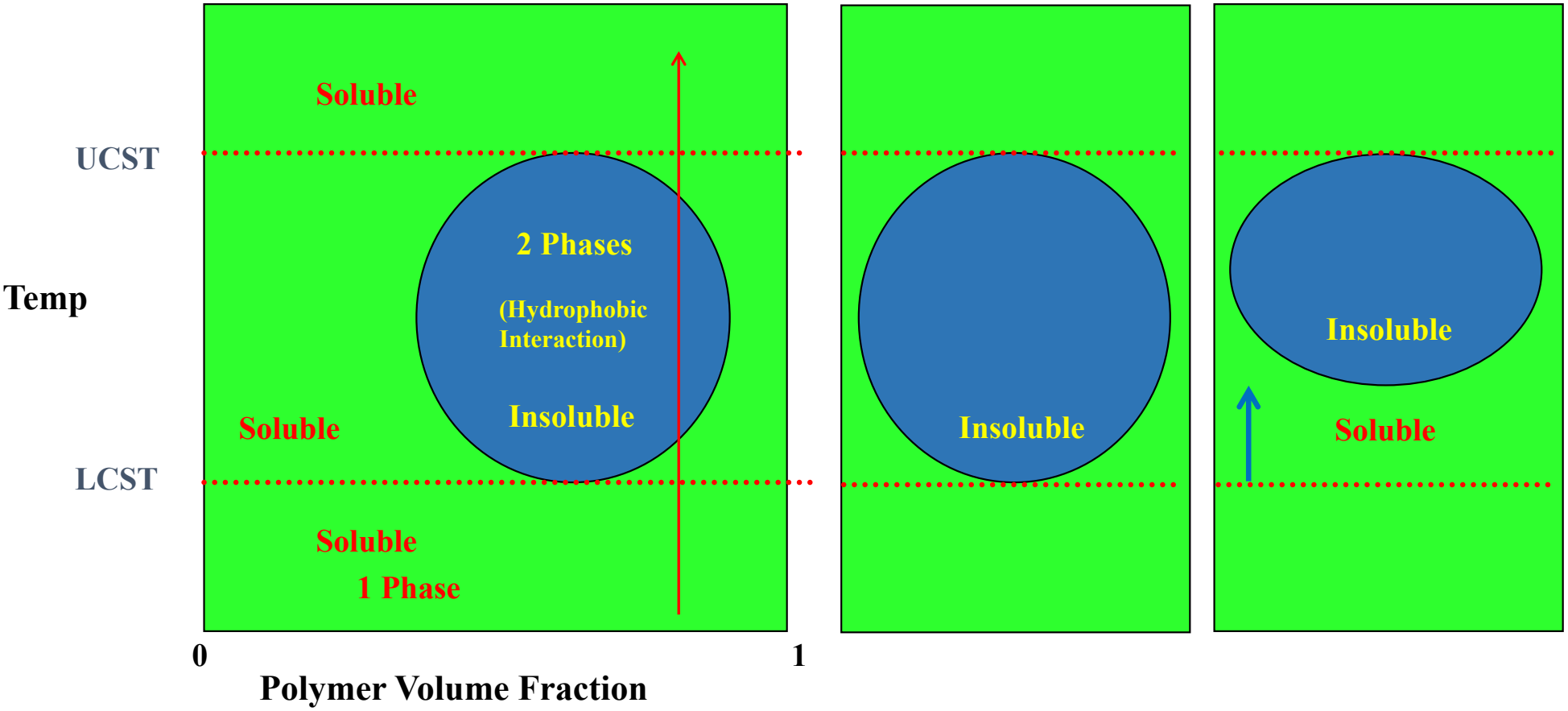

Temperature-Sensitive Polymers

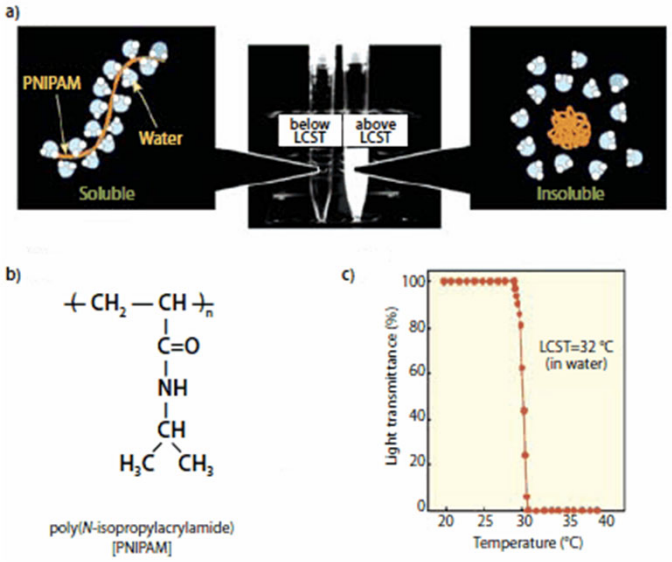

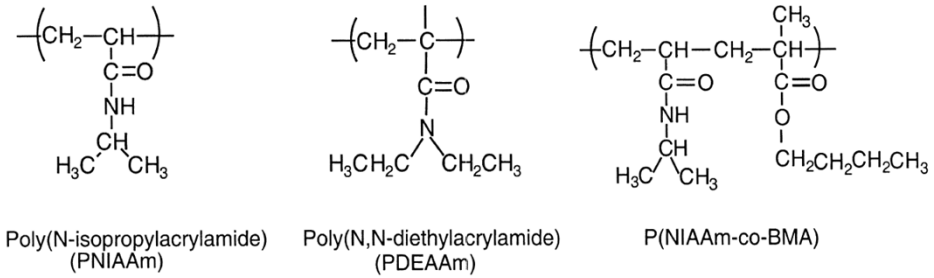

Fig. 1. Structures of some temperature-sensitive polymers.

Qiu 2001, Environment-sensitive hydrogels for drug delivery

Temperature-dependent polymers: The first smart polymers.
Lower critical solution temperature: lowest temperature at which all components are soluble.

Solution:	Soluble	→	Insoluble
Hydrogel:	Swollen	→	Collapsed
Surface:	Hydrophilic	→	Hydrophobic

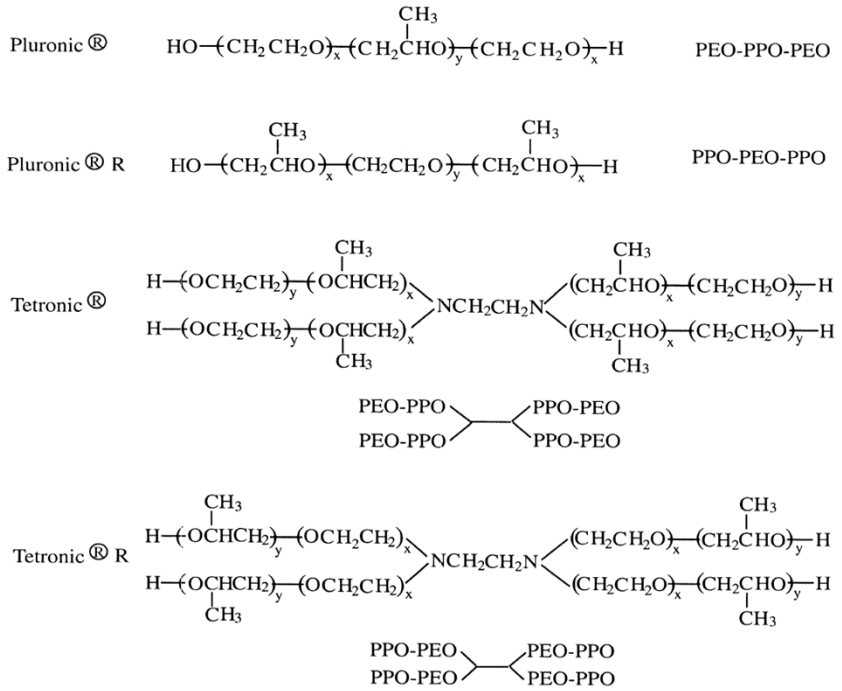

Fig. 2. Polymer structures of Pluronic®, Pluronic® R, Tetronic® and Tetronic® R.

PLGA

Poly(lactic-co-glycolic acid) (PLGA)

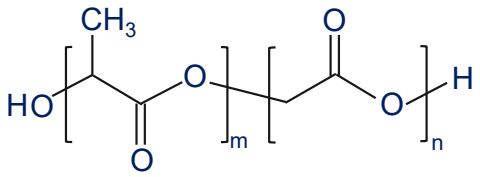

Lactic Acid Glycolic Acid

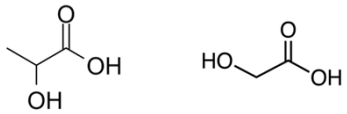

Poly(lactide-co-glycolide)

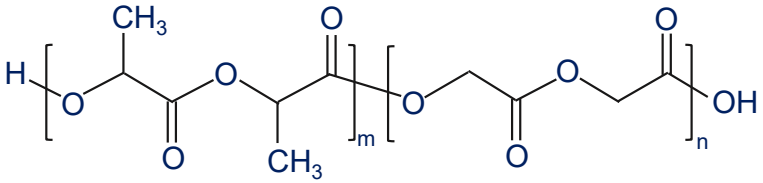

Lactide Glycolide

PEG-PLGA-PEG Triblock Copolymer

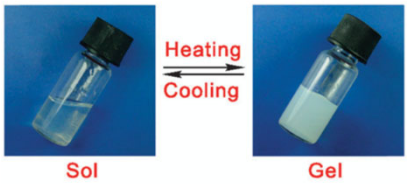

PLGA is hydrophobic and biodegradable.
PLGA is most widely used in drug delivery.
PEG is hydrophilic and biocompatible.

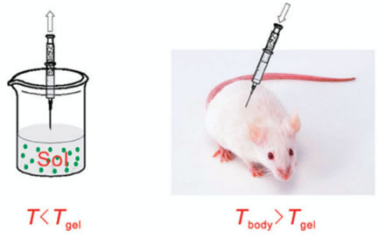

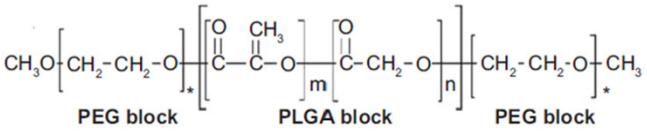

Jeong 1999, Thermoreversible gelation of PEG-PLGA-PEG triblock copolymer aqueous solutions

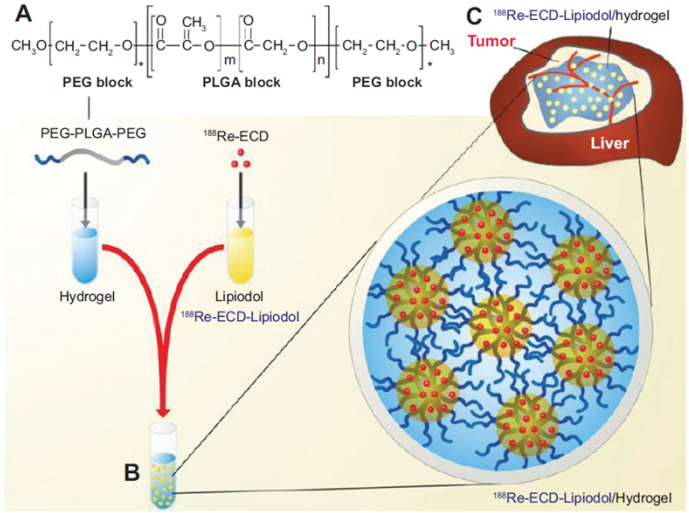

Shih 2014, Preparation and therapeutic evaluation of 188Re-thermogelling emulsion in rat model of hepatocellular carcinoma

Solubilities of Polyethers in Water

The solubilities of polyethers are surprisingly counter-intuitive. The best-known example is the difference between polyethylene glycol ($[-CH_2-CH_2-O-]_n$) which is infinitely soluble, and polyoxymethylene ($[-CH_2-O-]_n$) which is completely insoluble in water, exactly the opposite of what one expects from the C/O ratios of these molecules. Similar anomalies exist for oligomeric and cyclic polyethers. To solve this apparent mystery, we use femtosecond vibrational and GHz dielectric spectroscopy with complementary *ab initio* calculations and molecular dynamics simulations. We find that the dynamics of water molecules solvating polyethers is fundamentally different depending on their C/O composition. The *ab initio* calculations and simulations show that this is not because of steric effects (as is commonly believed), but because the partial charge on the O atoms depends on the number of C atoms by which they are separated. Our results thus show that inductive effects can have a major impact on aqueous solubilities.

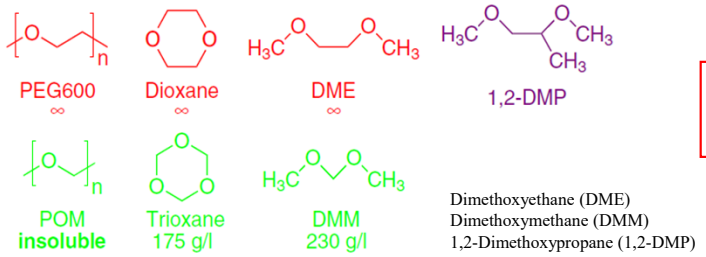

Dimethoxyethane (DME)
Dimethoxymethane (DMM)
1,2-Dimethoxypropane (1,2-DMP)

Fig. 1 Investigated polyethers and their solubilities[4].

The origin of the different solubilities is not well understood[5]. It is commonly explained by assuming that the distances between the O atoms in different polyethers have consequences for their solubility in water. As early as 1969, Blandamer et al.[6] suggested that water molecules solvating PEG can form a hydrogen-bond network similar to that of bulk water on the basis of the distances between O atoms in the trans-gauche-trans conformation of the OCCO backbone. The resulting good fit of the solvation hydrogen-bond network into that of the surrounding water would then explain the high solubility of PEG. Previous studies[7–22] have shown evidence for this intuitively appealing idea, but to date no systematic experimental investigation of the origin of the different solubilities of polyethers exists. Here, we investigate this issue using spectroscopic experiments in combination with *ab initio* calculations and molecular dynamics simulations. We find evidence that the solubility difference is not due to a difference in hydrogen-bond geometry but has a completely different origin: our results indicate that it is mainly the difference in partial charges on the oxygen atoms that determines the difference in solubility, a result that may be relevant for understanding the solubilities of many other compounds.

Poly(ethylene glycol) (PEG)
vs.
Poly(ethylene oxide) (PEO)

PEG3 molecules remain well dissolved in water.

POM3 precipitates by forming a single large aggregate.

The POM3 dissolves, if PEG's O charge is used.

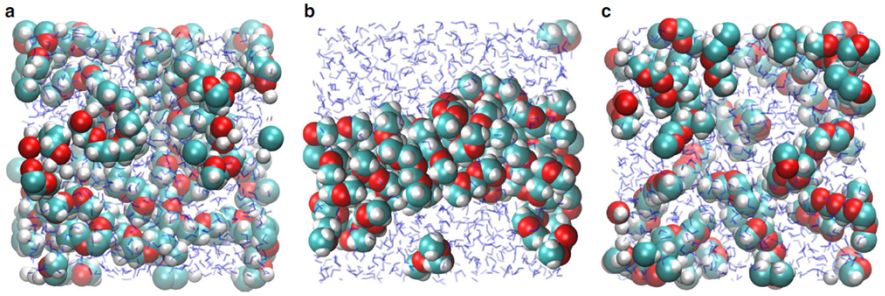

Fig. 6 Snapshots after 1 ns of FF-MD simulation. **a** PEG3, **b** POM3, and **c** fictitious POM3 molecules with modified atomic charges. Water molecules are indicated in blue. Time series of snapshots are provided in Supplementary Fig. 8, together with a clustering analysis obtained from a 50 ns simulation

Discussion

Our experimental and computational results suggest a new explanation for the different solubilities of polyethers: water interacts more strongly with PEG-like polyethers than with POM-like polyethers (Fig. 5) as a consequence of the larger partial charge on the O atoms in the former (Fig. 4). The larger partial charges of PEG-like polyethers would also result in a larger enthalpy of hydration as compared to POM-like polyethers, and this could partly explain the larger negative enthalpy of solution[2,3], and hence the better solubility. It should be noted that in general, solubility is determined not only by the hydration strength. Dissolving a substance can be regarded energetically as a process involving two steps, each of which is accompanied by an enthalpy change: (1) removing the molecules (or ions, in the case of a salt) from their pure solid or liquid phase, and (2) subsequent hydration of these free molecules (or ions). The net enthalpy change when dissolving a substance in water is the sum of these two contributions. In the case of polyethers, the enthalpy change of the first step (removing a molecule from its pure liquid phase) is very similar for PEG- and POM-like polyethers of similar size: for $CH_3OCH_2CH_2OCH_3$ and $CH_3OCH_2OCH_3$ the vaporization enthalpies at room temperature are $+36.6$ and $+31.2\,kJ\,mol^{-1}$ respectively[75,76], a difference of only $+5.4\,kJ\,mol^{-1}$. On the other hand, the heats ΔH_{sol}. released upon dissolving these substances are -59.1 and $-10.5\,kJ\,mol^{-1}$ for $CH_3OCH_2CH_2OCH_3$ and $CH_3OCH_2OCH_3$ respectively[3], a difference of $-48.9\,kJ\,mol^{-1}$. Using Hess' law we can therefore conclude that the hydration enthalpies of these two ethers differ $-54.3\,kJ\,mol^{-1}$ in favor of the PEG-like polyether. The difference in polyether solubility is thus predominantly due to the hydration interaction, i.e. to the difference in hydration enthalpies (the much smaller difference in the enthalpies required to remove the ethers from their pure liquid state actually works in the opposite direction); and the simulations indicate that this stronger hydration interaction is mostly due to the higher partial O charges (as observed in the simulations). The anchoring of the hydrating water molecules due to the presence of the neighboring hydrophobic groups (the excluded-volume effect[42]) probably further enhances the solubility.

Ensing 2019, On the origin of the extremely different solubilities of polyethers in water

Adjusting the LCST of Thermosensitive Polymers

PLGA-PEG-PLGA Thermo-responsive Copolymers

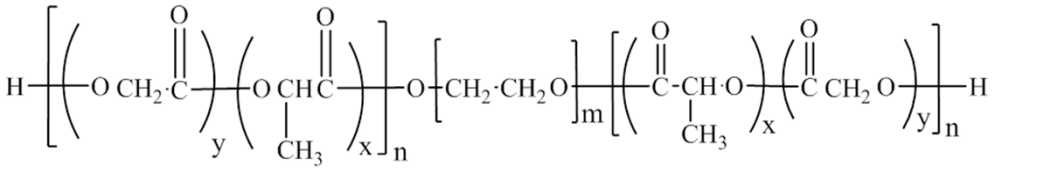

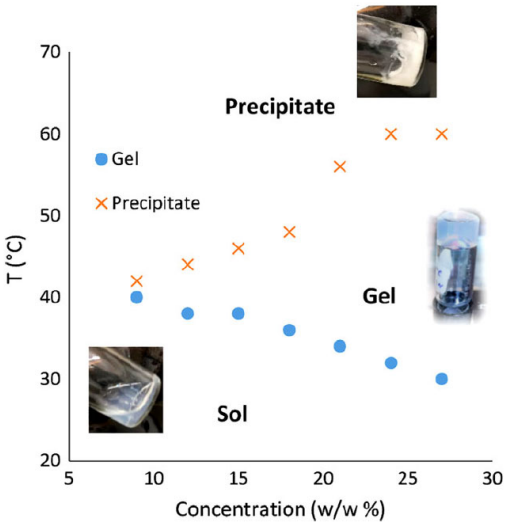

FIGURE 6. Representative phase diagram of PLGA-PEG-PLGA aqueous solutions. As temperature increases the solution turns to gel, and upon further heating a precipitate is formed.

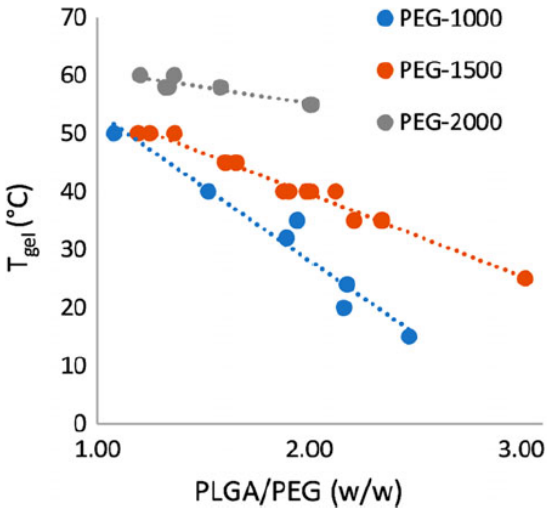

FIGURE 7. Dependence of T_{gel} on PLGA/PEG ratio. For each set of polymers based on a particular PEG MW, a linear relationship has been defined between the polymer's aqueous gelling temperature in a 20% solution and the polymer structure's PLGA/PEG ratio.

Steinman 2019, Effect of PLGA block molecular weight on gelling temperature of PLGA-PEG-PLGA thermoresponsive copolymers

Copolymer of acrylamide and n-tertbutylacrylamide
= Poly(acrylamide-co-n-tertbutylacrylamide)

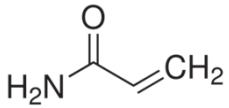

AAm: acrylamide

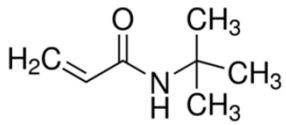

N-tBAAm: n-tertbutylacrylamide

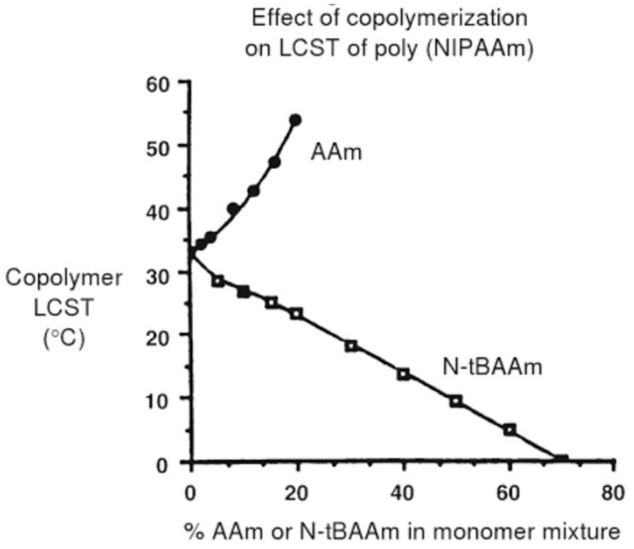

FIG. 3. Copolymerization of a thermally sensitive polymer, PNIPAAm, with a more hydrophilic comonomer, AAm, raises the LCST of the copolymer, whereas copolymerization with a more hydrophobic comonomer, N-tBAAm, lowers the LCST (Hoffman *et al.*, *Journal of Biomedical Materials Research* © 2000).

PEG-PLGA-PEG Triblock Copolymer

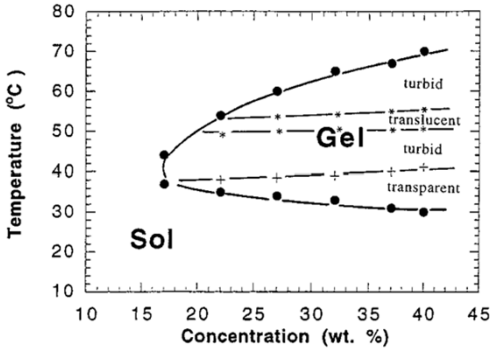

Figure 2. Phase diagram of $EG_{12}-(L_{31}G_9)-EG_{12}$ triblock copolymer aqueous solutions. Filled circles indicate sol–gel transition temperature, and the cross-bar is the temperature at which the transparent gels become turbid. The gel passes through a translucent region (*) and finally becomes turbid again with increasing temperature.

Effect of PLGA Molecular Weight

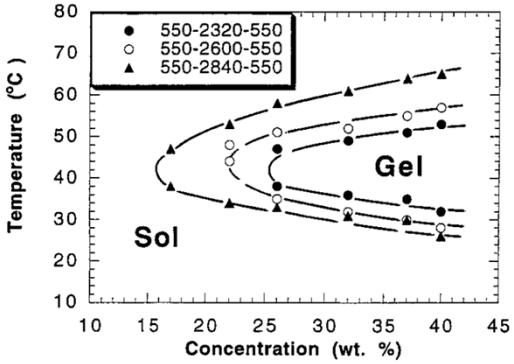

Figure 7. Phase diagram of PEG–PLGA–PEG triblock copolymers with various PLGA lengths: (●) $EG_{12}-(L_{26}G_7)-EG_{12}$; (○) $EG_{12}-(L_{29}G_8)-EG_{12}$; (▲) $EG_{12}-(L_{31}G_9)-EG_{12}$. The legend in the graph indicates molecular weight of constituting block.

Effect of L:G Ratio

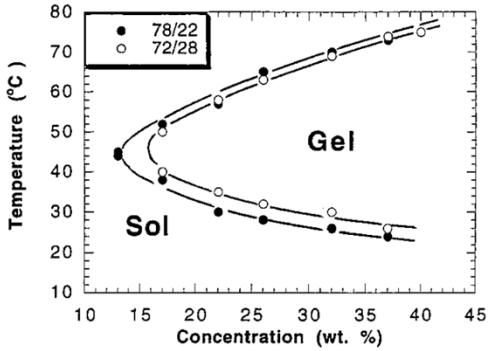

Figure 8. PLGA composition effect on the phase diagram of PEG–PLGA–PEG (550–2900–550) triblock copolymers: (●) $EG_{12}-(L_{32}G_9)-EG_{12}$; (○) $EG_{12}-(L_{31}G_{12})-EG_{12}$. The legend in the graph indicates the mole ratio of DLLA to GA.

Effect of PEG Molecular Weight

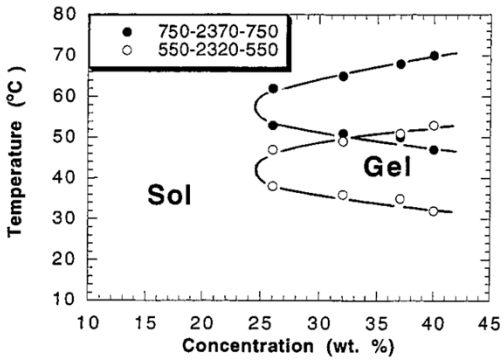

Figure 9. PEG length effect on the phase diagram of PEG–PLGA–PEG triblock copolymer aqueous solutions: (●) $EG_{17}-(L_{26}G_7)-EG_{17}$; (○) $EG_{12}-(L_{26}G_7)-EG_{12}$. The legend in the graph indicates molecular weight of constituting block.

Effect of the Solvent

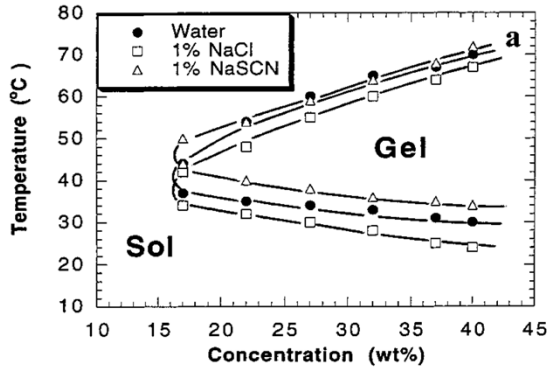

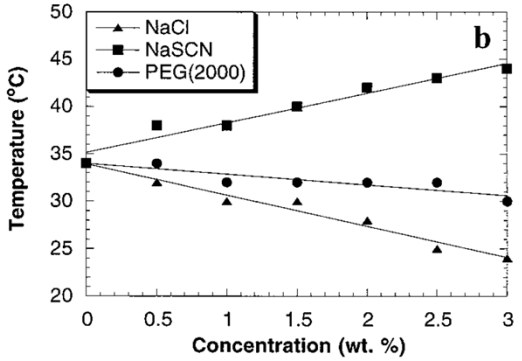

Figure 10. Additive effects on the phase transition of 27 wt % $EG_{12}-(L_{31}G_9)-EG_{12}$ triblock copolymer aqueous solutions: (a) salt effect; (b) concentration effects of NaCl, NaSCN, and PEG 2000.

Jeong 1999, Thermoreversible gelation of PEG-PLGA-PEG triblock copolymer aqueous solutions

Hofmeister Series

$CO_3^{2-} > SO_4^{2-} > S_2O_3^{2-} > H_2PO_4^- > F^- > Cl^- > Br^- > NO_3^- > I^- > ClO_4^- > SCN^-$

$N(CH_3)_4^+ > NH_4^+ > Cs^+ > Rb^+ > K^+ > Na^+ > Li^+ > Ca^{2+} > Mg^{2+} > Zn^{2+} > Ba^{2+}$

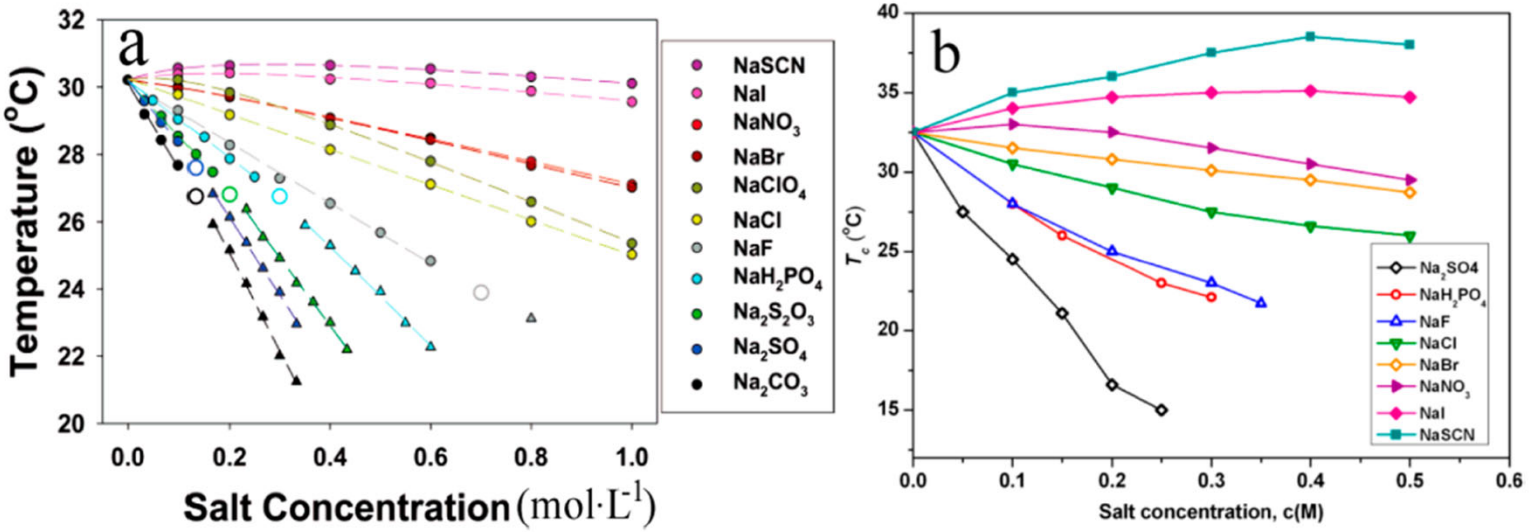

Figure 3. (a) **LCST** values of PNIPAM determined in the presence of sodium salts at different concentrations (0 to 1.0 M). The dashed lines are curve fits to the data calculated from eq 1.

(b) Change of the cloud point (T_c) of 10 $g \cdot L^{-1}$ HIPS solutions with the concentration of different sodium salts.

Kang 2020, Hofmeister Series- Insights of ion specificity from amphiphilic assembly and interface property

As shown in Figure 3, the ability of anions to decrease the LCST agrees with the HS sequence. The salting-out anions present a linear relationship at low salt concentration. When the concentration reaches a certain value, a two-step transition is observed, and the phase transition point is plotted. While for the chaotropic species such as $ClO4^-$ and SCN^-, the effect of anions on the LCST is nonlinear. In Figure 3a, the data calculated from eq 1 are shown with dashed lines. The experimental data coincide with the theoretical calculation. The values of c, B_{max}, and KA also fit the experimental data. Zhang et al. synthesized a novel thermoresponsive polymer, 2-hydroxy-3-isopropoxypropyl starches (HIPS), and studied the influence of sodium salts on its clou point (T_c). In the presence of kosmotropic salts, the hydrogen bonding between polymer and water would be destroyed; meanwhile, some water molecules released from the polymer chains, resulting in a reduction of polymer solubility and a dropping of T_c. On the contrary, chaotropic anions would increase the solubility of polymer and elevate the T_c with concentration, owing to the direct binding to polymer chains. At larger chaotrope concentrations, the T_c goes over a peak and then drops, due to the main driving force of hydrogen bonding between polymer and water, as shown in Figure 3b.

Temperature-Sensitive Block Copolymers and Crosslinked Micelles

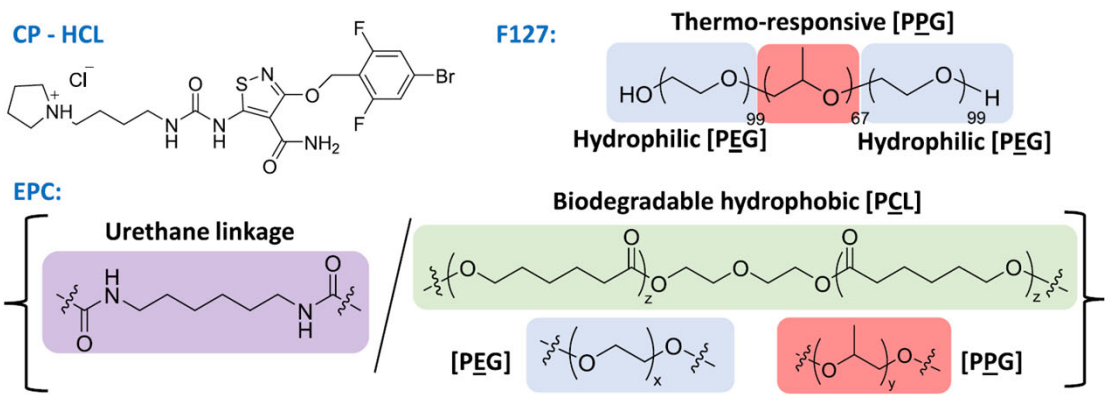

Figure 1. (A) Chemical structures of CP-547,632 hydrochloride (CP-HCl), EPC, and F127.
EPC: A thermogelling multiblock copolymer, which comprises poly(ethylene glycol) (PEG), poly-(propylene glycol) (PPG), and poly(ε-caprolactone) (PCL). The CP-EPC formulation was injectable at 4 °C and gelled spontaneously at body temperature without cross-linkers.

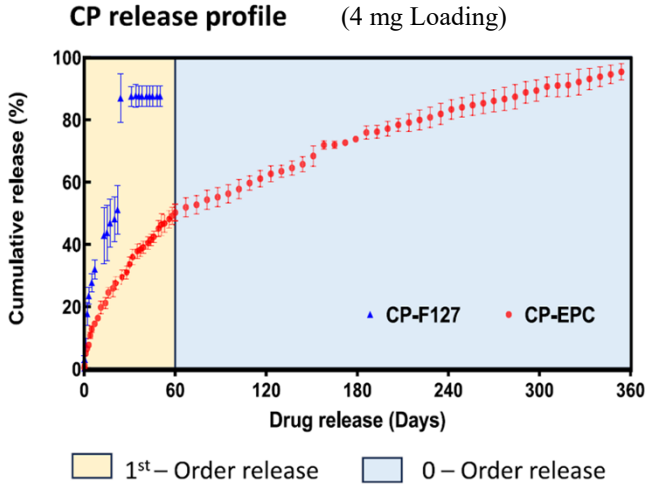

Figure 1. (B) In vitro drug-release profiles.

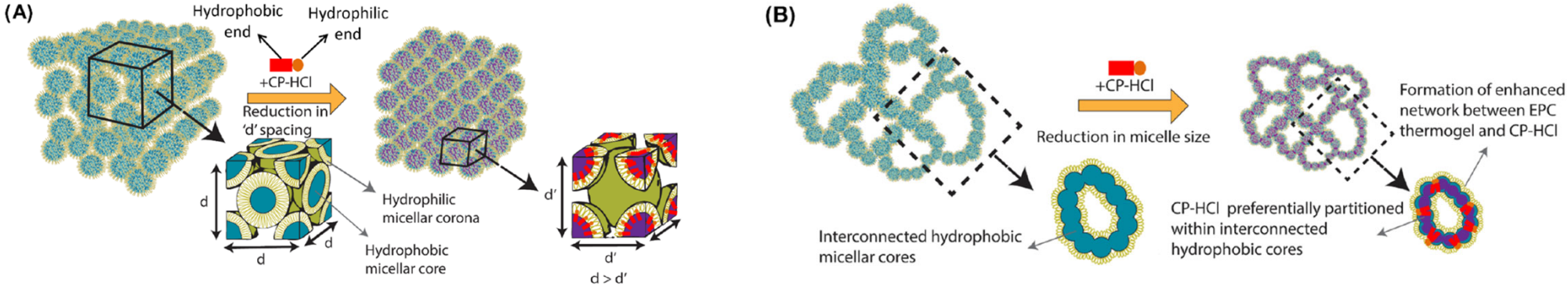

Figure 3. Schematic representation of plausible microstructural changes in (A) F127 and (B) EPC1 thermogels after incorporating CP-HCl.

Zhao 2025, One-year ultralong intravitreal release of tyrosine kinase inhibitor from supramolecular temperature-responsive hydrogel

Applications in Tissue Engineering

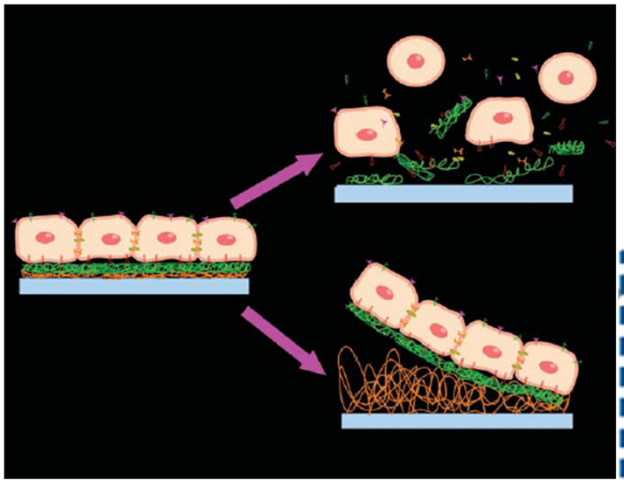

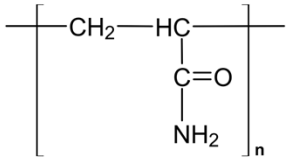

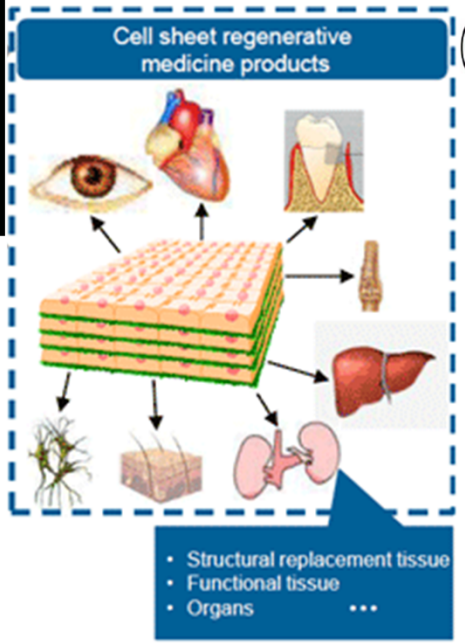

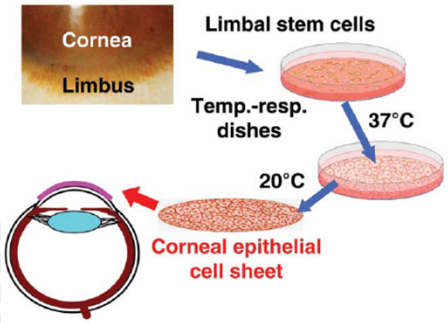

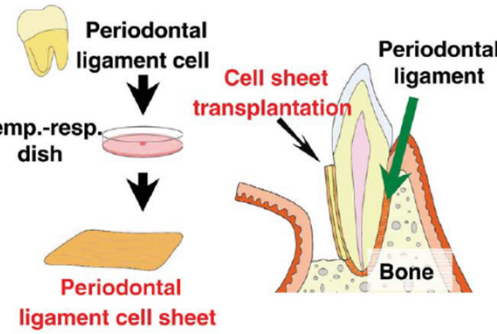

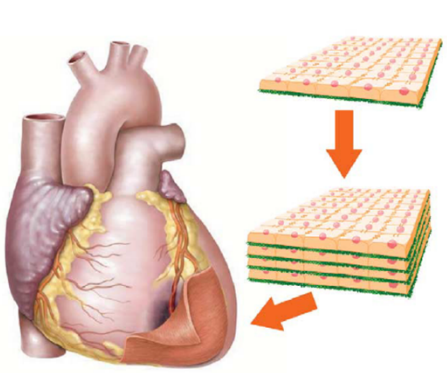

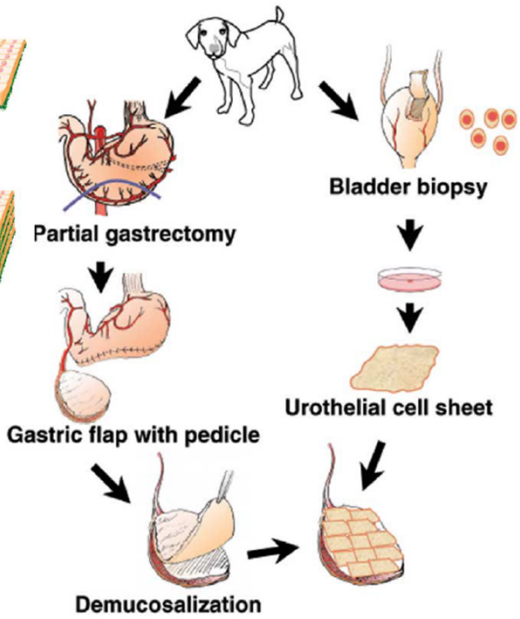

Fig. 2 Cell sheet harvest. Trypsin degrades deposited ECM (green) and membrane proteins, enabling the harvest of confluent monolayer cells as single cells (upper right). The temperature-responsive polymer (orange) covalently immobilized on the dish surface hydrates when the temperature is lowered, thereby decreasing its interaction with deposited ECM. All the cells connected via cell-cell junction proteins are harvested as a single, contiguous cell sheet without the need for proteolytic enzymes (lower right).

Yamato 2004, Cell sheet engineering
Teruo Okano (Professor, Tokyo Women's Medical University)

Thermo-Responsiveness

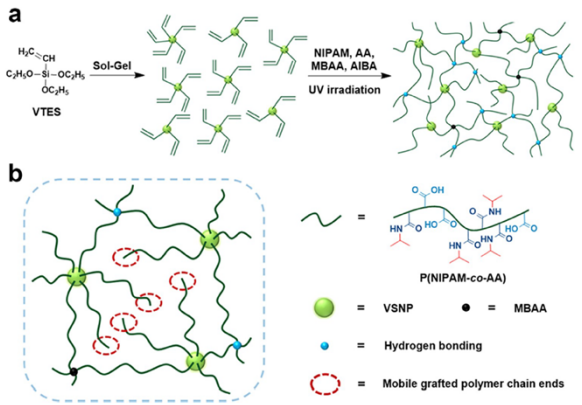

Vinyl Functionalized Silica Nanoparticles (VSNPs)
N,N′-methylenebisacrylamide (MBAA).

Figure 1. Thermo-responsive VSNPs-P(NIPAM-co-AA) hydrogels. (a) Synthesis and network structure of the hydrogels. The polymer network is constructed through the multivalent VSNPs (green balls), noncovalent hydrogen bonding (blue balls), and covalent cross-links by MBAA (black balls). AA monomer has carboxylic acid groups (in light blue), while NIPAM has both hydrophilic amide groups (in dark blue) and hydrophobic isopropyl groups (in red). (b) Schematic illustration of the mobile grafted polymer chain ends.

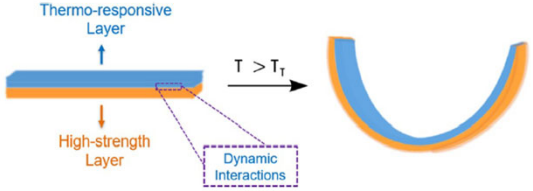

Figure 4. Design and actuating mechanism of the gradient thermo-responsive hydrogel actuators.

Li 2022, Biomimetic gradient hydrogel actuators with ultrafast thermo-responsiveness and high strength

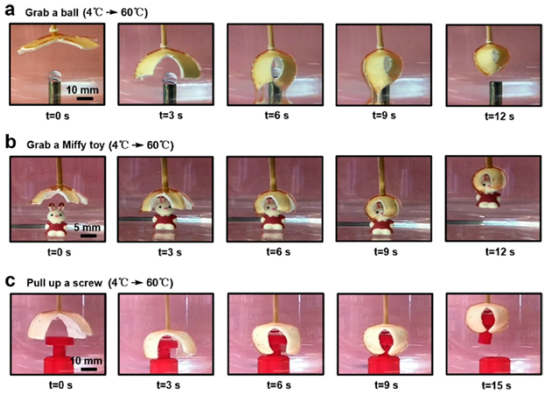

Figure 6. Schematic illustrations of the integrated gradient hydrogels as thermo-responsive grippers. (a) Grab a ball, (b) grab a Miffy toy, and (c) pull up a screw.

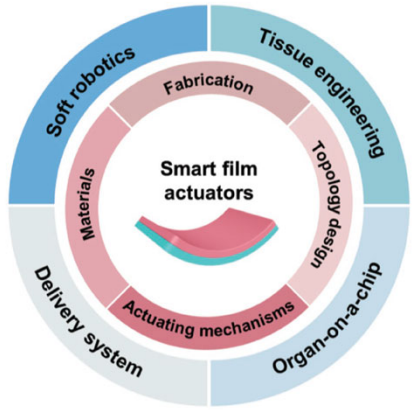

Figure 1. Overview of smart film actuators for biomedical applications.

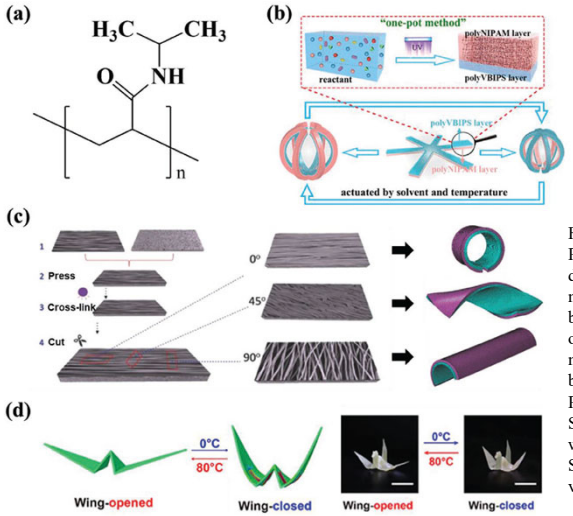

Figure 4. a) Chemical structure of the PNIPAM monomer. b) Schematic diagram of the preparation and working mechanism of the PNIPAM-PVBIPS bilayer hydrogel. c) Schematic diagram of the preparation and working mechanism of the anisotropic PNIPAM bilayer hydrogel with different internal PNIPAM fiber orientations. d) Schematic and images of the reversible wing-flapping of a crane-shaped 3D SMPs actuator triggered by temperature variation (Scale bar = 1 cm).

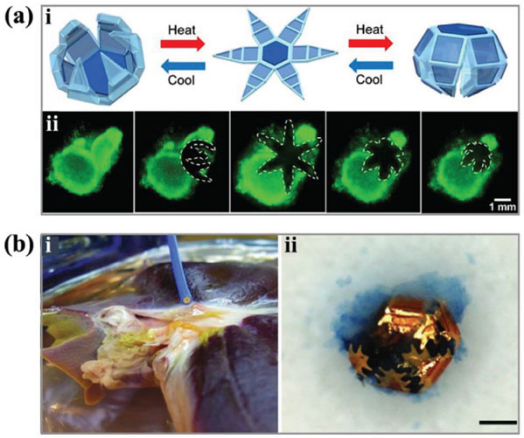

Figure 8. SFA-based soft medical robotics. a-i) Schematic diagram of the thermal-actuated soft robotics; a-ii) fluorescent images of the star-shaped microgripper capturing and excising cells from a living fibroblast clump. b-i) Photograph image of the control of the soft biopsy robotic using a magnetic catheter; b-ii) photograph image of the retrieved robotic with a piece of excised tissue, which was stained in blue (Scale bar = 100 μm).

Zhang 2022, Smart film activators for biomedical applications

Thermo-Responsive Polymers

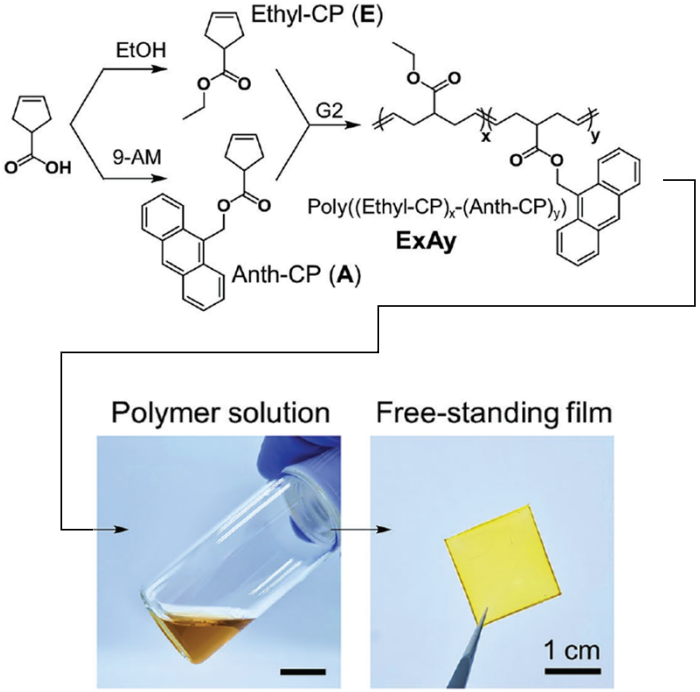

Figure 1. Anthracene-functionalized cyclopentene and its copolymers. a) Synthetic schemes for cyclopentene derivatives (**Ethyl-CP** (**E**) and **Anth-CP** (**A**)) and copolymers (**ExAy**). The resulting polymer was dissolved and then cast onto a silicone substrate, resulting in a free-standing film.

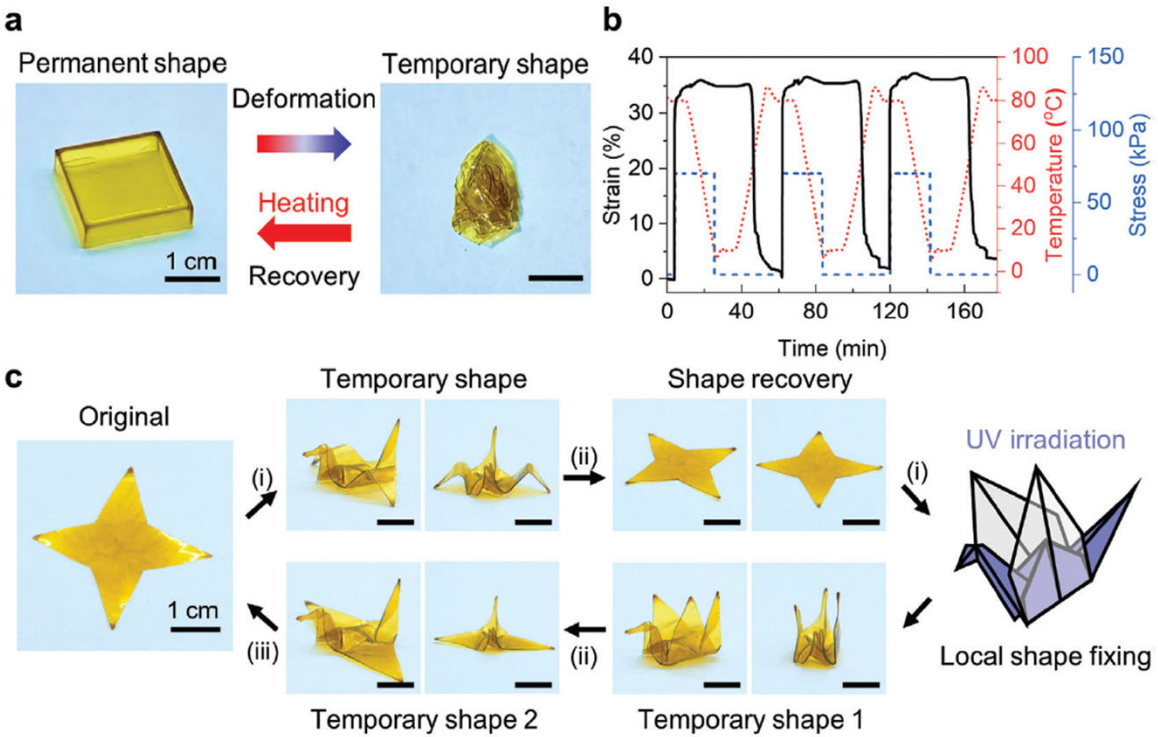

Figure 4. Evaluation of shape memory effect and local shape-programming process of **E1A1**. a) Thermal responsive dual shape memory behaviors. The temporary shape was made by deforming the sample at a temperature above its T_g and removing the applied force after cooling it to a temperature below the T_g. Then, the shape was recovered by re-heating above the T_g. b) Shape memory cyclic test under consecutive heating-cooling cycles. c) Demonstration of local shape programming and shape recovery behaviors. Step i) deformation above the T_g and cooling below the T_g. Step ii) re-heating above the T_g. Step iii) thermal cleavage of anthracene dimers above 130 °C.

Lee 2025, High-performance dynamic photo-responsive polymers with superior closed-loop recyclability

Temperature-Sensitive Polymers & Hydrogels

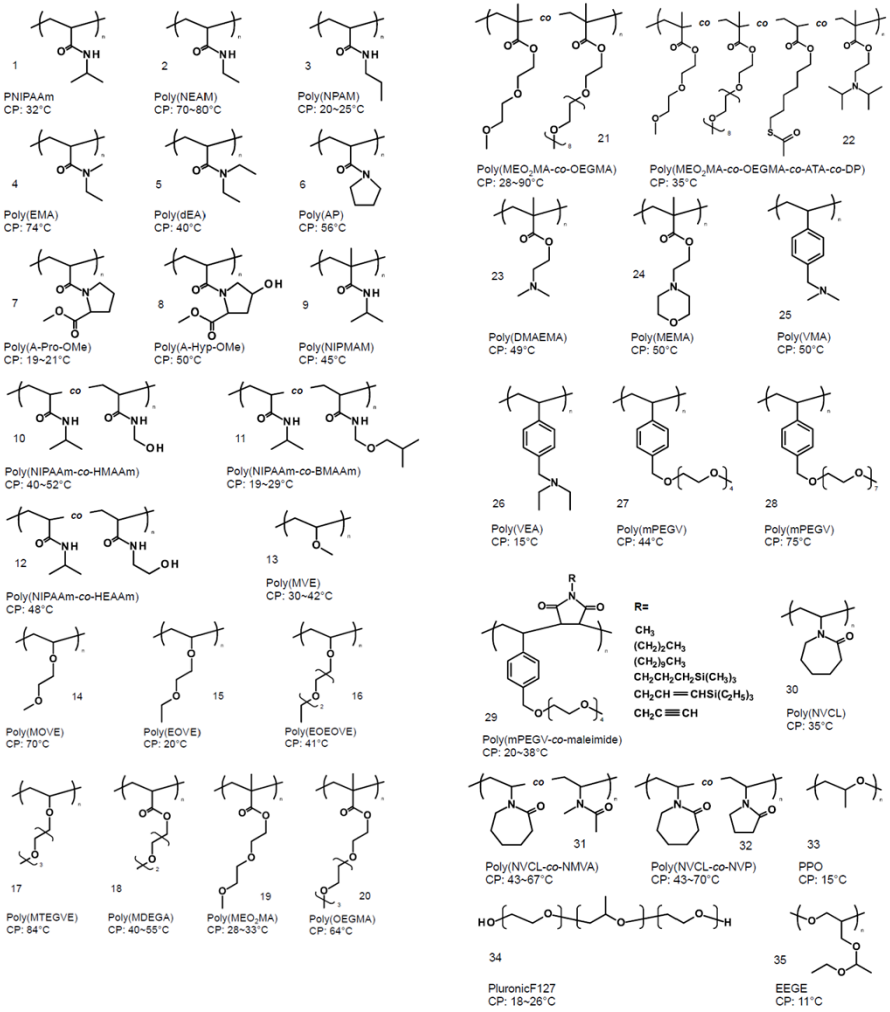

Figure 2. Structures of lower critical solution temperature (LCST) type of thermo-responsive copolymers for dual thermo-responsive block copolymers: CP: cloud point.
1. NIPAAm: N-isopropylacrylamide;
2. NEAM: N-ethylacrylamide;
3. NPAM: N-n-propylacrylamide;
4. EMA: N,N-ethylmethylacrylamide;
5. dEA: N,N-diethylacrylamide;
6. AP: N-acryloylpyrrolidine;
7. A-Pro-OMe: N-acryloyl-L-proline methylester;
8. A-Hyp-OMe: N-acryloyl-4-hydroxy-L-proline methylester;
9. NIPMAM: N-isopropyl methacrylamide;
10. HMAAm: N-hydroxymethyl acrylamide;
11. BMAAm: N-(isobutoxymethyl) acrylamide;
12. HEAAm: N-hydroxyethylacrylamide;
13. MVE: methyl vinyl ether;
14. MOVE: 2- methoxyethyl vinyl ether;
15. EOVE: 2-ethoxyethyl vinyl ether;
16. EOEOVE: 2-(2-ethoxy)ethoxyethyl vinyl ether;
17. MTEGVE: methyltriethylene glycol vinyl ether;
18. MDEGA: methoxydiethylene glycol acrylate;
19. MEO2MA: 2-(2-methoxyethoxy) ethyl methacrylate;
20–21. OEGMA: oligo(ethylethylene glycol)methyl ether methacrylate;
22. ATA: 6-acethylthiohexylacrylate, DP: 2- (diisopropylamino)ethyl methacrylate;
23. DMAEMA: 2-(dimethylamino)ethyl methacrylate;
24. 2-(N-morpholino)ethyl methacrylate;
25. VMA: N-(4-vinylbenzyl)-N,N-dimethylamine;
26. VEA: N-(4-vinylbenzyl)-N,N-diethylamine;
27–29. mPEGV: poly(ethyleneglycol)methyl ether vinyl phenyl;
30. NVCL: N-vinylcaprolactam;
31. NMVA: N-methyl-N-vinylacetamide;
32. NVP: Nvinylpyrrolidone;
33. PPO: poly(propylene oxide);
34. PluronicF127: poly(oxyethylene)- poly(oxypropylene)-poly(oxyethylene);
35. EEGE: ethoxyethylglycidyl ether.

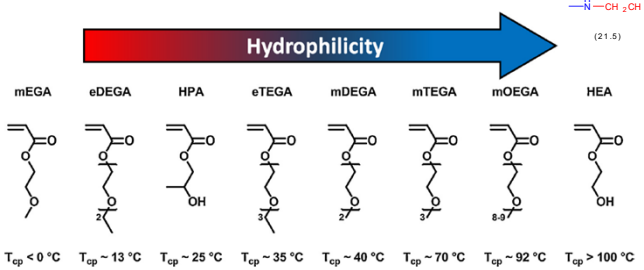

Fig. 4. Overview of the selected OEGA monomers arranged according to increased hydrophilicity, with average cloud point temperatures (T_{cp}) of the corresponding homopolymer.

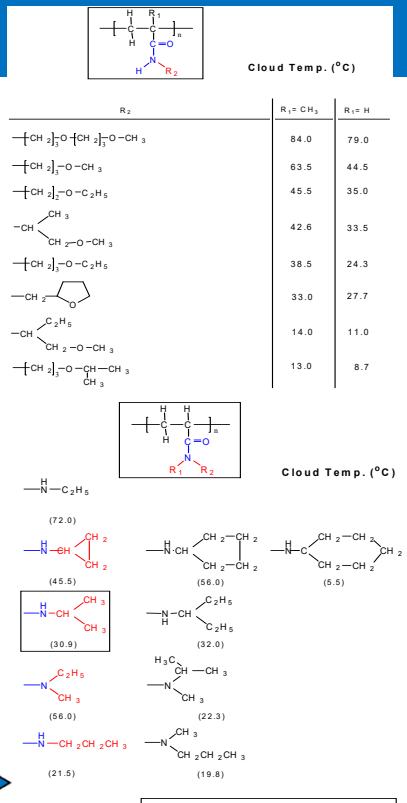

Kotsuchibashi 2016, Recent advances in dual temperature responsive block copolymers and their potential as biomedical applications

Vancoillie 2014, Thermoresponsive poly(oligo ethylene glycol acrylates)

Thermo-Sensitive Hydrogels Induced by Divalent Counterions

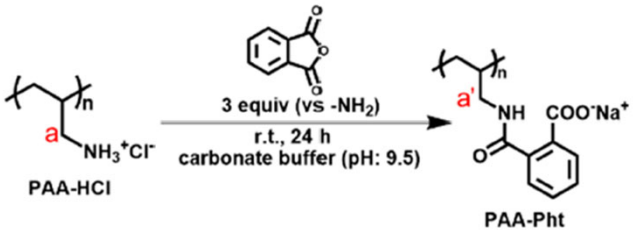

Scheme 1. Thermoresponsiveness of Carboxylated Polyallylamine (PAA) Induced by Divalent Counterions

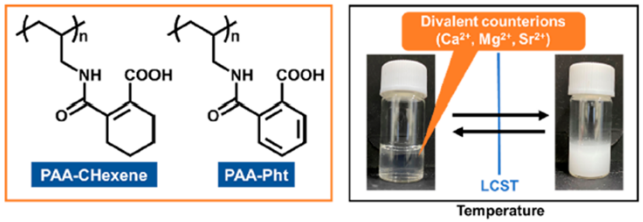

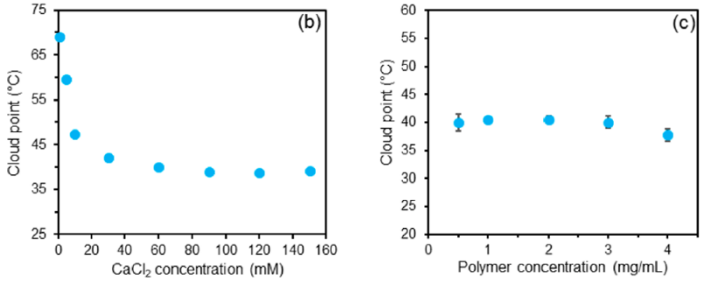

Figure 2. Plots of cloud points against $CaCl_2$ concentration (b) and polymer concentration (c) (pH 5.2, 150 mM $CaCl_2$ aq).

PAA-HCl was dissolved in carbonate buffer (pH 9.5) (2.5 mg/mL), and the pH was adjusted to 9.5 by using a 1 M sodium hydroxide aqueous solution.

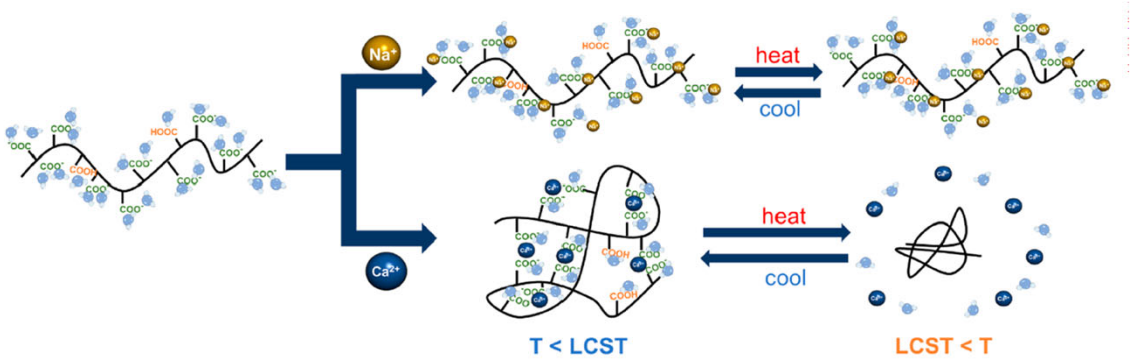

Figure 3. Schematic image of the thermoresponsive mechanism of PAA-Pht with divalent counterions.

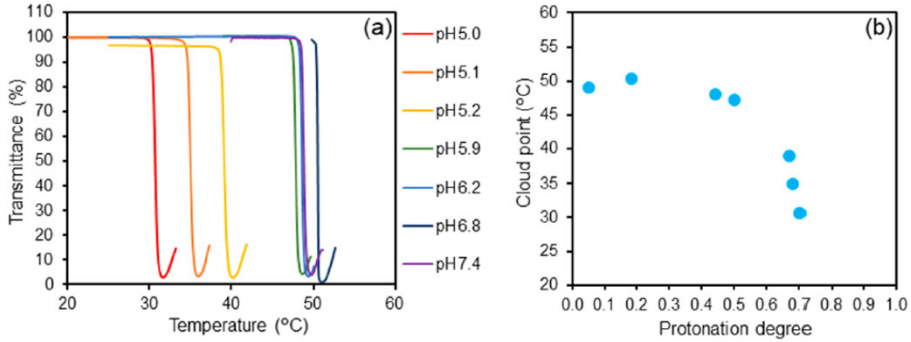

Figure 4. Changes in the transmittance of PAA-Pht in an acidic solution with $CaCl_2$ (150 mM) (pH 5.0, 5.1, 5.2, 5.9, 6.2, 6.8, and 7.4; 4.0 mg/mL) (a). Plots of cloud points against protonation degrees (b). The protonation degrees were determined by acid-base titration (Figure S1).

Emoto 2022, Thermoresponsiveness of carboxylated polyallylamines induced by divalent counterions as ionic effectors

Thermo-Sensitive Hydrogels for Batteries

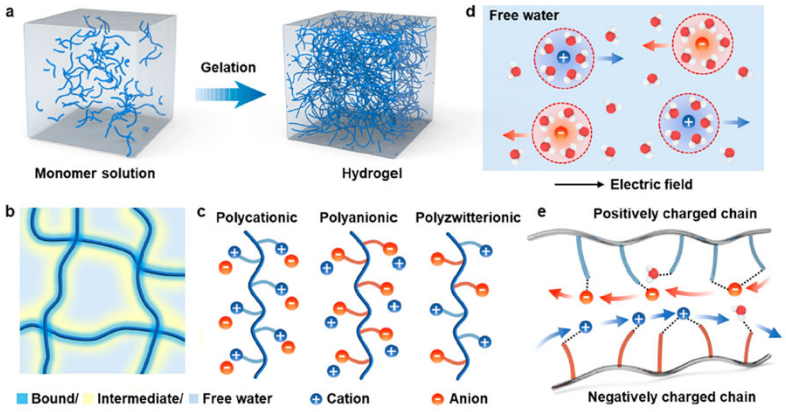

Figure 1. Hydrogel formation and basic properties. (a) Polymer networks cross-linking from monomers. (b) Water states in the hydrogel. (c) Polyionic hydrogel chains. (d) Diffusion of solvated ions in free water. (e) Interaction of ions with polyionic polymer chains.

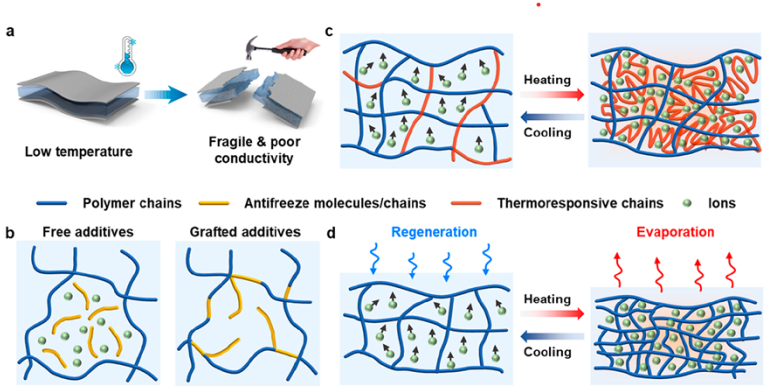

Figure 3. Temperature adaptability of aqueous batteries enabled by hydrogels. (a) Performance deterioration due to freezing of aqueous electrolyte at low temperatures. (b) Antifreezing by introducing additives to hydrogel. (c) Phase transition of hydrogel electrolyte that regulates the migration of ions. (d) Reversible water evaporation and regeneration in hygroscopic hydrogel electrolyte.

The temperature tolerance of rechargeable batteries determines whether they can operate in intercontinental regions.

Beyond Room Temperature. Temperature adaptability of rechargeable batteries determines whether they can be operatable in intercontinental regions.[68] As a typical example, hydrogel electrolytes in Zn−MnO_2 batteries can be stable over a wide temperature range from −40 to 60 °C.[69] At low temperatures, the electrolyte needs to have prominent conductivity to keep the battery running. In terms of antifreezing thermodynamics and ion diffusion kinetics, double networks, functional groups, and additives that interact with water can be introduced in the hydrogels to restrain the formation of hydrogen bonds between water molecules.[70−72] In contrast, at excessive temperatures, the battery should preferably be in a shutdown state to ensure safety. The thermal self-protection function is achievable by employing thermo-sensitive groups to control ion mobility. Research may be directed to the engineering of polymer chains by appropriately designing polyanionic, water-interactive, and thermal-responsive groups in one hydrogel electrolyte. Hence, high-performance and stable batteries for all seasons can be realized in the near future.

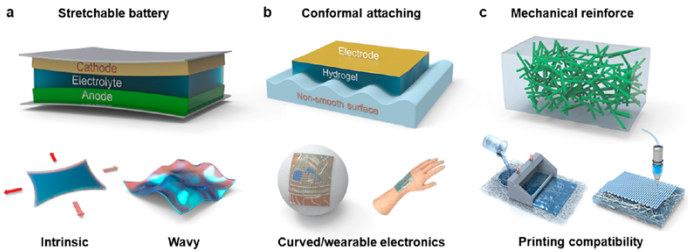

Figure 4. Mechanical regulation of batteries with hydrogel electrolytes. (a) Stretchable battery enabled by wavy structures. (b) Conformal design for structural batteries and wearable electronics. (c) Schematic of framework-reinforced hydrogel electrolyte

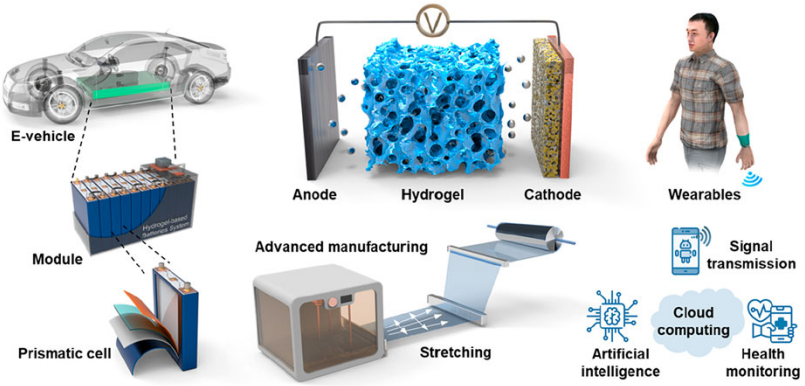

Figure 5. Perspective of hydrogels for future smart batteries

Yang 2022, Hydrogels enable future smart batteries

Liquid Crystal Elastomer

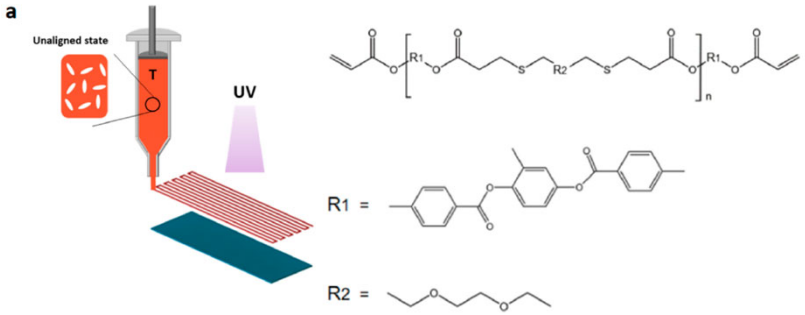

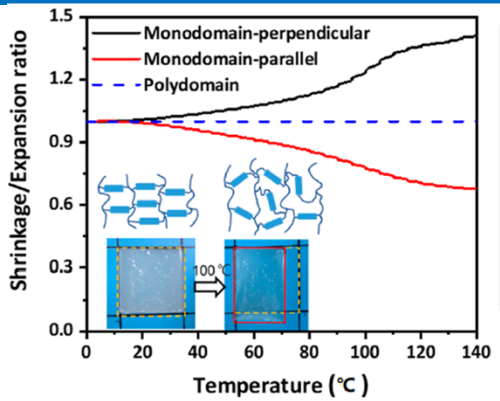

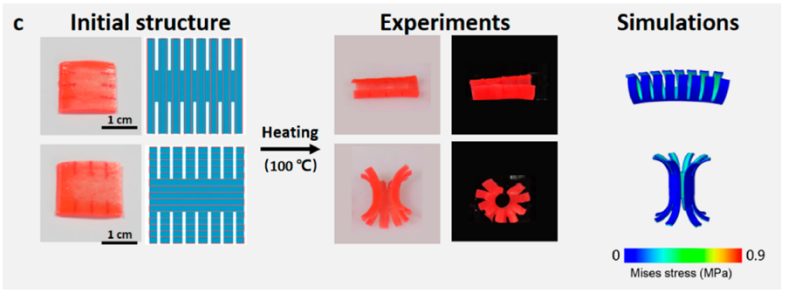

Liquid crystal elastomer (LCE) is a typical thermally responsive soft material, which is an ideal candidate for fabricating programmable shape changing structures. The anisotropic shape changes of LCEs caused by the mesogen reorientation are inherently different from those of other stimulus-responsive soft materials, such as hydrogels and dielectric elastomers.

Liquid crystal elastomer (LCE) is a thermally driven actuating material which combines **an elastic polymer network and anisotropic liquid crystal mesogens**. It has attracted much attention recently because of its unique properties, such as large and reversible actuation, easy processability, and programmability. The LCE can undergo nematic-toisotropic (N−I) phase transition under **external stimuli, such as heat, light, electric field, and magnetic field**. In the aligned LCEs, the mesogen orientation can change upon the phase transition process, leading to a macroscopic shape change. Various methods have been applied to adjust the mesogenic alignment, such as mechanical stretching, surface alignment, or external magnetic/electric field. The LCEs prepared by these conventional methods are usually presented as an extremely thin film. It is challenging to fabricate LCE structures with complex geometries and alignment patterns.

Wang 2025, Shape morphing of 3D printed liquid crystal elastomer structures with precuts

Anisotropic liquid crystal mesogens.
Anisotropic liquid crystal mesogens are elongated or disc-shaped molecules that form liquid crystal phases, exhibiting properties that vary with direction (anisotropy), like alignment and light interaction, crucial for smart materials (LCEs) that change shape with stimuli (heat, light, fields) due to their self-organization into ordered liquid-like states between solids and isotropic liquids.

- Mesogen (Mesophase): A molecule that can exist in a liquid crystalline state (mesophase) and drives the material's ordered behavior, often having rigid, anisotropic shapes (rod-like or disc-like).
- Anisotropy: Means properties (optical, mechanical, electrical) differ depending on the direction measured, unlike isotropic materials, where properties are uniform.
- Self-Organization: Mesogens align themselves, giving liquid crystals their unique order, which can be controlled by external fields.

How They Work:

- Molecular Structure: Mesogens typically have a rigid core (e.g., aromatic rings) and flexible tails, promoting alignment.
- Phases: They transition between disordered (isotropic) and ordered (nematic, smectic) states with temperature or other stimuli, unlike normal liquids that just freeze.
- Stimuli Response (in LCEs): When mesogens are part of a polymer network (Liquid Crystal Elastomers - LCEs), their alignment changes with heat, light, or fields, causing the whole material to deform or change properties.

Applications:

- Smart Materials: Creating responsive actuators, soft robotics, and adaptive surfaces.
- Displays (LCDs): Controlling light polarization for screens (TVs, monitors).
- Biomaterials: Developing scaffolds that guide cell alignment in tissue engineering.

Thermochromic Polymers

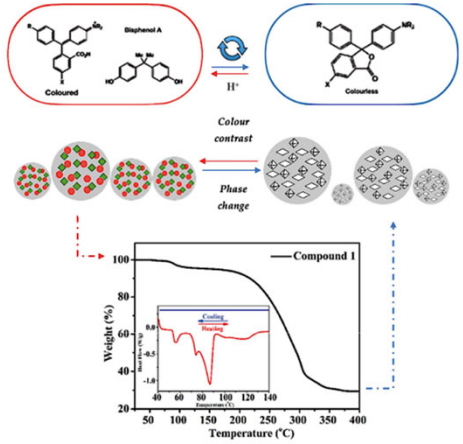

Figure 2. Schematic relationship between temperature and colour change in a specific reversible composite organic thermochromic pigment.

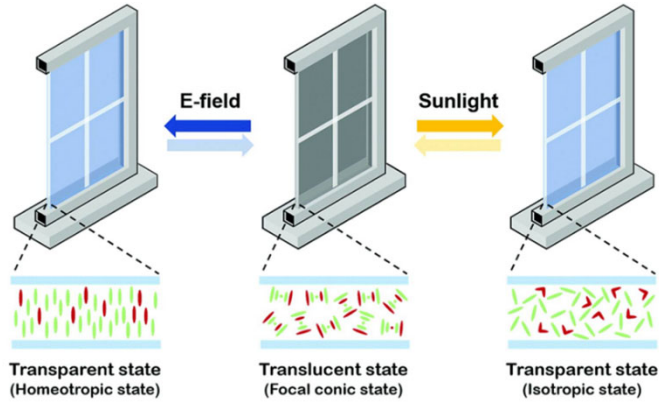

Figure 6. Schematic representation of reversible liquid crystal thermochromic material on smart window using a push–pull chemical compound of functional group R−N = N−R′.

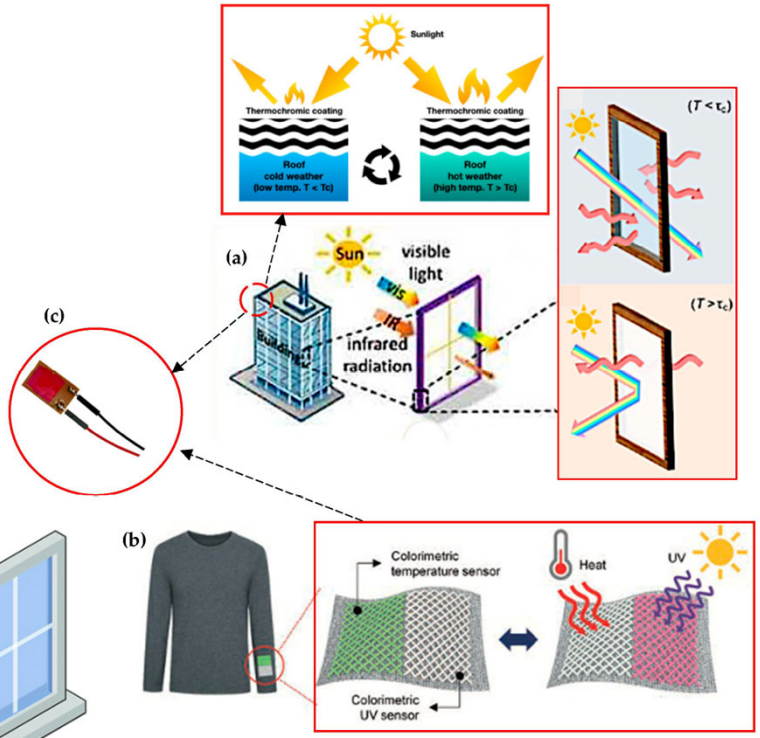

Figure 15. Versatile applications of thermochromic materials for smart application technology. (**a**) Hydrophobic roof coating and smart window module from thermochromic material [138,235]. (**b**) Calorimetric temperature and UV sensors applied by weaving thermochromic materials [236]. (**c**) Highly thermochromic temperature sensor membrane in fire detector sensor and temperature detection application [191].

In situ polymerization
Solution mixing (Themochromic chemical & polymer dissolved in a solvent)
Melt blending

Thermochromism is the property of materials, such as specific pigments or inks, to reversibly change color or shade in response to temperature fluctuations. These "smart materials" function by using heat-sensitive molecules (leuco dyes or liquid crystals) that change their molecular structure and how they reflect light when heated or cooled.
Thermochromic pigments can be incorporated into inks, plastics, and paints, allowing for creative, functional, and interactive design.

Applications
Consumer Goods: Novelty items like mood rings, t-shirts, and mugs.
Safety & Logistics: Temperature-sensitive labels for cold-chain monitoring (food/vaccines) and baby bottle indicators.
Industrial/Environmental: Smart packaging, coatings for energy-efficient buildings to reduce solar heat gain, and specialized inks.

Types
Liquid Crystals: Often used for precise, reversible temperature sensing, changing color based on the pitch of their structure (e.g., forehead thermometers).
Leuco Dyes: Commonly used in inks, changing from a colored state to colorless upon heating.

Limitations: These materials may have limited, temporary life spans, especially when exposed to high UV light or extreme temperatures.

Supian 2024, Thermochromic polymer nanocomposites for the heat detection system

Shape Memory Polymers

Important Aspects of Shape Memory Polymer Systems

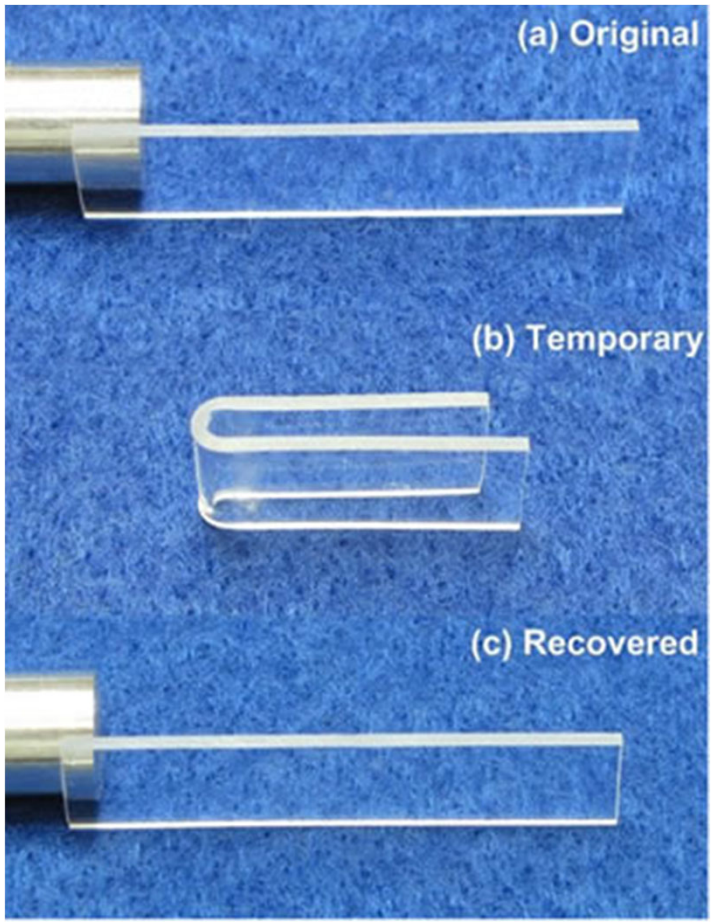

Shape memory polymers have 2 key identifying features

Shape fixity
Shape recovery

Shape fixity allows the material to maintain a temporary shape after molding

Shape recovery allows the material to return to the original shape of the material

Polymer Origami

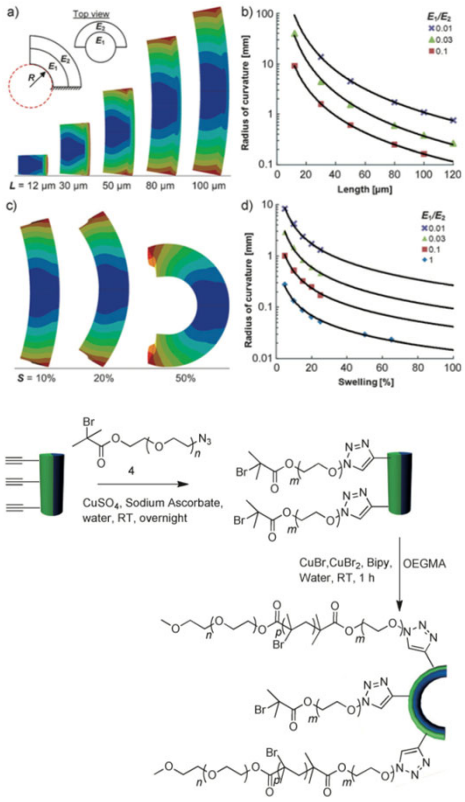

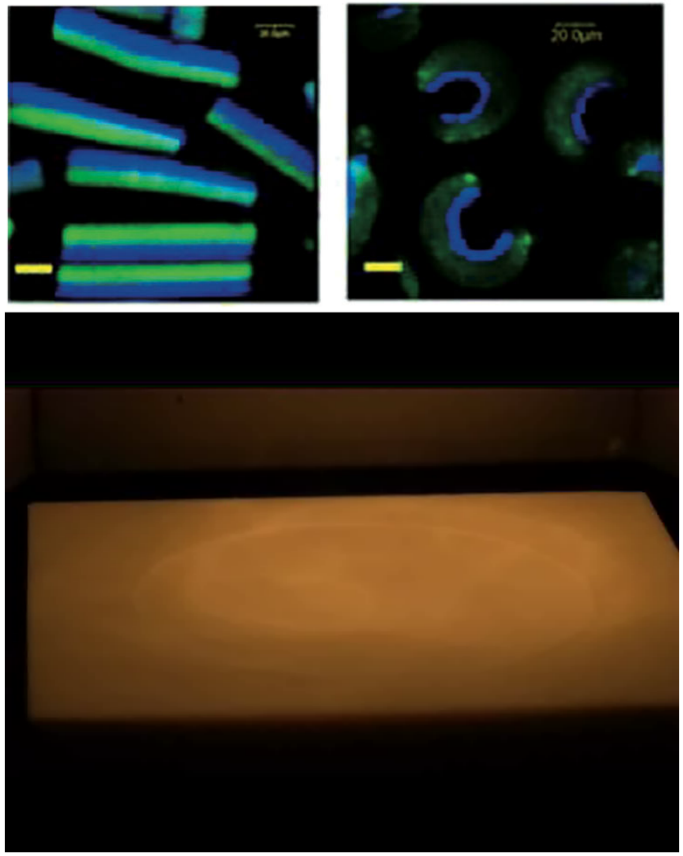

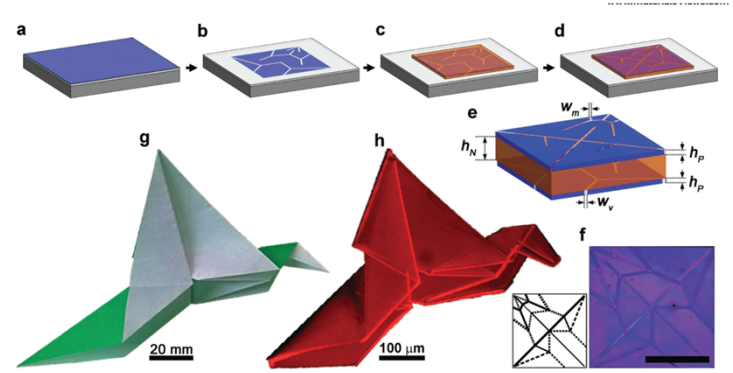

Figure 1. Fabrication of self-folding polymer origami. a) A thin layer of a photo-crosslinkable glassy polymer (PpMS) on a substrate precoated with a sacrificial layer is b) photolithographically patterned with open stripes of width W_v to define the positions and angles of the valley folds. c) Next, a thicker layer of a photo-crosslinkable temperature-responsive polymer (PNIPAM) is coated on top and uniformly crosslinked over the entire area of the bottom PpMS sheet. d) Finally, a third layer of PpMS is coated and patterned with open stripes of width W_m to define the positions and angles of the mountain folds. e) A magnified schematic of the resulting trilayer film (dimensions not to scale), with h_N and h_P as the respective thicknesses of PNIPAM and PpMS layers. f) An optical image of a trilayer film patterned to fold into Randlett's flapping bird (scale bar: 400 µm), along with a schematic indicating the locations and widths of mountain (solid lines) and valley (dotted lines) folds. g) A photograph of Randlett's flapping bird folded using paper, h) alongside a fluorescence image of the self-folded trilayer film.

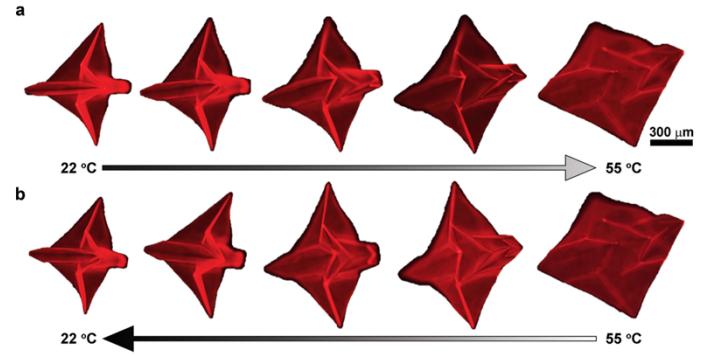

Figure 4. Thermal actuation of self-folding origami. a) When the temperature is increased, the hydrogel polymer layer deswells, causing the Randlett's bird to revert to an unfolded, nearly flat, shape by 55 °C. b) Upon cooling to 22 °C, reswelling back to the folded state occurs through a similar pathway. Dry thicknesses of h_P = 70 nm and h_N = 1.5 µm are used, while the size of the square sheet is 800 µm on a side.

Stimulus allows for folding of a polymer into predefined shape in response to an external stimulus.

Angew. Chem. Int. Ed. 2012, 51, 660 –665

Science Advances 08 Jan 2016: Vol. 2, no. 1, e1501297 DOI: 10.1126/sciadv.1501297

Adv. Mater. 2015, 27, 79–85

Shape Memory Polymers in Aerospace Applications

http://acadia.org/papers/2QPH7Y

Figure 6: The sequential recovery of a multimaterial flower.

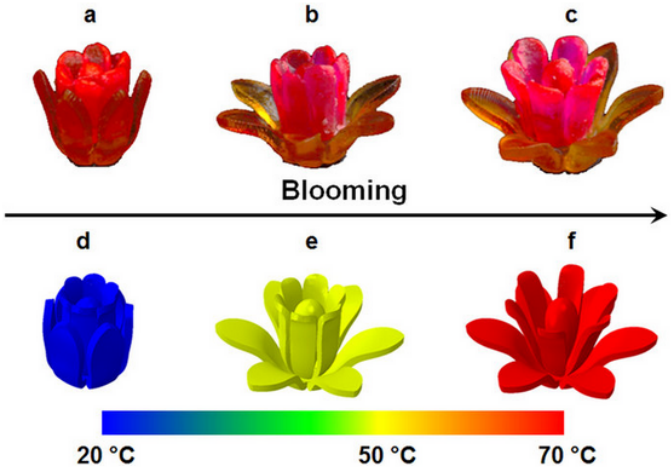

The multimaterial flower in the original shape (**c**) was first programmed into the temporary bud state at 20 °C (**a**). The outer petals opened first after heating to 50 °C (**b**) and then, the flower fully bloomed at 70 °C (**c**). (**d**)–(**f**) represent the FE simulations of the corresponding flower blooming process.

http://www.nature.com/articles/srep31110

Figure 5: 3D printed multimaterial grippers.

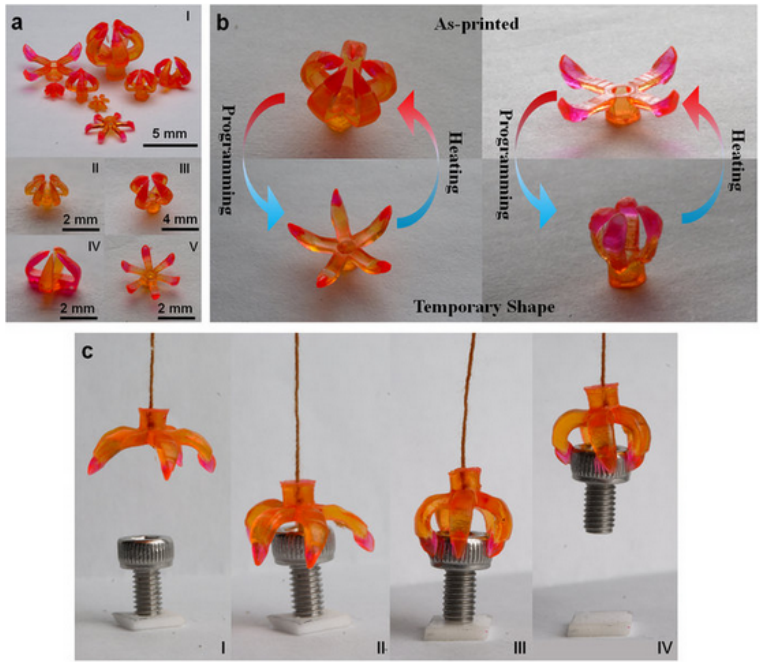

(**a**) Multimaterial grippers were fabricated with different designs. (**b**) The demonstration of the transition between as printed shape and temporary shape of multimaterial grippers. (**c**) The snapshots of the process of grabbing an object.

Stimuli-Responsive Shape Memory Polymer Composites

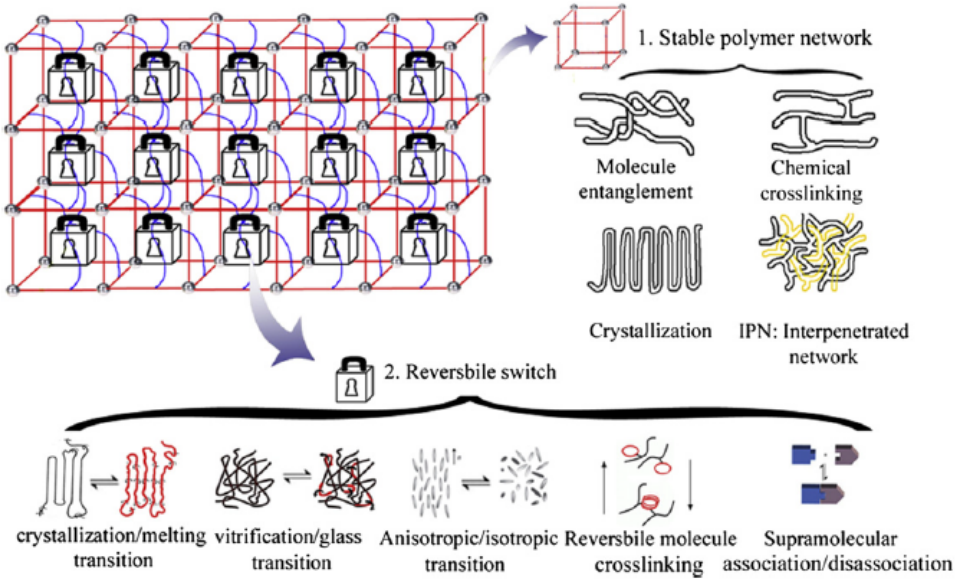

Fig. 1. Various molecular structures of SMPs. A stable network and a reversible switching transition are the prerequisites for the SMPs to show SME. The stable network can be molecule entanglement, chemical cross-linking, crystallization, and IPN; the reversible switching transition can be crystallization melting transition, vitrification-glass transition, anisotropic-isotropic transition, reversible chemical cross-linking, and associatione-disassociation of supramolecular structures

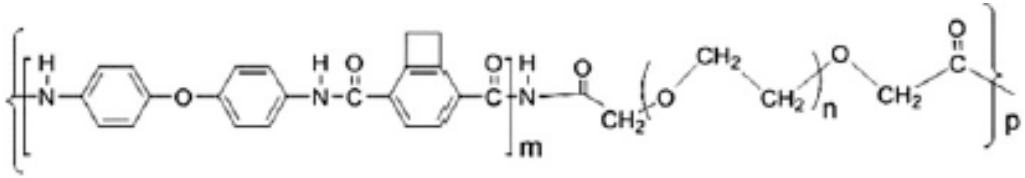

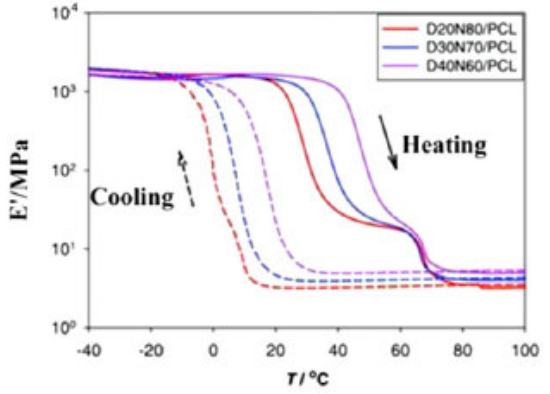

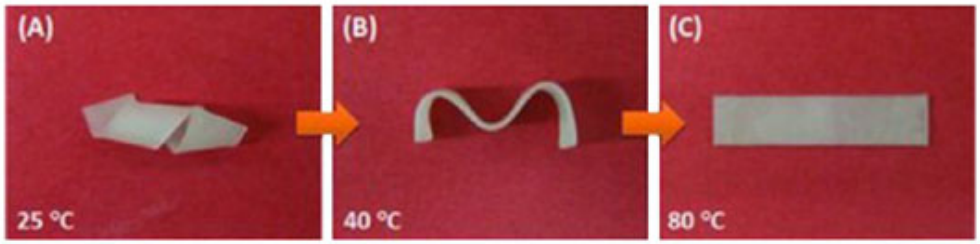

The sequential recovery of the epoxy/polycaprolactone composite (A) from a temporary shape, (B) to temporary shape b, and (C) to permanent shape c.

Harper Meng, Guoqiang Li. A review of stimuli-responsive shape memory polymer composites. Polymer 54: 2199-2221, 2013.

Hydrogel with Fast Shape Memory and On-demand Drug Release

Fig. 2 | Mechanical and shape-memory properties of PTK hydrogel. a Tensile stress-strain curves of PMI, PKG, PTA, and PTK hydrogels. **b** Successive loading-unloading test of PMI and PTK hydrogels. **c** The retention ratio of the initial stress at the 0, 20, 200, 1000, 3000, 6000, 10000, and 20000 cycles during the successive loading-unloading test of PMI and PTK hydrogel. **d** The lap-shear adhesive strength of PTA and PTK hydrogels with cartilage. Photographs of the shape-memory performances of PTK hydrogel with the temporary helix shape (**e**) and coil shape (**f**). Scale bar: 5 mm. Data in **d** are presented as mean values ± SD. ($n = 3$ independent samples).

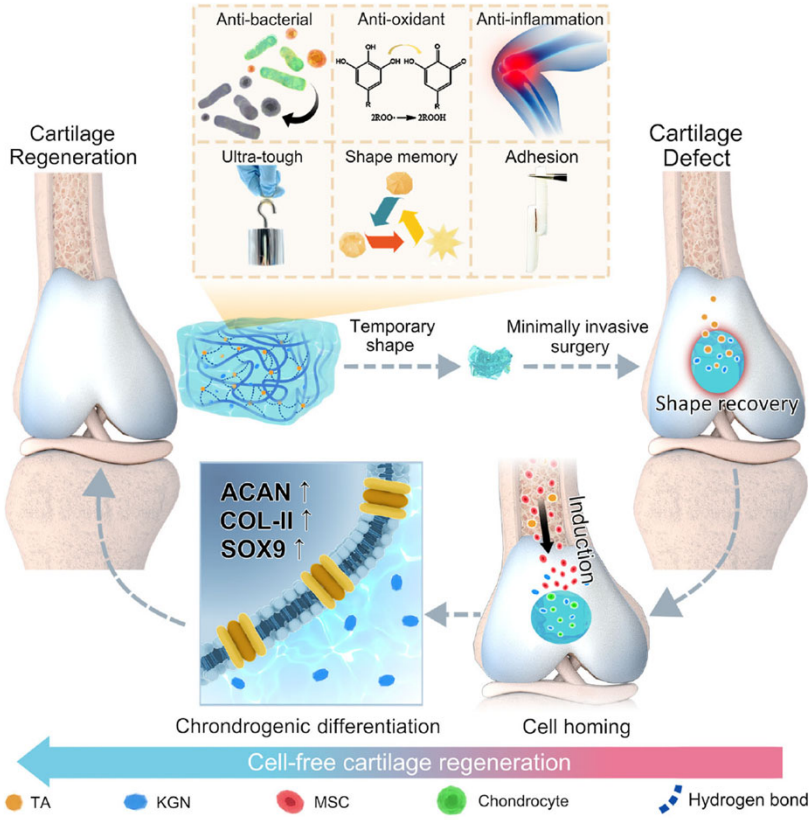

Yang 2023, Ultra-durable cell-free bioactive hydrogel with fast shape memory and on-demand drug release for cartilage regeneration

Is This A Shape Memory Polymer?

Is Slinky a shape memory polymer?

pH-Sensitive Systems

Intelligent Gels

Soft aggregations of long-chain molecules can shrink or swell in response to stimuli. They may form the basis of a new kind of machine. Yoshihito Osada and Simon B. Ross-Murphy. Scientific American. May 1993, p. 83)

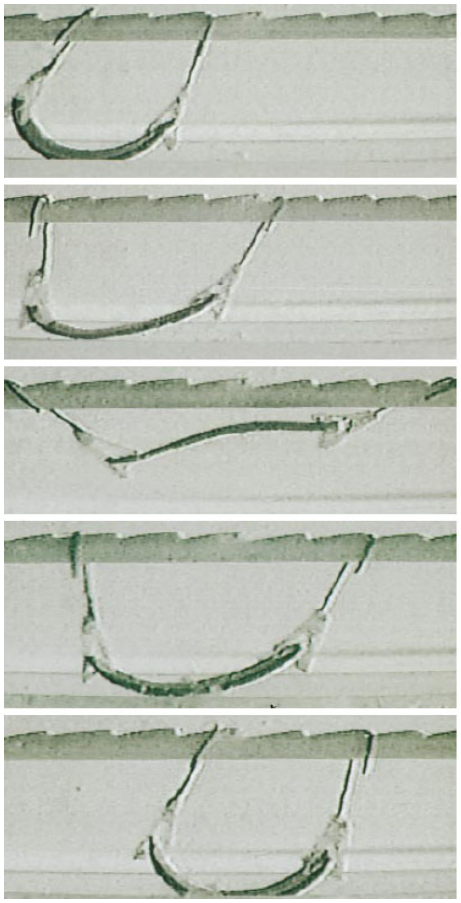

Gel Looper, and inchwormlike device that moves by repeatedly curling and straightening itself, was developed by Osada. Surfactant molecules in the liquid surrounding the looper collect on the gel's top surface under the influence of an electric field, causing the gel to shrink. When the polarity of the electric field is changed, the surfactant goes back into the solution.

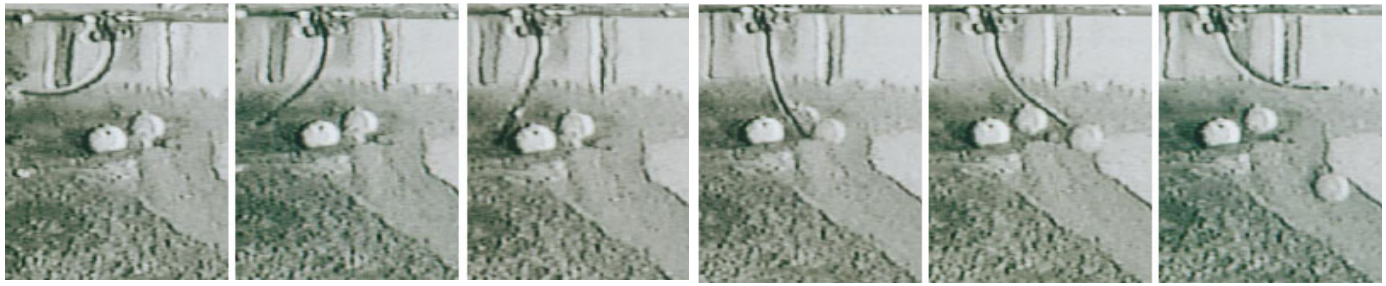

Gel Golf demonstrates the ability of an intelligent gel to act on its surroundings. A strip of gel made of the same material as the gel looper curls first one way and then the other under the influence of an electric field. During this transition, it strikes a gold ball, propelling it down a slope. Although the "club" material is sturdy enough to strike a ball directly, it must be submerged in liquid and so an actual use would probably be encases in a protective container.

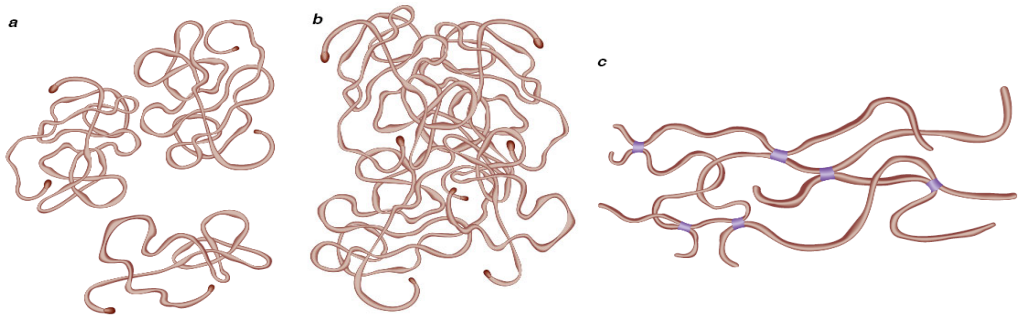

Long-chain molecules cause a solution to become viscous (a) because they interfere with one another as the solution flows. As their concentration increases, the molecules become entangled, yielding viscoelastic behavior that partakes of both solid and liquid traits (b). If the intertwined molecules bond with one another, the result is a gel (c)

pH-Sensitive Polymers (Polyelectrolytes)

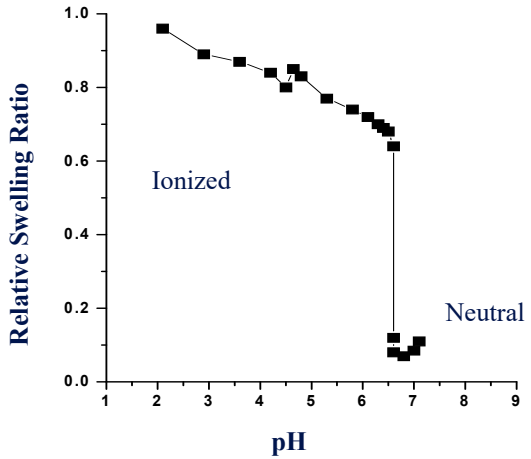

	Monomer	pH-sensitive group
Acidic (Anionic)	(Meth)acrylic acid	-COOH
	Sodium styrene sulfonate	$-SO_3^-$ Na^+
	Sulfoxyethyl methacrylate	$-SO_3H$
Basic (Cationic)	Aminoethyl (meth)acrylate	$-NH_2$
	N,N-dimethylaminoethyl (meth)acrylate	$-N(CH_3)_2$
	N,N-diethylaminoethyl (meth)acrylate	$-N(CH_2CH_3)_2$
	Vinylpyridine	
	Vinylbenzyl triethylammonium chloride	$-N^+(CH_3)_3Cl^-$

Brondsted and Kopecek, ACS Symp. Ser. 480, pp. 285-304 (1992)

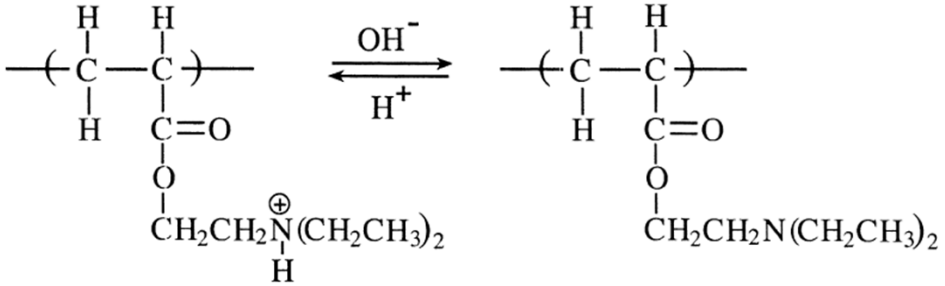

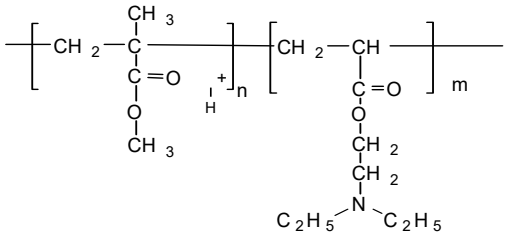

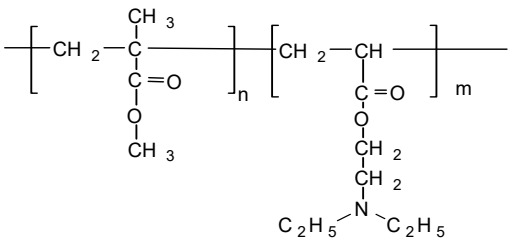

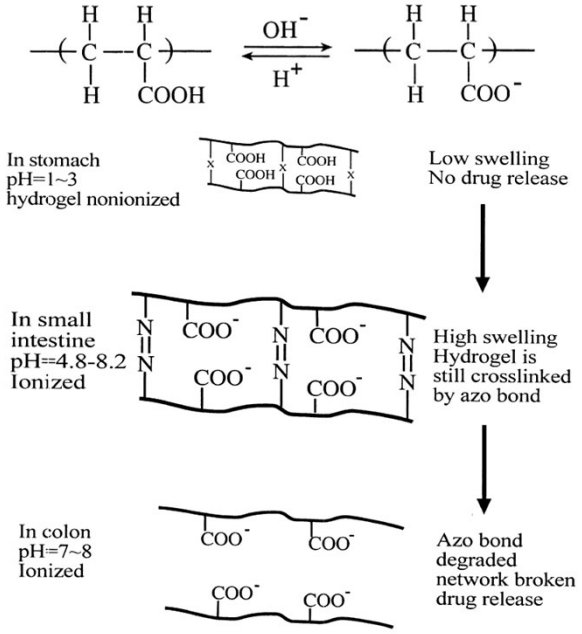

Fig. 5. Schematic illustration of oral colon-specific drug delivery using biodegradable and pH-sensitive hydrogels. The azoaromatic moieties in the cross-links are designated by –N=N–; from Ref. [62].

pH-Sensitive Polymers for Controlled Insulin Release

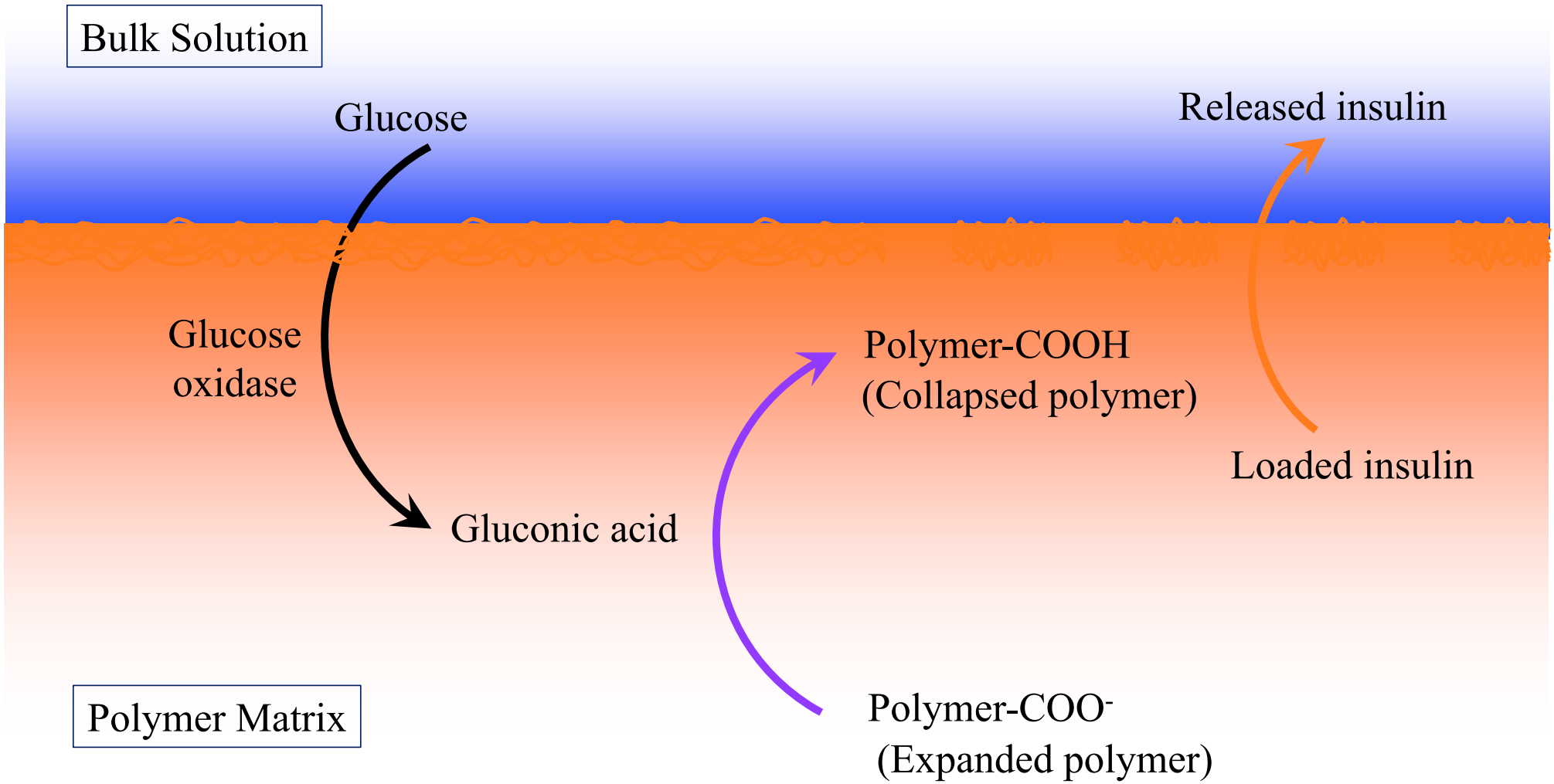

pH-Activatable Polymeric Prodrugs

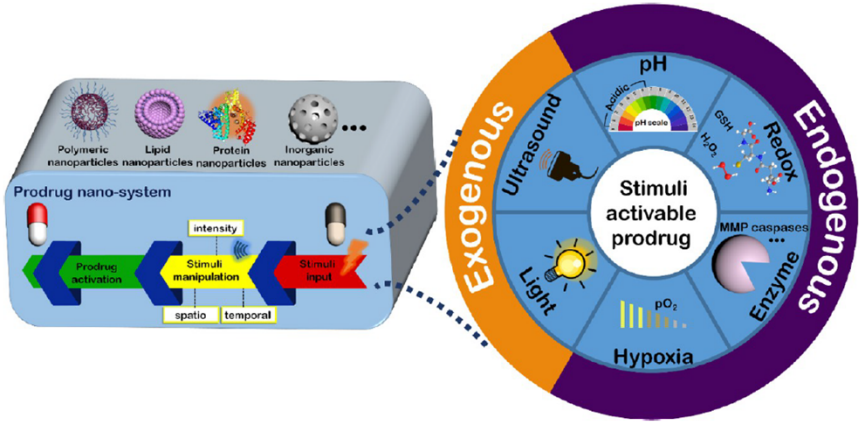

Scheme 1. Schematic illustration of stimuli-responsive activation process of prodrug nanosystems and various kinds of stimuli for prodrug activation

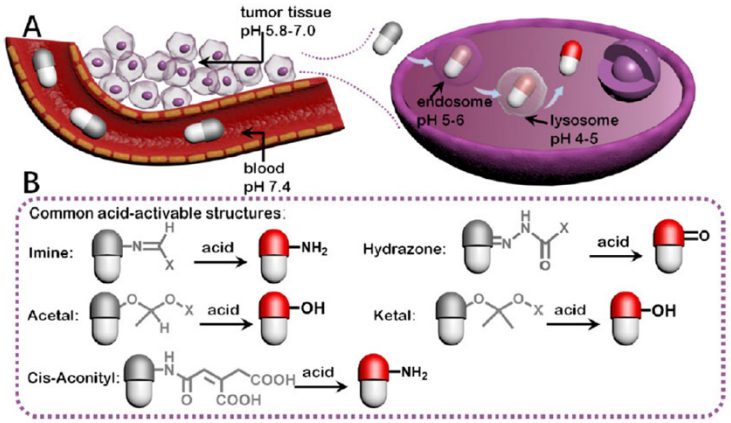

Scheme 2. (A) pH Values in blood, tumor microenvironment, endosome, and lysosome and (B) Representative acid-activable chemical structures

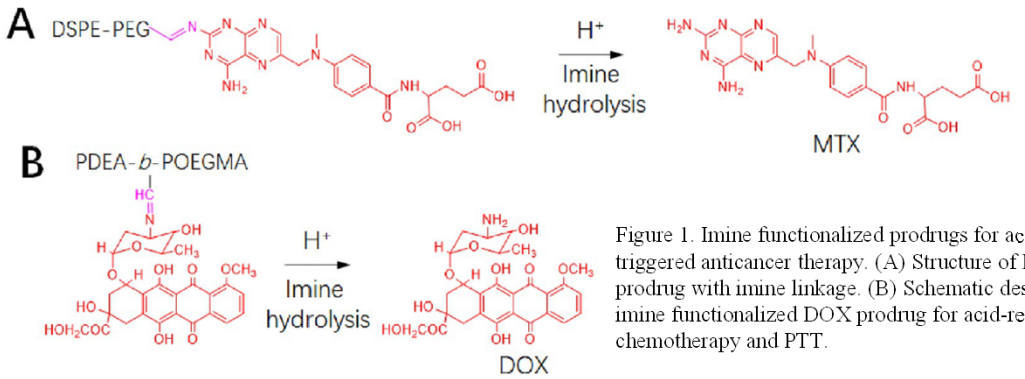

Figure 1. Imine functionalized prodrugs for acid-triggered anticancer therapy. (A) Structure of MTX prodrug with imine linkage. (B) Schematic design of imine functionalized DOX prodrug for acid-responsive chemotherapy and PTT.

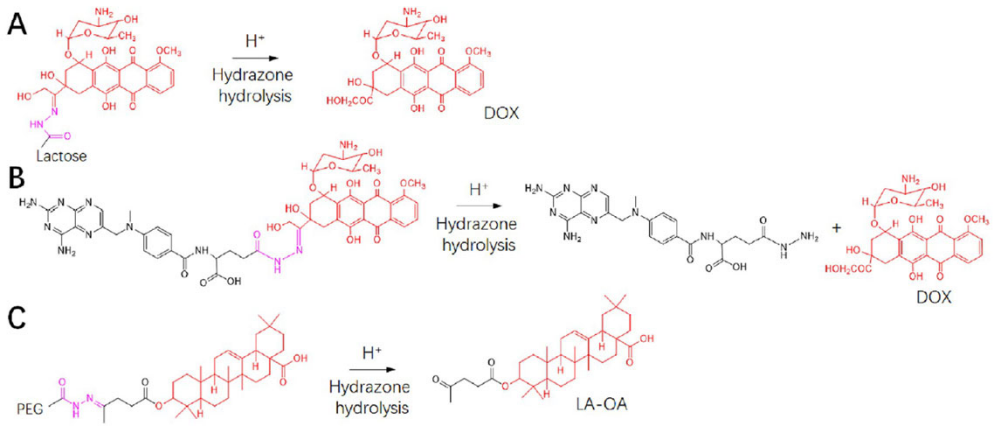

Figure 2. Prodrugs containing hydrazone linkage for acid-responsive activation. (A) Structure of DOX−lactose conjugated amphiphilic prodrug and working mechanism of the acid-triggered activation. (B) Hydrazone-based MTX−DOX prodrug and action mechanism of acid-responsive activation for cancer therapy. (C) Hydrazone functionalized PEG−OA macromolecule and schematic illustration of pH-induced OA activation

Ding 2022, Emerging strategies in stimuli-responsive prodrug nanosystems for cancer therapy

pH-Dependent Hydrogels Cross-Linked via Thia-Michael Addition Bonds

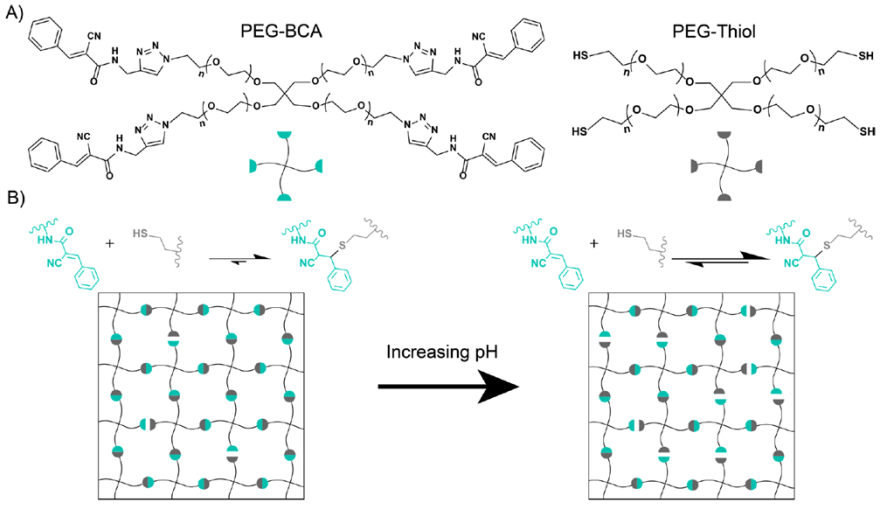

Figure 1. (A) Chemical structures for the two macromers used in this study. The conjugate acceptor is a four-arm benzylcyanoacetamide-functionalized poly(ethylene glycol) (PEG-BCA). The nucleophile is a four-arm PEG-thiol. (B) Schematic of the effect pH plays on the reaction. With increasing pH, both the forward and reverse rate constants increase, while the equilibrium constant decreases.

Dynamic covalent bonds

ABSTRACT: Hydrogels cross-linked with dynamic covalent bonds exhibit time-dependent properties, making them an advantageous platform for applications ranging from biomaterials to self-healing networks. However, the relationship between the cross-link exchange kinetics, material properties, and stability of these platforms is not fully understood, especially upon addition of external stimuli. In this work, pH was used as a handle to manipulate cross-link exchange kinetics and control the resulting hydrogel mechanics and stability in a physiologically relevant window. Poly(ethylene glycol)-based hydrogels were cross-linked with a reversible thia-Michael addition reaction in aqueous buffer between pH 3 and pH 7. The rate constants of bond exchange and equilibrium constants were determined for each pH value, and these data were correlated with the resulting mechanical profiles of the bulk hydrogels. With increasing pH, both the forward and the reverse rate constants increased, while the equilibrium constant decreased. These changes led to faster stress relaxation and less stiff hydrogels at more basic pH values. The elevated pH values also led to an increased mass loss and a faster rate of release of an encapsulated model bovine serum albumin fluorescent protein. The connection between the kinetics, mechanics, and molecular release profiles provides important insight into the structure–property relationships of dynamic covalent hydrogels, and this system offers a promising platform for controlled release between physiologically relevant pH values.

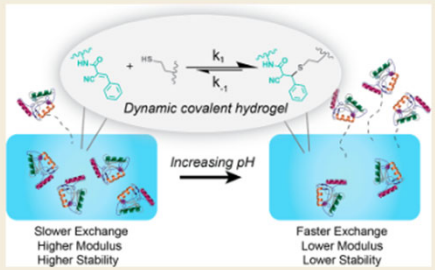

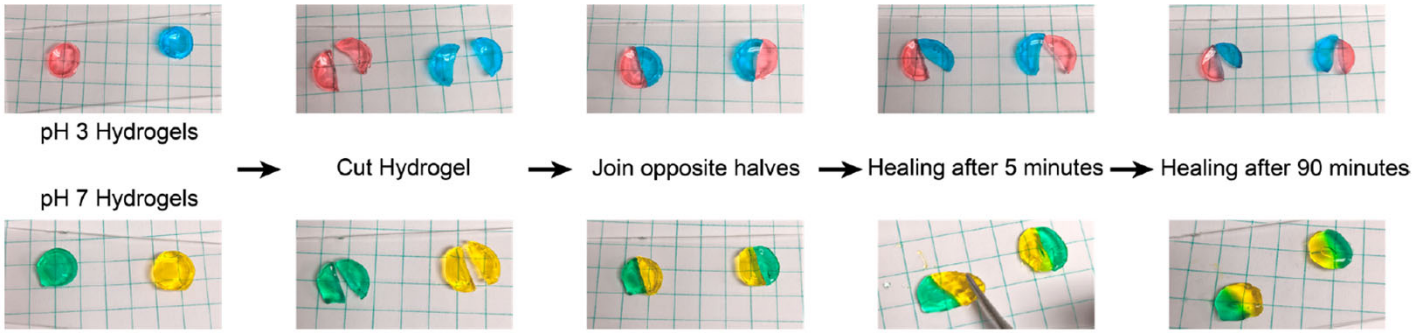

Figure 4. Self-healing ability for pH 3 (top) or pH 7 (bottom) hydrogels. Two hydrogels for each pH were dyed, cut, and the opposing halves were joined. After 5 min, the pH 7 hydrogels healed the defect, and after 90 min, the pH 3 hydrogels were still unhealed.

pH-dependent thiol reactivity

The deprotonated thiolate form is a much better nucleophile than the protonated thiol. As the pH increases and more thiolates are formed, the reactivity of the thiol (e.g., in Michael addition or thiol-disulfide exchange) increases.

FitzSimons 2025, Effect of pH on the properties of hydrogels cross-linked via dynamic thia-Michael addition bonds

pH-Tunable Hydrogels

Scheme 1. Schematic Illustration of the pH-Tunable Dynamic Properties of the Dynamic Hydrogel through Regulating the Binding Kinetics and Equilibrium Constants of the Reversible KC Reaction

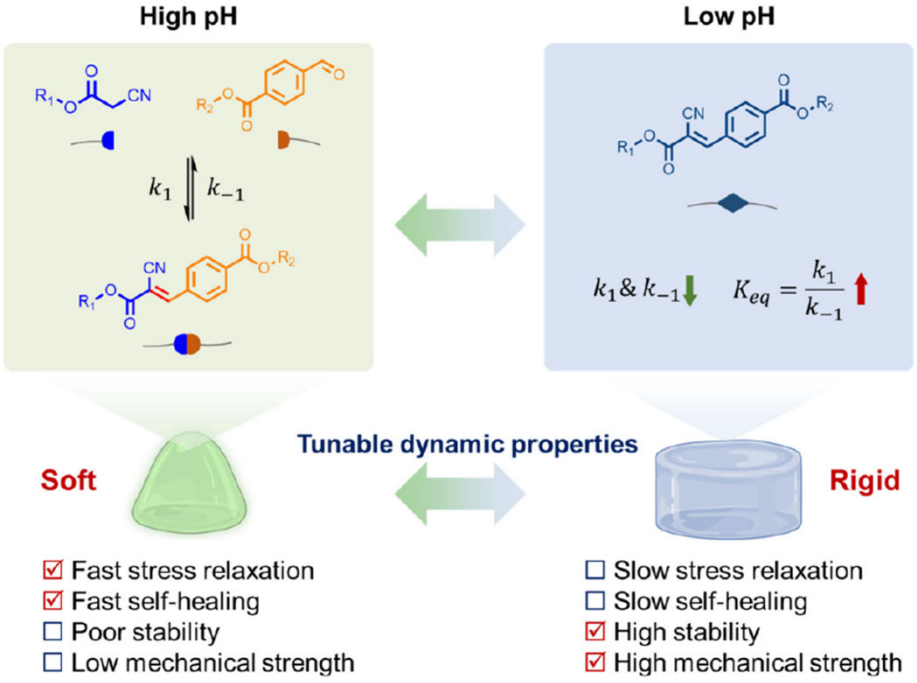

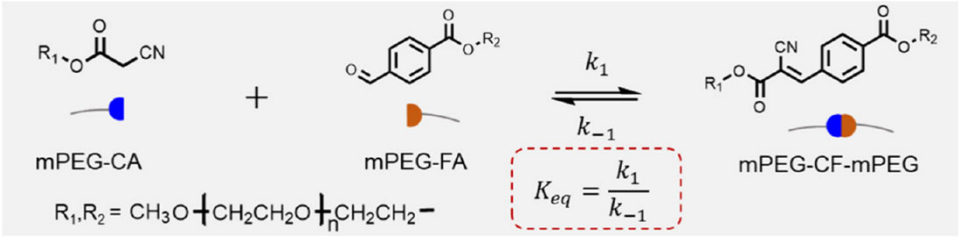

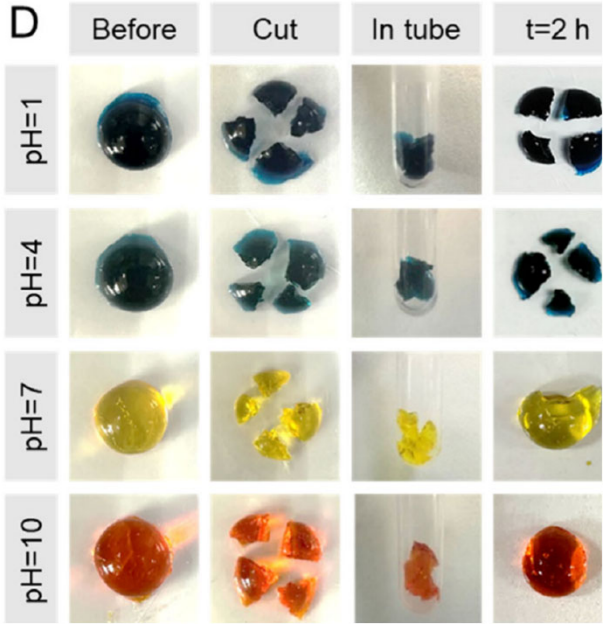

Yan 2025, Knoevenagel condensation reaction-empowered hydrogels with pH-tunable dynamic properties

Thermo- and pH-Responsive Antimicrobial Hydrogels

Semi-interpenetrating polymer networks (semi- IPNs) composed of poly(2-(dimethylamino)ethyl methacrylate) (PDMAEMA) and various concentrations of N-(2-hydroxyprop-yl)-3-trimethylammonium chitosan chloride (HTCC) (5, 10, and 25% w/w) were synthesized and evaluated as matrices for papain loading and sustained delivery.

Scheme 1. General Procedure for Synthesizing Hydrogels through the Quaternization of CH (a), Free-Radical Polymerization of DMAEMA and Crosslinking with BIS in the Presence of HTCC (b), and Incorporation of Papain (c)[a]

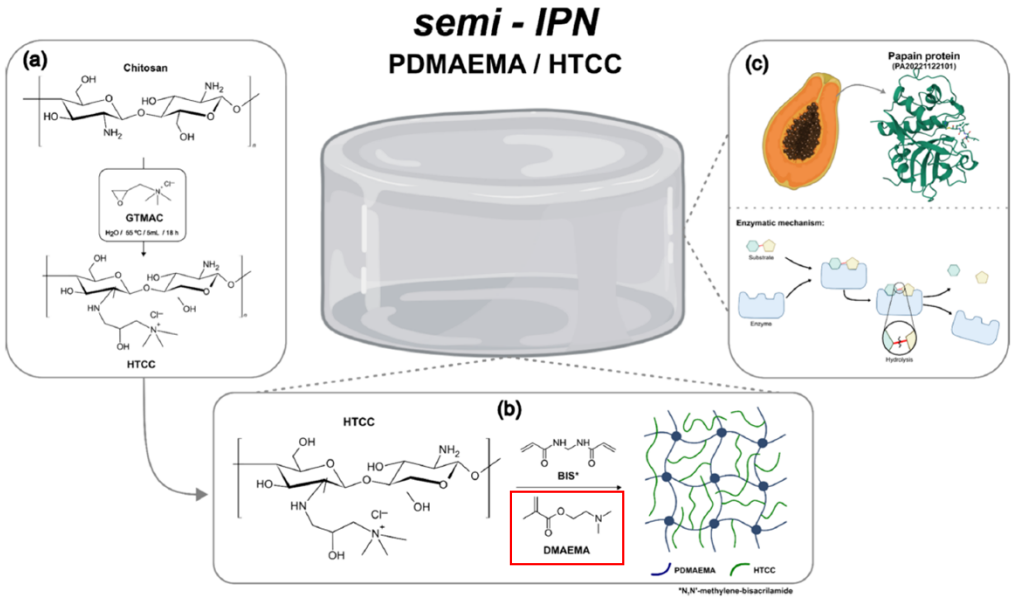

[a]This process results in the formation of semi-interpenetrating (semi-IPN) networks, where HTCC physically entangles with the PDMAEMA matrix. Created with BioRender (2025).

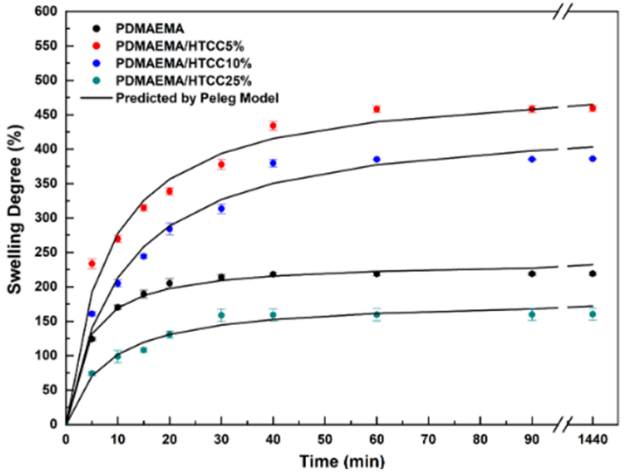

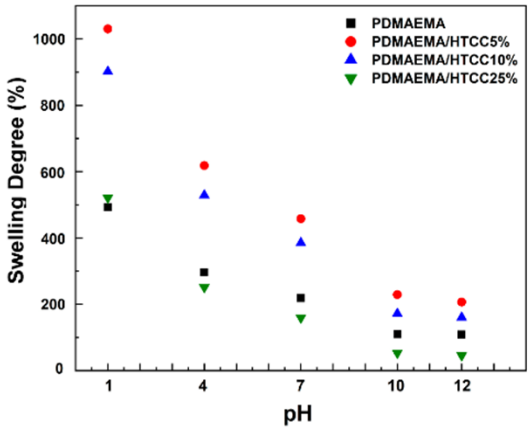

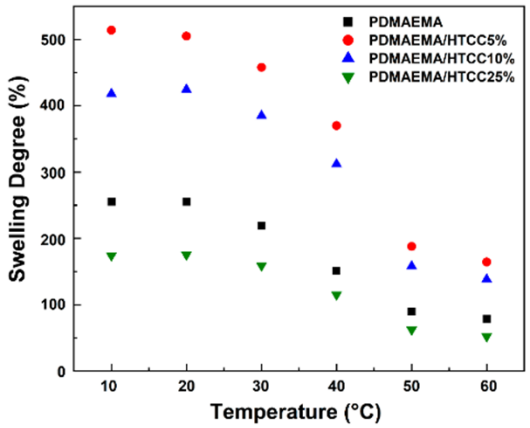

Ferreira 2026, Thermo- and pH-responsive antimicrobial hydrogels from poly(2-(dimethylamino)ethyl methacrylate) and cationic-modified chitosan

Light-Responsive Systems

Light-Sensitive Polymer and Hydrogels

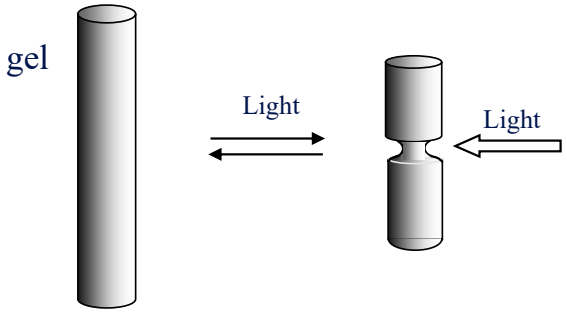

Figure 3. Effect of light irradiation on the structure of some photosensitive groups:
(A) trans-to-cis isomerization,
(B) ionization and
(C) zwitterion formation.

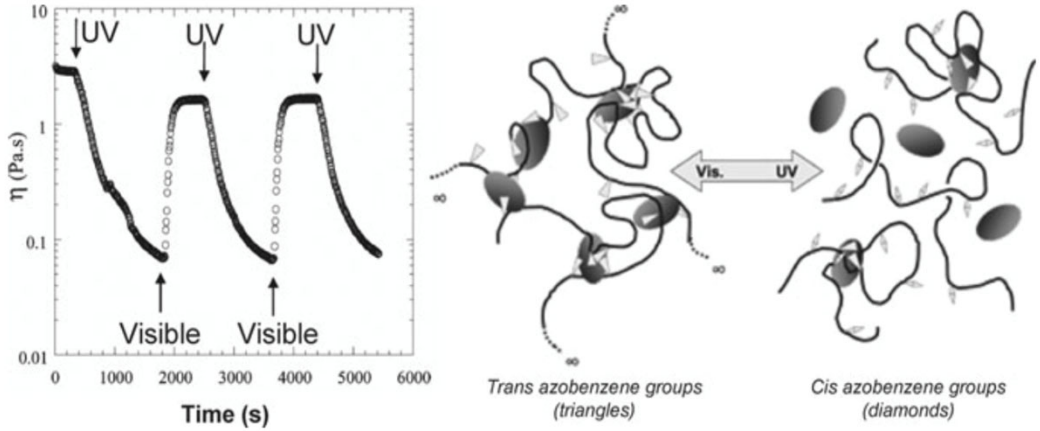

Figure 4. Variation of viscosity of 1 wt% poly(acrylic acid)-1,2-aminoundecilamido-4-phenylazobenzene micellar solution in the presence of bovine seroalbumin under exposure to light, alternating the wavelength between UV (365 nm) and visible (436 nm). Proteins mostly bound under exposure to visible light show significant release under UV exposure.

Alvarez-Lorenzo 2009, Light-sensitive intelligent drug delivery systems

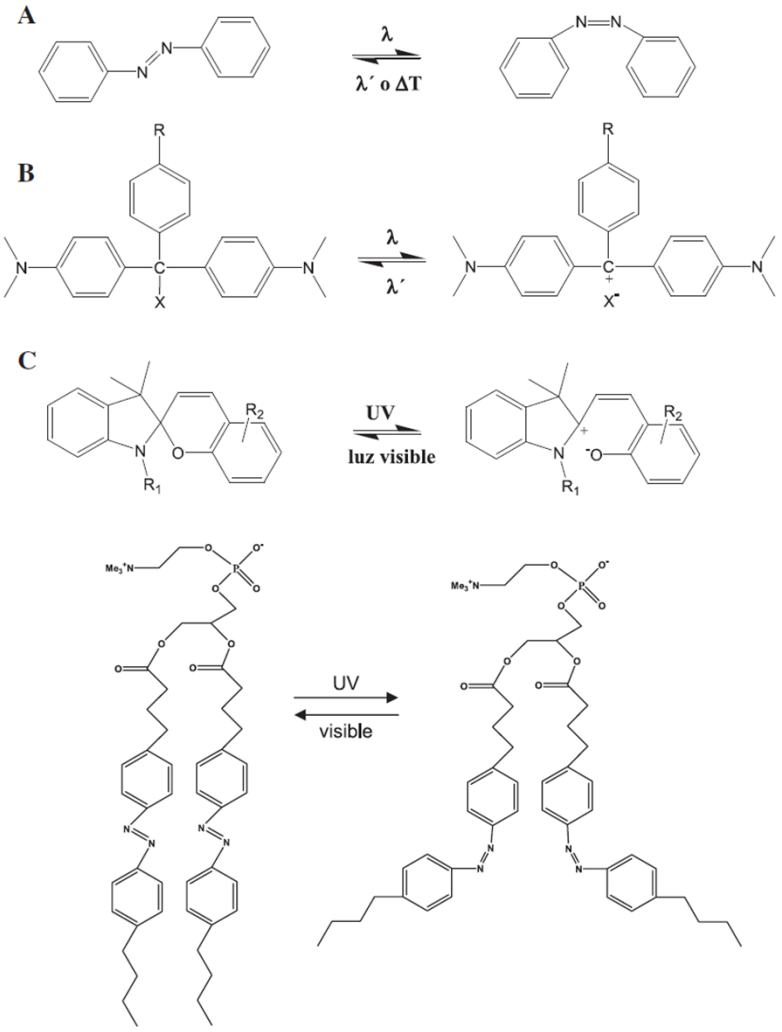

Figure 12. Structure of the photochromic lipid Bis-Azo PC.

Photosensitive (Photochromic) Systems

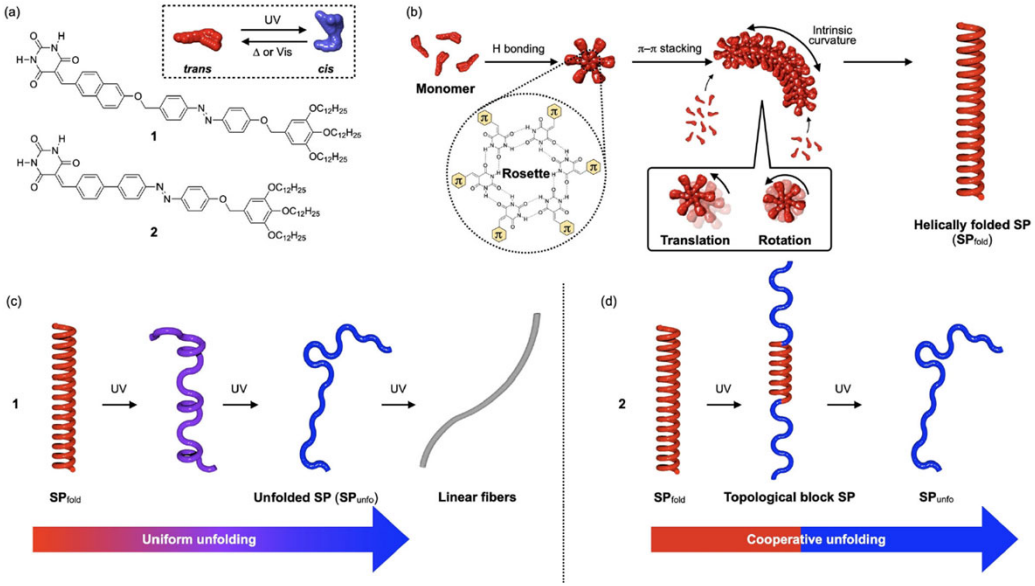

Figure 1. a) Molecular structures **1** and **2**. b) Formation mechanism of the SP_{fold}. c,d) Photo-induced unfolding processes of SP_{fold} composed of **1** (c) and **2** (d).

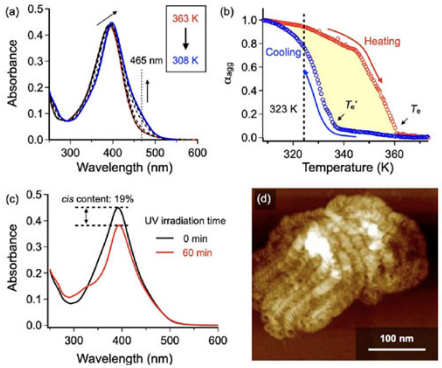

Figure 2. a) Temperature-dependent UV–Vis spectra of **2** ($c = 10$ μM) in MCH upon cooling from 373 to 308 K at a rate of 1.0 K min^{-1}. The cooling was ceased at 308 K to avoid precipitation upon further cooling to room temperature. b) Cooling (blue) and heating (red) curves of **2** ($c = 10$ μM) at a rate of 1.0 K min^{-1} obtained by plotting degree of aggregation α_{agg} (calculated from absorption change at 465 nm) as a function of temperature in MCH. c) UV–Vis absorption spectra of SP_{fold} of **2** in MCH before and after UV-light irradiation at 308 K for 60 min. d) AFM image of the SP_{fold} of **2** spin-coated onto highly oriented pyrolytic graphite (HOPG) after UV-light irradiation in MCH at 308 K for 60 min.

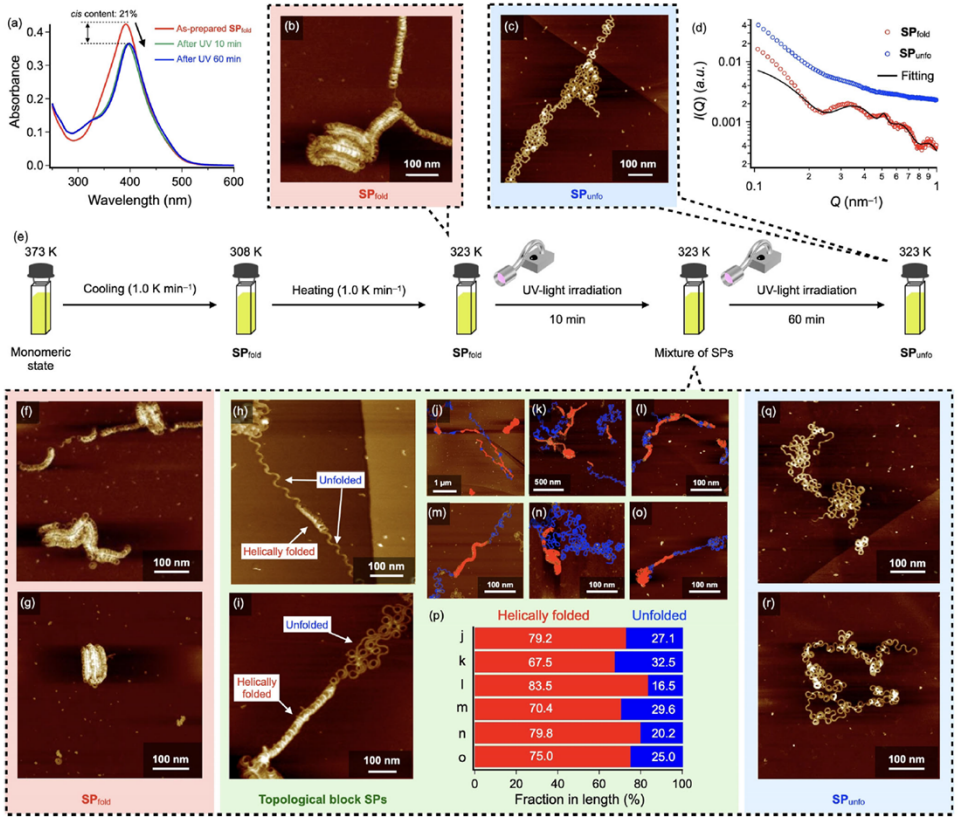

Figure 3. a) UV–Vis spectra of a MCH solution of **2** ($c = 10$ μM) during UV-light irradiation at 323 K. b,c) AFM images of SP_{fold} of **2** before UV-light irradiation (b) and SP_{unfo} of **2** after UV-light irradiation for 60 min at 323 K (c). d) Change of SAXS profiles of a SP_{fold} solution of **2** ($c = 50$ μM) upon UV-light irradiation at 323 K (from red to blue). The black line is a fit to the data using a core-multishell cylinder model. e) Schematic representation of procedure on photo-induced unfolding of SP_{fold} of **2** (f-o,q,r) AFM images of SP_{fold} (f,g), topological block SPs (h-o), and SP_{unfo} (q,r) found in a solution of **2** upon UV-light irradiation for 10 min at 323 K. In (j-o), helically folded and unfolded domains were colored with with red and blue, respectively. p) Fractions in length of helically folded and unfolded domains in the topological block SPs.

Tashiro 2021, Non-uniform photoinduced unfolding of supramolecular polymers leading to topological block nanofibers

Photo-Responsive Polymers

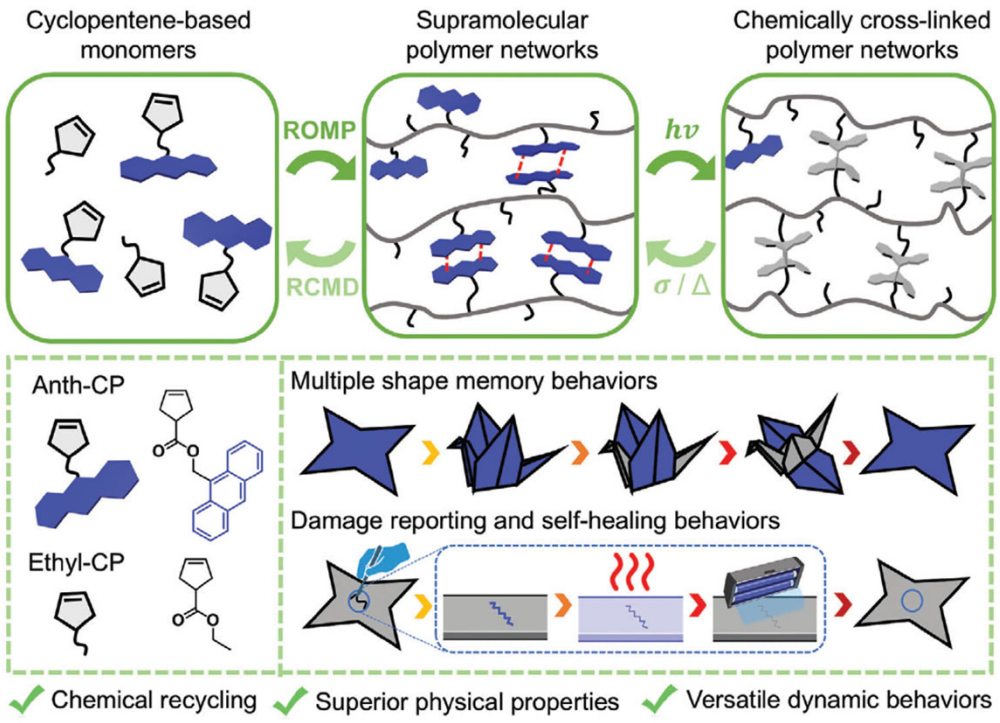

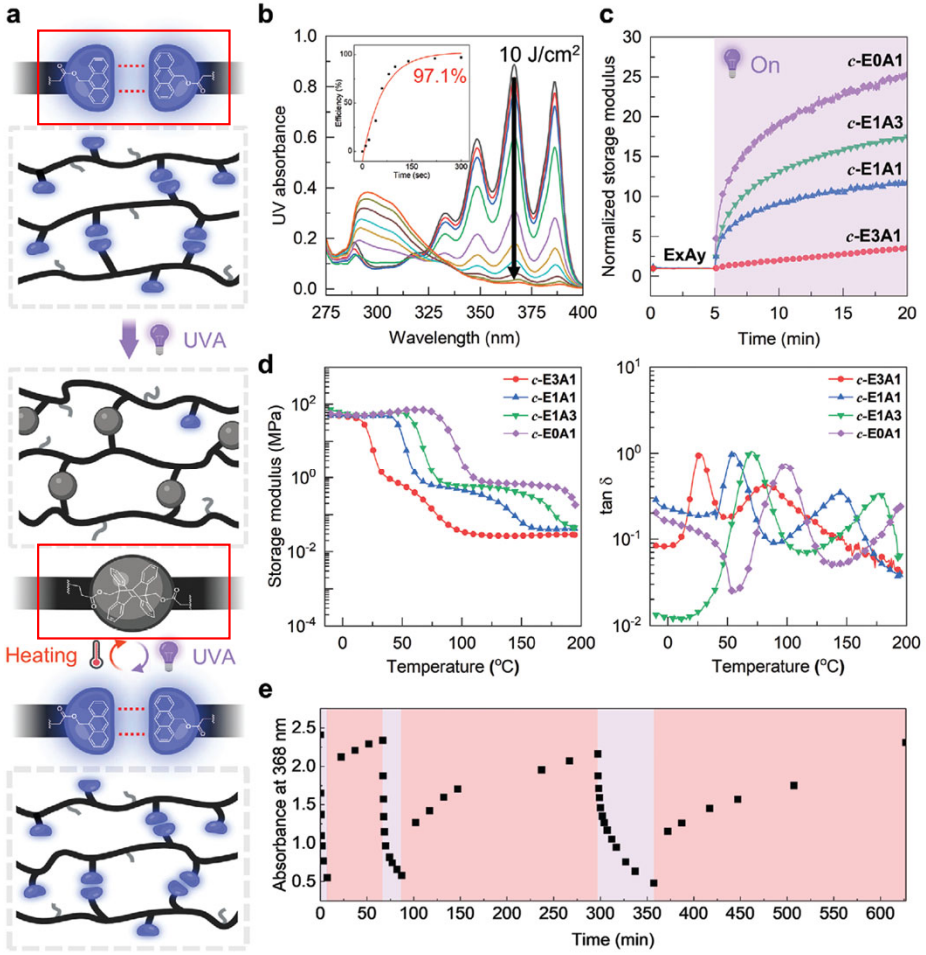

Lee 2025, High-performance dynamic photo-responsive polymers with superior closed-loop recyclability

Light-Sensitive Polymers

Metal-ligand complexes have attracted considerable interest for the design of stimuli-responsive metallosupramolecular polymers (MSPs), as the association and dynamicity of the interactions can be tuned by the nature of the metal salt and the ligand. Heat is arguably the most widely employed stimulus to manipulate MSPs in their solid state, for example, to achieve healing, debonding, or to program shape-memory polymers. Even though heat can be generated by the conversion of light, an oscillating magnetic field, or an electrical current, the level of control achievable is limited if the underlying process driving supramolecular (dis)assembly ultimately involves a temperature change.

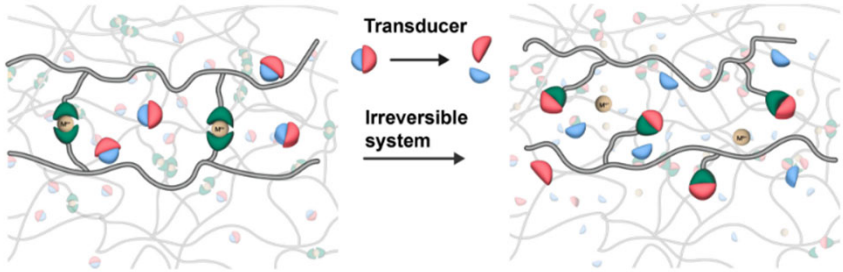

Figure 1. Schematic of the design and function of the metallosupramolecular polymer (MSP) systems investigated here. They consist of a photoacid generator (PAG) as a transducer and an MSP network. Upon light-triggered activation of the PAG and in situ acid production, the metal−ligand complexes that cross-link the polymer dissociate due to protonation of the ligand.

Bertossi 2025, Light-triggered switching of metallosupramolecular polymer systems

Metallosupramolecular polymers (MSPs).

- Poly(n-butyl acrylate) (PBA), a rubbery, amorphous polymer with subambient glass-transition temperature (T_g)
- 6-bis(1′-methyl-benzimidazolyl)pyridine (Mebip)-acrylate (MBA)
- 2-(4-methoxystyryl)-4,6-bis(trichloromethyl)-1,3,5-triazine (MBTT)

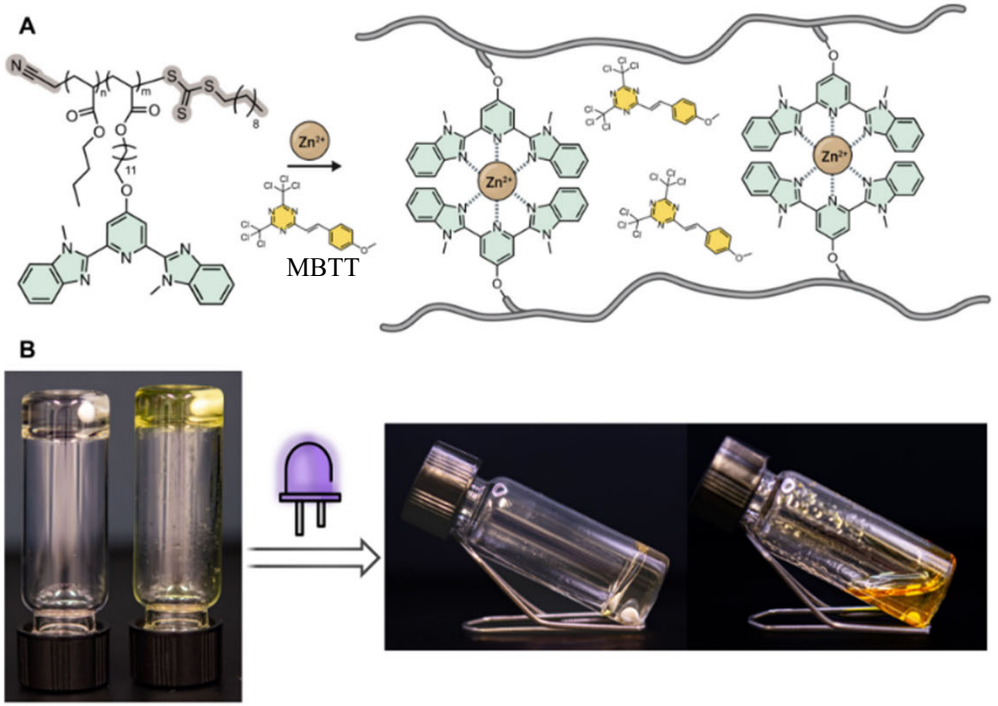

Figure 5. MSP gels were prepared using the copolymers of **PBA-*co*-MBA$_{xx}$-YY** following the addition of $Zn(OTf)_2$. (A) Chemical structure of **PBA-*co*-MBA$_{xx}$-YY** and an illustration of the components in **Zn(PBA-*co*-MBA$_5$-43)/MBTT** gels. (B) Pictures of as-prepared **Zn(PBA-*co*-MBA$_5$-43)** (colorless) and **Zn(PBA-*co*-MBA$_5$-43)/MBTT** (yellow) gels in chlorobenzene (left) and the solution obtained after irradiating the gels for 10 min with UV light (365 nm, 90 mW/cm^2). Both gels contain 12 wt % of the MSP and the MBTT gel additionally 1.2 wt % of MBTT ([MBTT]: [**Zn(MBA)$_2$**] = 1.5).

Irreversible Light-Sensitive systems

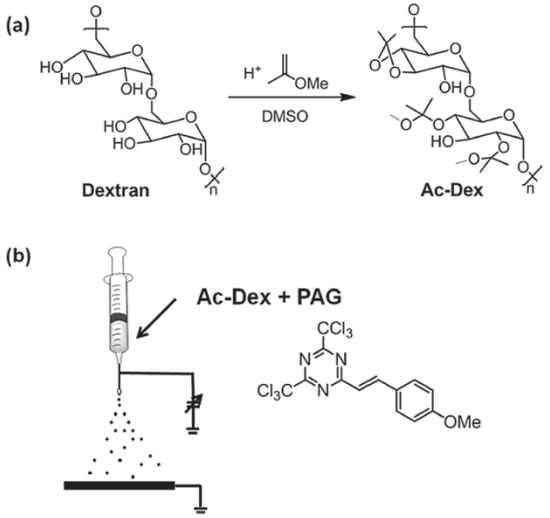

Figure 1. (a) Synthesis of acetal-modified dextran (Ac-Dex).[10] Illustration of (b) preparation of photodegradable Ac-Dex nanoparticles by electrospraying a solution of Ac-Dex (7.5 w/v%) and 2-(4-methoxystyryl)-4,6-bis(trichloromethyl)-1,3,5-triazine (3 wt% based on Ac-Dex) as a photoacid generator (PAG).

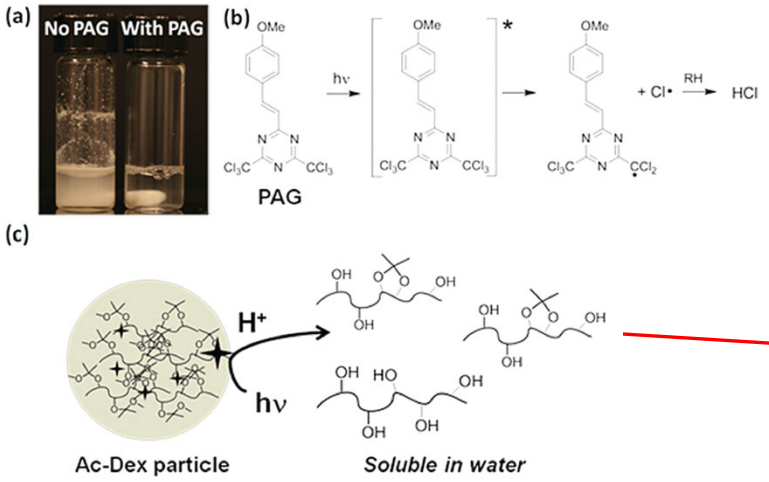

Figure 3. (a) Digital image after illuminating a PAG-free Ac-Dex particle suspension (left) and a PAG-encapsulating Ac-Dex particle suspension (right) with a UV-lamp (345 nm, 4 W) for 20 min (image contains stir bar). (b) Photoacid generation scheme by exciting 2-(4´-methoxystyryl)-4,6-bis(trichloromethyl)-1,3,5-triazine (PAG). (c) Schematic illustration of photoacid triggered deprotection of Ac-Dex and subsequent degradation of particles by dissolution.

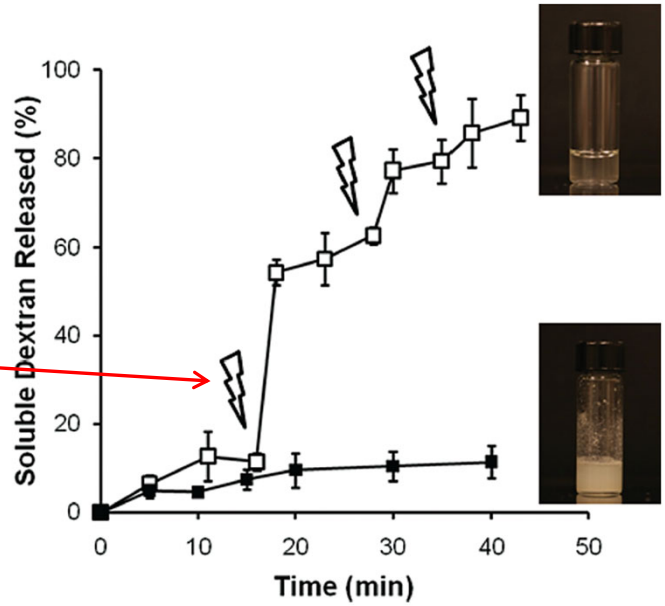

Figure 5. Photoacid triggered dissolution of dextran from Ac-Dex particles either in the dark (closed squares) or exposed to a UV light (open squares) in H_2O. The particle suspensions were illuminated using a UV-lamp (345 nm, 4 W) for 1 min at the points indicated by lightning bolt symbols. The digital images of both suspensions were taken after a reaction time of 45 min.

Acetylated Dextran is not soluble; the acetylation is sensitive to acidic conditions. Light induces a change in pH solubalizing the dextran.

Figure 3a displays a digital image of the particle suspensions after irradiation with a portable UV lamp (345 nm, 4 W) for 20 min. While the suspension of Ac-Dex particles without a photoacid generator (PAG) remained turbid, that of the Ac-Dex particles containing PAG turned clear after UV light exposure. As direct excitation of PAG leads to photocleavage of one of the carbon-chlorine bonds and subsequent hydrogen abstraction by the chlorine atom generates HCl (Figure 3b), UV illumination on Ac-Dex particles encapsulating PAG leads to the deprotection of the acetal groups by photo-generated HCl within the particles and concomitantly dissolution of deprotected dextran in water, as illustrated in Figure 3c.

Park 2013, Photoswitchable particles for on-demand degradation and triggered release

Light- or Electric-Sensitive Hydrogels

ABSTRACT: In our continuing pursuit to generate, understand, and control the morphology of organic nanofilaments formed by molecules with a bent molecular shape, we here report on two bent-core molecules specifically designed to permit a phase or morphology change upon exposure to an applied electric field or irradiation with UV light. To trigger a response to an applied electric field, conformationally rigid chiral (*S,S*)-2,3-difluorooctyloxy side chains were introduced, and to cause a response to UV light, an azobenzene core was incorporated into one of the arms of the rigid bent core. The phase behavior as well as structure and morphology of the formed phases and nanofilaments were analyzed using differential scanning calorimetry, cross-polarized optical microscopy, circular dichroism spectropolarimetry, scanning and transmission electron microscopy, UV−vis spectrophotometry, as well as X-ray diffraction experiments. Both bent-core molecules were characterized by the coexistence of two nanoscale morphologies, specifically helical nanofilaments (HNFs) and layered nanocylinders, prior to exposure to an external stimulus and independent of the cooling rate from the isotropic liquid. The application of an electric field triggers the disappearance of crystalline nanofilaments and instead leads to the formation of a tilted smectic liquid crystal phase for the material featuring chiral difluorinated side chains, whereas irradiation with UV light results in the disappearance of the nanocylinders and the sole formation of HNFs for the azobenzene-containing material. Combined results of this experimental study reveal that in addition to controlling the rate of cooling, applied electric fields and UV irradiation can be used to expand the toolkit for structural and morphological control of suitably designed bent-core molecule-based structures at the nanoscale.

KEYWORDS: *bent-core liquid crystal, B4 phase, morphology, chirality, electric field, UV irradiation*

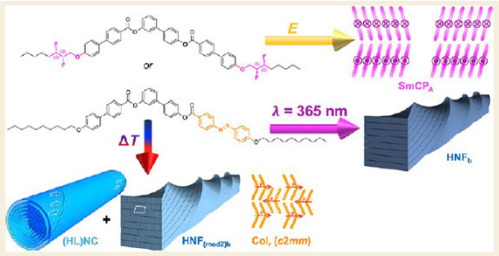

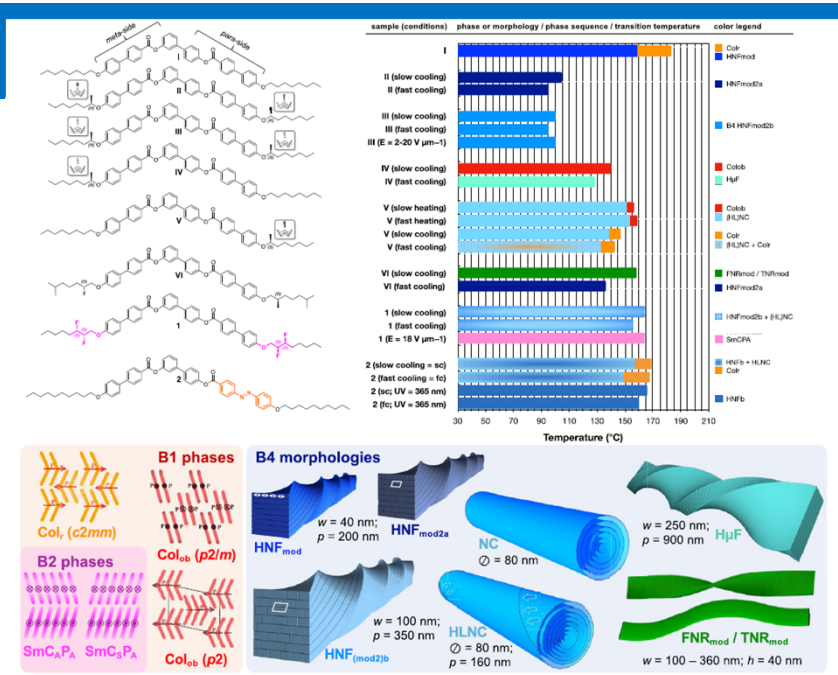

Figure 1. Comparison of the phase sequence, phase structure, B4 morphology, and phase transition temperatures depending on the chemical structure—position, branching points, as well as the number and configuration of chiral center(s) in the aliphatic side chains—of the parent compounds **I**–**VI**[20,22,23,25,26] (chiral center configurations only affect the handedness of the final filaments) with the here-investigated new compounds **1** and **2** (Arabic numerals). Models for the different B1 and B2 phase structures as well as the B4 morphologies are shown at the bottom. The color coding in the bar diagram and models is used throughout in the data plots for various B4 morphologies and B1 or B2 phases.

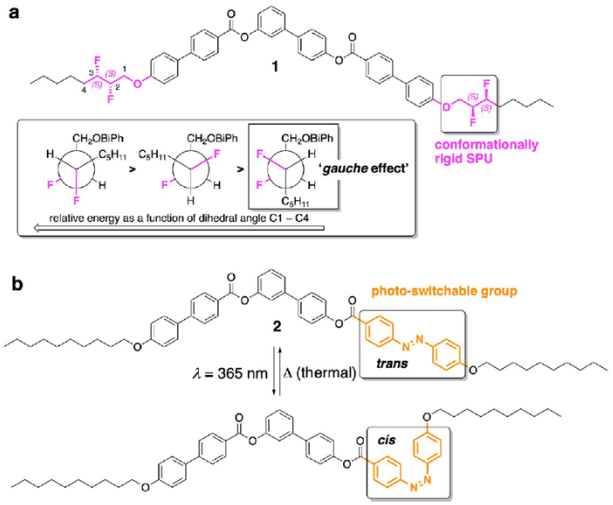

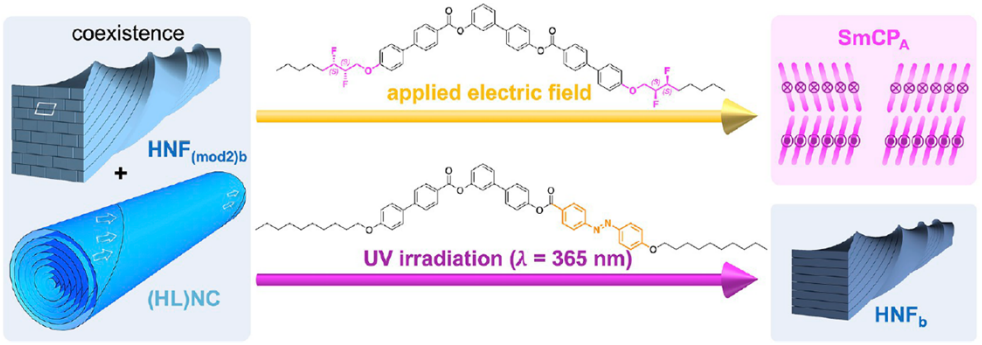

Figure 12. Graphical summary of the response of compounds **1** and **2** to applied external stimuli in addition to thermal control by adjusting the cooling rate from the isotropic liquid phase.

Sezgin 2023, Controlling the structure and morphology of organic nanofilaments using external stimuli

Light-Sensitive Hydrogels

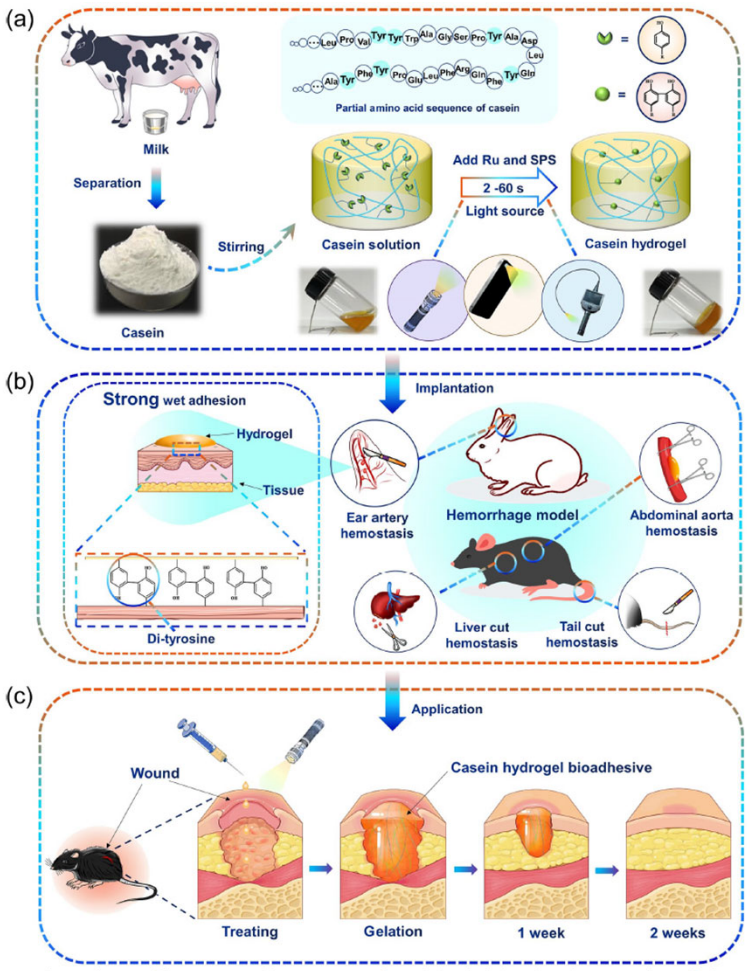

Fig. 1 Schematic illustration of the preparation and the reaction process of casein hydrogels which accelerates hemostasis and wound healing. (**a**) Casein from milk can be crosslinked through white-light activated di-tyrosine bonds formation initiated by Ru/SPS to form hydrogel; (**b**) Adhesion mechanism and hemostatic property of the casein hydrogel bioadhesive for massive arterial and visceral hemorrhage; (**c**) The process of wound healing with casein hydrogel bioadhesive treatment

Abstract. Background Post-traumatic massive hemorrhage demands immediately available first-aid supplies with reduced operation time and good surgical compliance. In-situ crosslinking gels that are flexibly adapting to the wound shape have a promising potential, but it is still hard to achieve fast gelation, on-demand adhesion, and wide feasibility at the same time. **Methods.** A white-light crosslinkable natural milk-derived casein hydrogel bioadhesive is presented for the first time. Benefiting from abundant tyrosine residues, casein hydrogel bioadhesive was synthesized by **forming di-tyrosine bonds under white light with a ruthenium-based catalyst**. We first optimized the concentration of proteins and initiators to achieve faster gelation and higher mechanical strength. Then, we examined the degradation, cytotoxicity, tissue adhesion, hemostasis, and wound healing ability of the casein hydrogels to study their potential to be used as bioadhesives. **Result.** Rapid gelation of casein hydrogel is initiated with an outdoor flashlight, a cellphone flashlight, or an endoscopy lamp, which facilitates its usage during first-aid and minimally invasive operations. The rapid gelation enables 3D printing of the casein hydrogel and excellent hemostasis even during liver hemorrhage due to section injury. The covalent binding between casein and tissue enables robust adhesion which can withstand more than 180 mmHg blood pressure. Moreover, the casein-based hydrogel can facilitate post-traumatic wound healing caused by trauma due to its biocompatibility. **Conclusion.** Casein-based bioadhesives developed in this study pave a way for broad and practical application in emergency wound management.

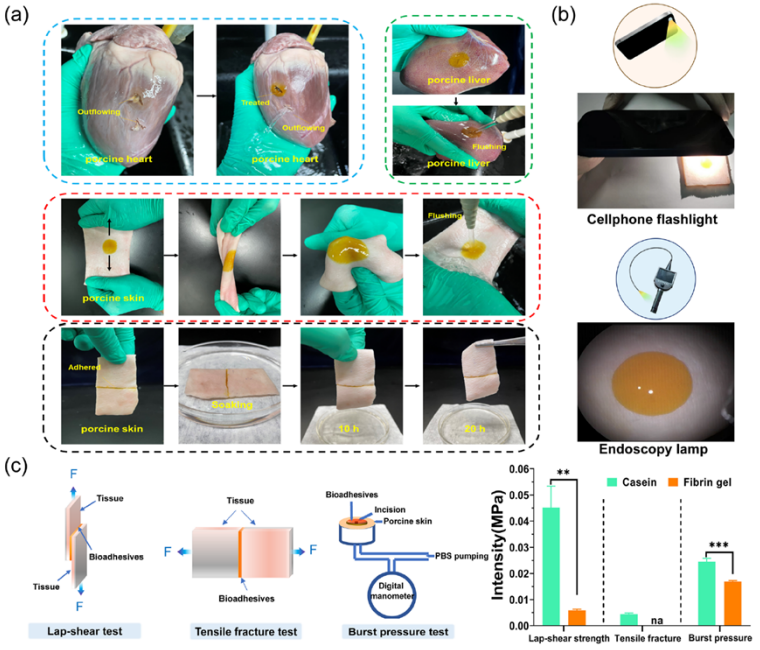

Fig. 3 (a) Quick adhesion of casein hydrogel bioadhesives gelling in-situ in porcine heart, liver and skin, (b) Casein hydrogel photographs under cellphone flight and endoscopy lamp, (c) The lap-shear testing, tensile fracture testing and testing of adhesion performance with casein hydrogel bioadhesive and fibrin gel gelling in-situ on porcine skin (n = 3).

Zhu 2023, White-light crosslinkable milk protein bioadhesive with ultrafast gelation for first-aid wound treatment

Light-Sensitive Drug Release

On-Demand Opioid Effect Reversal with an Injectable Light-Triggered Polymer-Naloxone Conjugate

Wei Zhang, Dali Wang, Claire A. Ostertag-Hill, Yiyuan Han, Xiyu Li, Yueqin Zheng, Berwyn Lu, and Daniel S. Kohane*

Cite This: *Nano Lett.* 2023, 23, 10545−10553 Read Online

ACCESS | Metrics & More | Article Recommendations | Supporting Information

ABSTRACT: Misuse of opioids can lead to a potential lethal overdose. Timely administration of naloxone is critical for survival. Here, we designed a polymer−naloxone conjugate that can provide on-demand phototriggered opioid reversal. Naloxone was attached to the polymer poly(lactic-*co*-glycolic acid) via a photocleavable coumarin linkage and formulated as injectable nanoparticles. In the absence of irradiation, the formulation did not release naloxone. Upon irradiation with blue (400 nm) light, the nanoparticles released free naloxone, reversing the effect of morphine in mice. Such triggered events could be performed days and weeks after the initial administration of the nanoparticles and could be performed repeatedly.

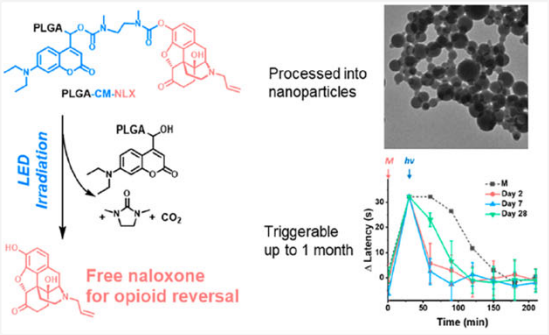

KEYWORDS: *Stimulus-responsive, photocleave, drug delivery, prodrug, naloxone, opioid*

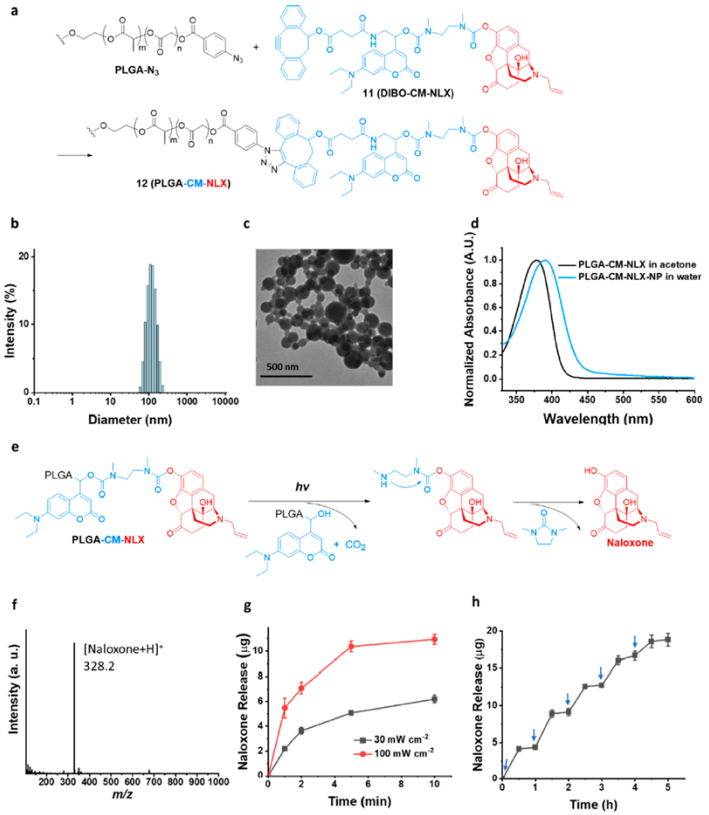

Figure 1. Synthesis, characterization, and in vitro photocleavage. (a) Synthesis of PLGA-CM-NLX. (b) DLS of the PLGA-CM-NLX nanoparticles. (c) TEM image of the PLGA-CM-NLX nanoparticles. (d) UV−vis spectra of the PLGA-CM-CM-NLX in acetone and nanoparticles in water. (e) Scheme of photocleavage releasing naloxone from PLGA-CM-NLX. (f) Mass spectrum of the cleaved naloxone. (g) Release of naloxone by photocleavage of NLX-NP (10 mg mL−1) over time with a 400 nm LED at different irradiances (n = 4, data are means ± SD). (h) Repeated phototriggered naloxone release from NLX-NP (arrows represent 2 min of irradiation with a 400 nm LED at 30 mW cm−2, n = 4, data are means ± SD).

Zhang 2023, On-demand opioid effect reversal with an injectable light-triggered polymer-naloxone conjugate

Polymers Responsive to Electric and Magnetic Fields

Electrifying Plastics

Flexible circuits by lamination

PLASTIC ELECTRONICS

Researchers at Bell Laboratories and the University of Texas at Austin, led by John A. Rogers, have developed a new method to fabricate plastic circuits with organic semiconductors using 'soft', conformable electrical contacts and a lamination process [*PNAS* (2002) 99, 10252-10256]. The printed circuits have excellent flexibility and are able to withstand stirred, soapy water for long periods. Low cost, flexible, durable, and lightweight plastic circuits have great potential for many devices, including electronic paper, wearable sensors, and smart cards.

The key aspect of the approach is the fabrication of different parts of the circuit on different substrates. The two substrates are then bonded together. "A thin elastomeric substrate supports the electrodes and interconnections. Laminating this substrate against another plastic substrate that supports the gate, dielectric, and semiconductor levels establishes effective electrical contacts and completes the circuits," explain the authors. The electrical properties of these laminated transistors are similar to other organic semiconductor devices produced using more standard techniques.

The laminated circuits have two advantages over other fabrication technologies. The embedded circuits have much better mechanical flexibility than circuits deposited in the usual way on the surfaces of substrates. The flexibility arises because the circuit lies near the neutral mechanical plane (0% strain) at the center of the device. The embedded circuits are also naturally encapsulated, providing protection from the environment. Negligible changes in the transistor properties after 15 minutes in stirred, soapy water were observed.

The researchers hope that their work will provide a general method for providing non-invasive electrical contacts to fragile or ultra-thin organic materials, and will be useful for measuring charge transport in these systems.

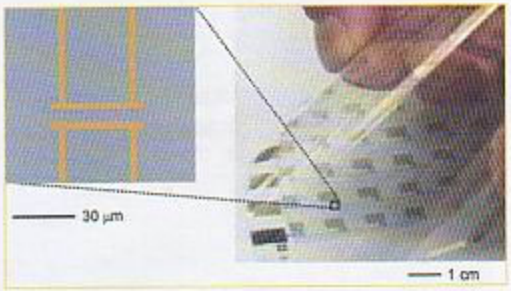

A laminated circuit. Inset shows source/drain electrodes (gold) laminated against a pentacene layer (blue). (Courtesy of PNAS.)

news of the week

ELECTRIFYING PLASTICS

Nobel Prize in Chemistry honors three who pioneered a new materials field

Alan G. MacDiarmid missed the fateful phone call from Stockholm that many scientists can't help dreaming about. But he learned the momentous news soon enough from a colleague who had seen it on the Internet: MacDiarmid, 73, a chemistry professor at the University of Pennsylvania, had won the 2000 Nobel Prize in Chemistry along with Alan J. Heeger, 64, a professor of physics and materials science at the University of California, Santa Barbara, and Hideki Shirakawa, 64, a chemistry professor who retired earlier this year from the University of Tsukuba, in Japan.

The three were honored last week by the Royal Swedish Academy of Sciences, which administers the Nobel Prizes, for opening and developing the important new field of electrically conductive polymers. They will share the monetary award of more than $900,000.

Before Shirakawa, MacDiarmid, and Heeger made their seminal discovery in 1977, the idea that a plastic could conduct electricity as well as a metal would have seemed ludicrous. Organic polymers were—and for the most part, still are—known as insulators. But the three researchers found that by doping a known conjugated polymer (polyacetylene), they could make it conduct a charge with unprecedented ease.

Since then, scientists have synthesized a number of other conducting polymers as well as a host of related polymers that have semiconducting and light-emitting properties. All applications that involve the movement of charge through a polymer "owe some debt" to the 1977 discovery, says organic chemist Howard E. Katz of Lucent Technologies' Bell Laboratories in Murray Hill, N.J.

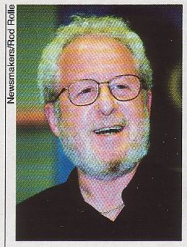
Newsmakers/Reuters/Rick Rickle

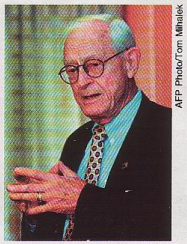
AFP Photo/Tom Mihalek

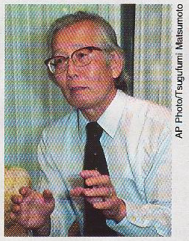
AP Photo/Tsugufumi Matsumoto

Clockwise from above: Heeger, MacDiarmid, and Shirakawa

That discovery, he adds, led to new types of organic materials that combine the processing advantages and mechanical properties of plastics with the electronic and optical properties of metals and inorganic semiconductors. And these materials, in turn, led to the development of organic and polymeric light-emitting diodes, field-effect transistors, and photovoltaic devices.

Conducting polymers have yet to take the marketplace by storm, but they are beginning to have a commercial impact, says Arthur J. Epstein, a professor of physics and chemistry at Ohio State University.

For example, conducting polymers are being used as antistatic coatings and corrosion inhibitors, and one even plays "a major role as a radar-absorbing screen coating in stealth bombers," according to chemistry professor Andrew B. Holmes, who directs the Melville Laboratory for Polymer Synthesis at the University of Cambridge. He tells C&EN that one conductive polymer is making its way into mobile phone displays based on a light-emitting polymer.

Other applications of conducting polymers that could emerge in coming years include lightweight batteries for cars, electromagnetic shielding, ultrathin computer monitors and TV sets, artificial nerves, and sensors, according to Daryle H. Busch, president of the American Chemical Society.

As often happens in science, the 1977 discovery began with an accident. In the early 1970s, a graduate student in Shirakawa's lab at Tokyo Institute of Technology prepared a new form of polyacetylene after he mistakenly added 1,000 times more catalyst to the reaction mixture than the recipe called for. The film of all-*trans*-polyacetylene produced in the reaction looked like aluminum foil, not the dark material the chemists had been expecting.

MacDiarmid later met Shirakawa in Tokyo and heard about his discovery. MacDiarmid invited the Japanese chemist to Penn to collaborate with him and Heeger, who then was also on the Penn faculty, on further studies of this metallic-looking polymer.

During that visit at Penn in 1977, the three researchers tried doping the polyacetylene with iodine. Not only did the silvery polymer film become golden, but its conductivity increased more than a billionfold—to 10^5 siemens per meter. By comparison, DuPont's Teflon has a conductivity of 10^{-16} S m^{-1} and silver and copper have conductivities of 10^8 S m^{-1}.

On exposure to iodine, polyacetylene is oxidatively doped: The polymer chain loses an electron, leaving a hole or positive charge, while the pilfered electron resides on the counterion I_3^-. When such a hole is filled by an electron jumping in from a neighboring position, a new hole

Some conjugated polymers can be made conductive

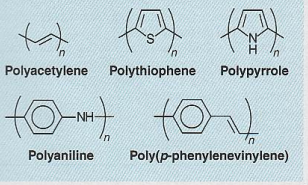

Organic Light-Emitting Diode

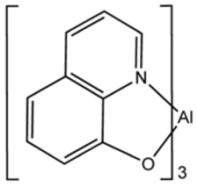

Tris(8-hydroxyquinolinato) aluminium

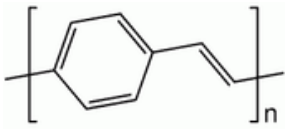

Poly(*p*-phenylene vinylene)

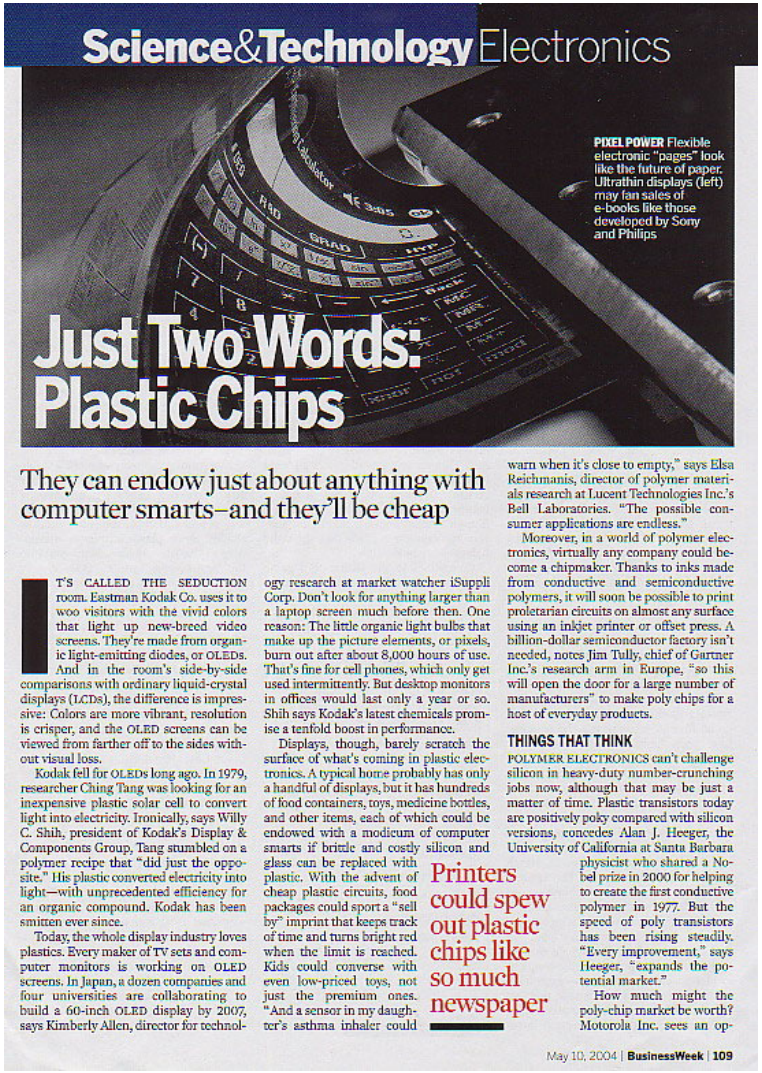

Science&Technology Electronics

PIXEL POWER Flexible electronic "pages" look like the future of paper. Ultrathin displays (left) may fan sales of e-books like those developed by Sony and Philips

Just Two Words: Plastic Chips

They can endow just about anything with computer smarts—and they'll be cheap

IT'S CALLED THE SEDUCTION room. Eastman Kodak Co. uses it to woo visitors with the vivid colors that light up new-breed video screens. They're made from organic light-emitting diodes, or OLEDs. And in the room's side-by-side comparisons with ordinary liquid-crystal displays (LCDs), the difference is impressive: Colors are more vibrant, resolution is crisper, and the OLED screens can be viewed from farther off to the sides without visual loss.

Kodak fell for OLEDs long ago. In 1979, researcher Ching Tang was looking for an inexpensive plastic solar cell to convert light into electricity. Ironically, says Willy C. Shih, president of Kodak's Display & Components Group, Tang stumbled on a polymer recipe that "did just the opposite." His plastic converted electricity into light—with unprecedented efficiency for an organic compound. Kodak has been smitten ever since.

Today, the whole display industry loves plastics. Every maker of TV sets and computer monitors is working on OLED screens. In Japan, a dozen companies and four universities are collaborating to build a 60-inch OLED display by 2007, says Kimberly Allen, director for technology research at market watcher iSuppli Corp. Don't look for anything larger than a laptop screen much before then. One reason: The little organic light bulbs that make up the picture elements, or pixels, burn out after about 8,000 hours of use. That's fine for cell phones, which only get used intermittently. But desktop monitors in offices would last only a year or so. Shih says Kodak's latest chemicals promise a tenfold boost in performance.

Displays, though, barely scratch the surface of what's coming in plastic electronics. A typical home probably has only a handful of displays, but it has hundreds of food containers, toys, medicine bottles, and other items, each of which could be endowed with a modicum of computer smarts if brittle and costly silicon and glass can be replaced with plastic. With the advent of cheap plastic circuits, food packages could sport a "sell by" imprint that keeps track of time and turns bright red when the limit is reached. Kids could converse with even low-priced toys, not just the premium ones. "And a sensor in my daughter's asthma inhaler could warn when it's close to empty," says Elsa Reichmanis, director of polymer materials research at Lucent Technologies Inc.'s Bell Laboratories. "The possible consumer applications are endless."

Moreover, in a world of polymer electronics, virtually any company could become a chipmaker. Thanks to inks made from conductive and semiconductive polymers, it will soon be possible to print proletarian circuits on almost any surface using an inkjet printer or offset press. A billion-dollar semiconductor factory isn't needed, notes Jim Tully, chief of Gartner Inc.'s research arm in Europe, "so this will open the door for a large number of manufacturers" to make poly chips for a host of everyday products.

THINGS THAT THINK

POLYMER ELECTRONICS can't challenge silicon in heavy-duty number-crunching jobs now, although that may be just a matter of time. Plastic transistors today are positively poky compared with silicon versions, concedes Alan J. Heeger, the University of California at Santa Barbara physicist who shared a Nobel prize in 2000 for helping to create the first conductive polymer in 1977. But the speed of poly transistors has been rising steadily. "Every improvement," says Heeger, "expands the potential market."

How much might the poly-chip market be worth? Motorola Inc. sees an op-

> Printers could spew out plastic chips like so much newspaper

Graphene

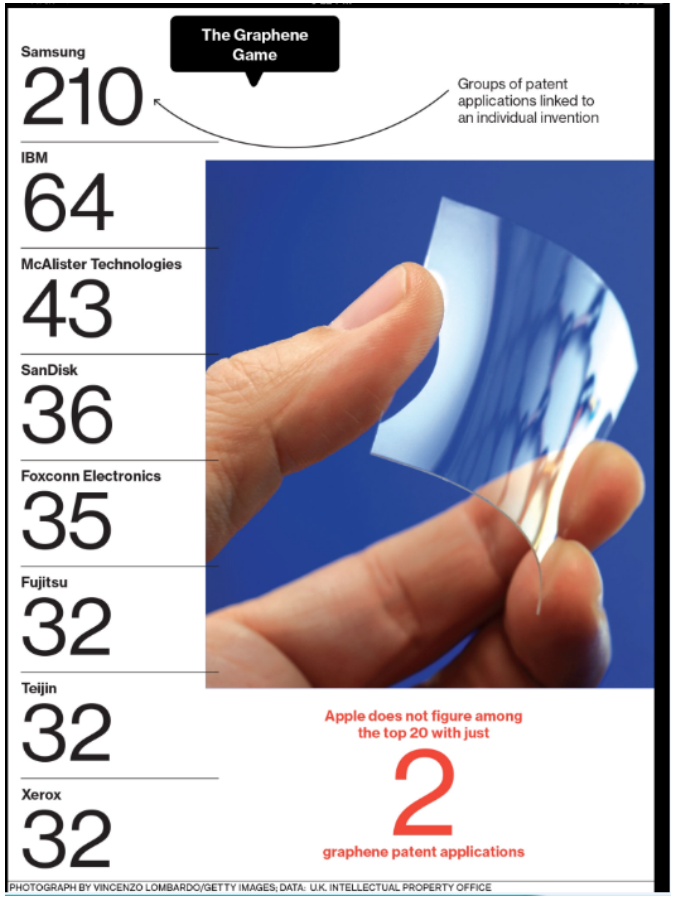

Electrochromic Polymers

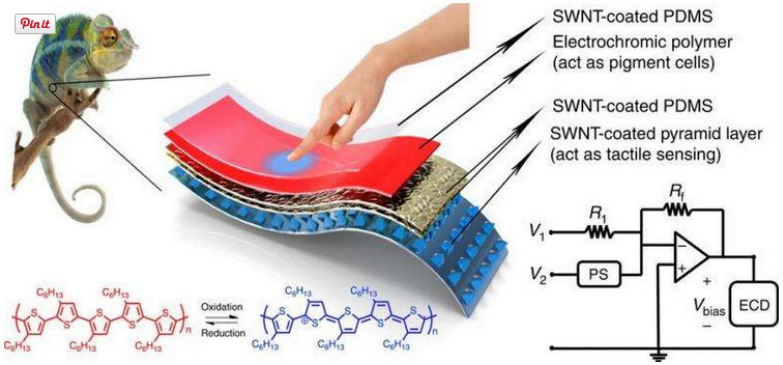

http://phys.org/news/2015-09-chameleon-inspired-stretchable-e-skin.html

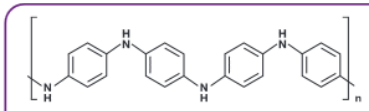	Leucoemeraldine	Colourless Fully reducing Insulating
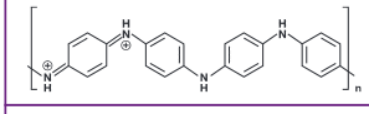	Emeraldine salt	Green Partially oxidised Conducting
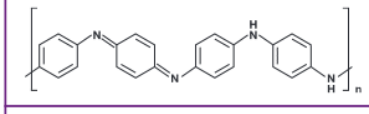	Emeraldine base	Blue Partially oxidised Insulating
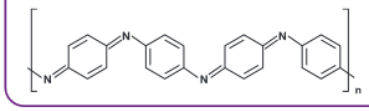	Pernigraniline	Purple Fully oxidised Insulating

http://www.rsc.org/images/RSCelectro_tcm18-159224.pdf

'Green' Paper- Thin, Flexible Electronics

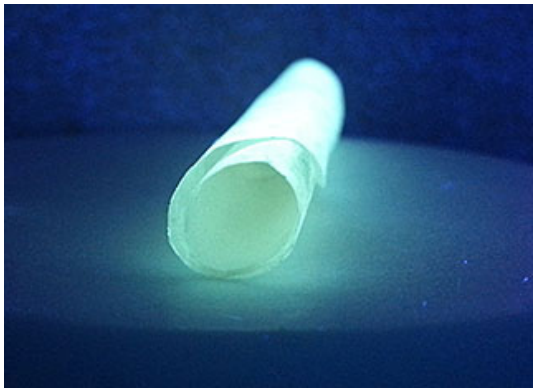

The researchers developed a thin, clear nanocellulose paper made out of wood flour and infusaed it with biocompatible quantum dots—tiny, semiconducting crystals—made out of zinc and selenaium. The paper glowed at room temperature and could be rolled and unrolled without cracking.

http://www.rdmag.com/news/2015/05/toward-green-paper-thin-flexible-electronics?et_cid=4581167&et_rid=54728378&location=top

New printing process makes three-dimensional objects glow

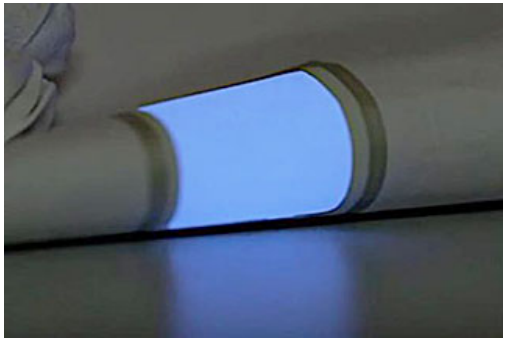

Conventional electroluminescent (EL) foils can be bent up to a certain degree only and can be applied easily onto flat surfaces. The new process developed by Karlsruhe Institute of Technology (KIT) in cooperation with the company of Franz Binder GmbH & Co. now allows for the direct printing of electroluminescent layers onto three-dimensional components. Such EL components might be used to enhance safety in buildings in case of power failures. Other potential applications are displays and watches or the creative design of rooms. The development project was funded with EUR 125,000 by the Deutsche Bundesstiftung Umwelt (German Foundation for the Environment).

http://www.rdmag.com/news/2015/05/new-printing-process-makes-three-dimensional-objects-glow?et_cid=4581167&et_rid=54728378&type=cta

Metal Rubber: Layer by Layer (LBL) Coating

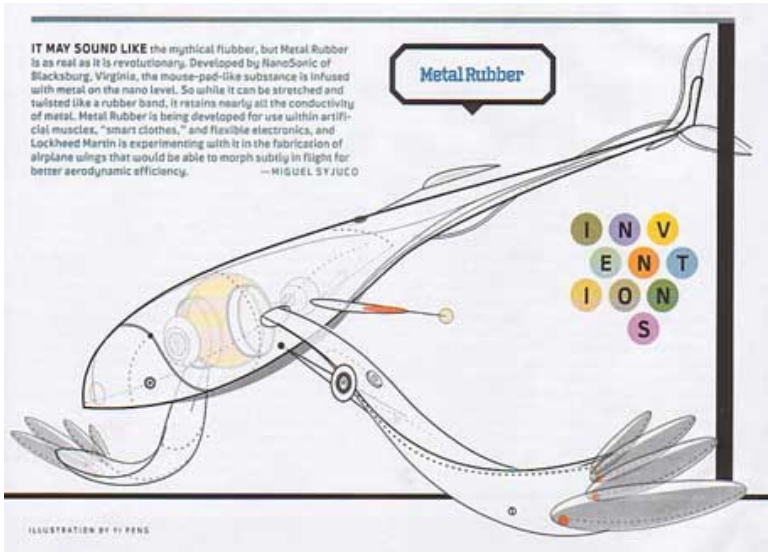

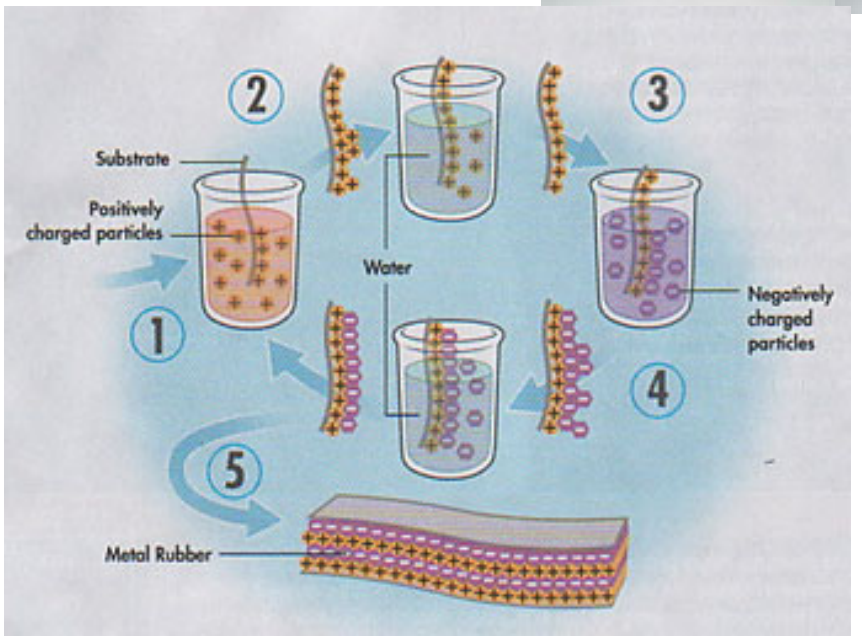

MAKING METAL RUBBER FROM SCRATCH
Dip charged substrate into container of positively charged water-based solution (1). Rinse substrate in water to remove unbound particles (2). Dip substrate into negatively charged solution (3). Rinse and repeat (4, 5).

NanoSonic's Metal Rubber™ is a highly electrically conductive and highly flexible elastomer. It can be mechanically strained to greater than 1000 percent of its original dimensions while remaining electrically conductive. As Metal Rubber can carry data and electrical power and is environmentally rugged, it opens up a new world of applications requiring robust, flexible and stretchable electrical conductors in the aerospace/defense, electronics and bioengineering markets.

http://www.nanosonic.com/80/4/metalrubber.html
http://videos.howstuffworks.com/sciencentral/2938-metal-rubber-video.htm

Popular Science. August 2004. p. 36.

Conductive Polymers

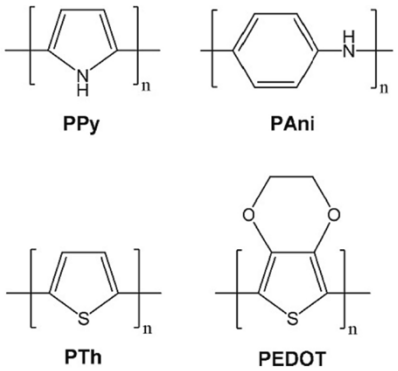

Fig. 2. Structures of most widely investigated CPs in biomedical applications.

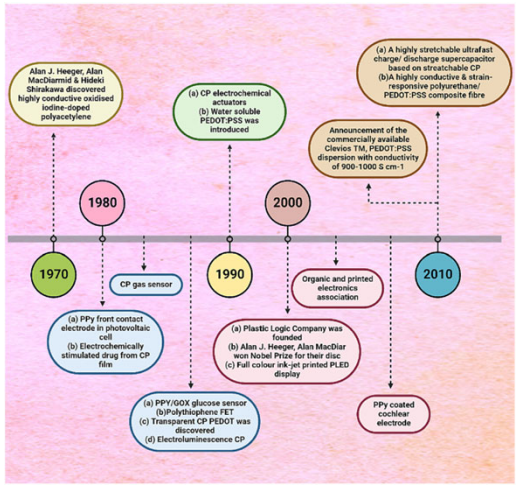

Fig. 3. A timeline detailing the evolution of CPs and their applications over past decades.

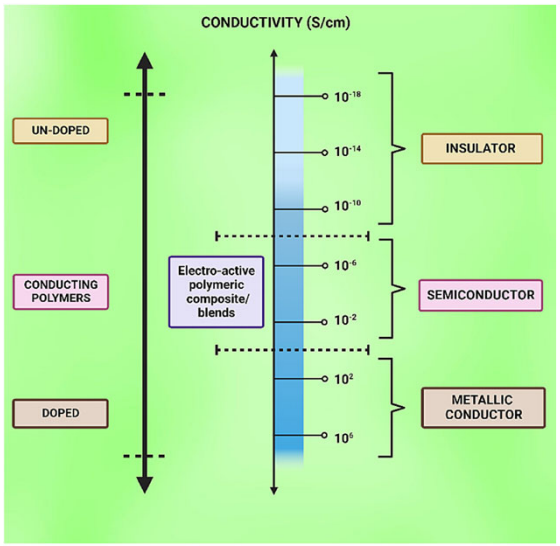

Fig. 1. Range of conductivity for CPs, CPs composites, and blends.

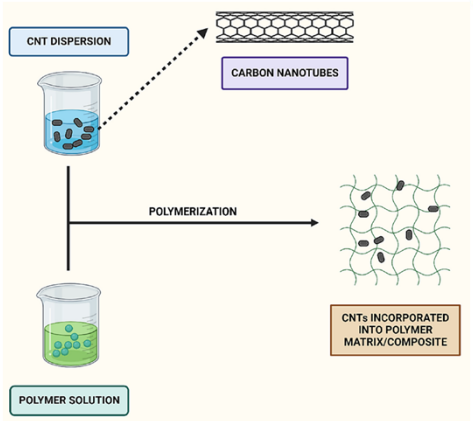

Fig. 7. Overview of in-situ polymerization method for the synthesis of CPs composites.

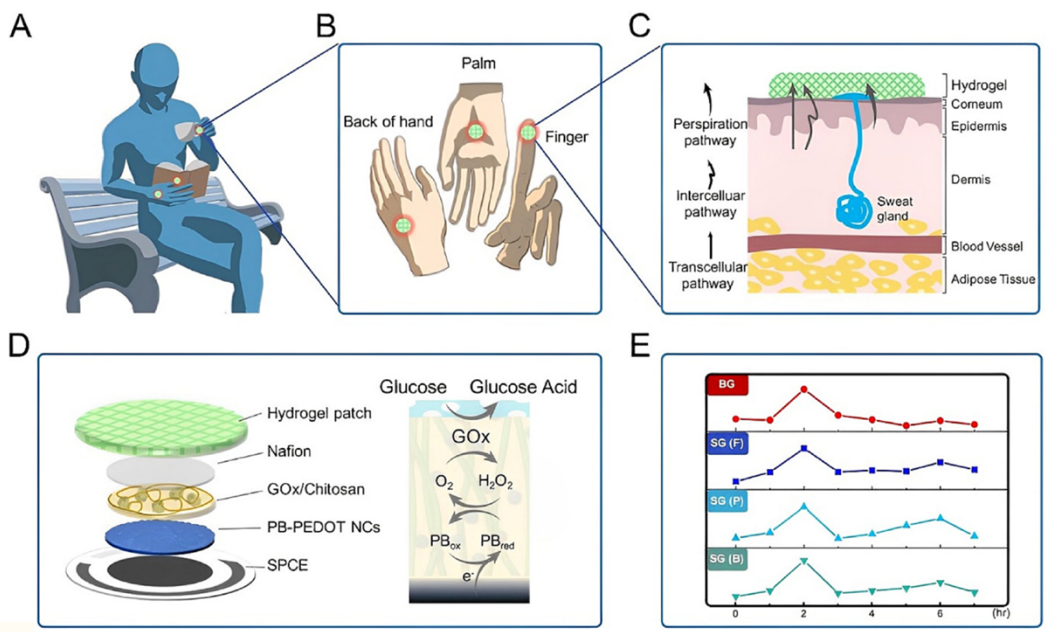

Fig. 11. Schematic representation of the design, mechanism involved, and the usage of natural sweat as a sample for glucose sensor. (A) The hydrogel patch can be placed at different positions on the body for the sampling of sweat during resting time. (B) The positions to place the patch on the hand for sweat collection are the palm, back of the hand, and fingers. (C) The favourable glucose sweat sampling pathways for natural sweat hydrogel patches. (D) Schematic representation of the multiple layers in PB-PEDOT NC enzymatic electrode of the sweat glucose monitoring device and the working mechanism GOx with the PB probe. (E) The sweat glucose monitoring device can identify sweat glucose levels without externally applied stimulation or high-intensity physical activity at various locations such as the palm, back of the hand, and finger.

Raj 2023, Conductive polymers and composites-based systems

Conductive Hydrogels

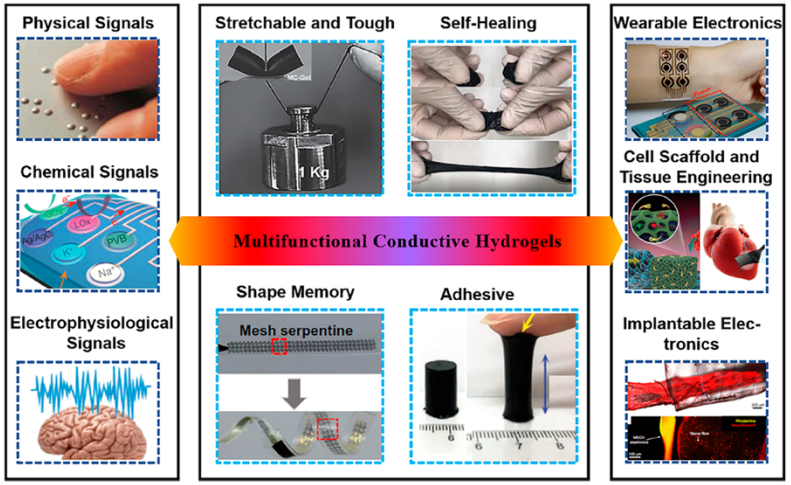

Figure 1. Functional conductive hydrogels for bioelectronics in biomedical applications. The left column presents the conductive hydrogels used for physical, chemical, and electrophysiological signals detection, respectively. The middle column summarizes important functions of conductive hydrogels. The right column shows the application of conductive hydrogels in the areas of wearable electronics, cell scaffold and tissue engineering, and implantable electronics, respectively.

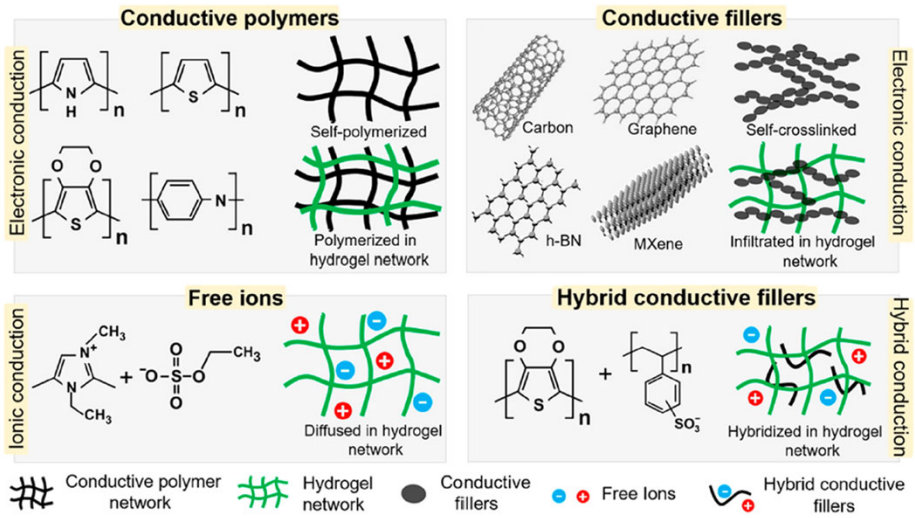

Figure 2. Structures of several types of conductive hydrogels. Conductive hydrogel can be synthesized by using conductive polymers, conductive fillers, free ions, and their mixtures. The formed hydrogels can be classified as electronic, ionic, and the hybrid electronic-ionic conducting hydrogels.

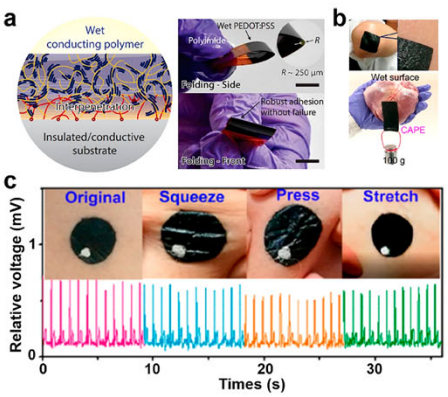

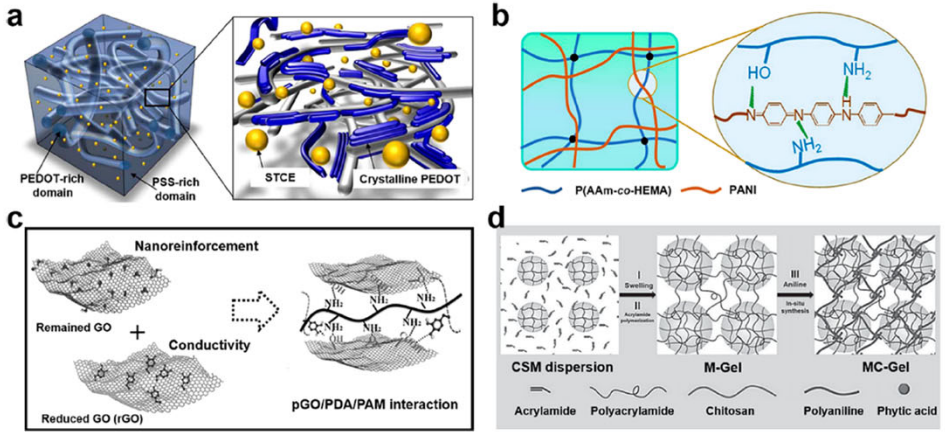

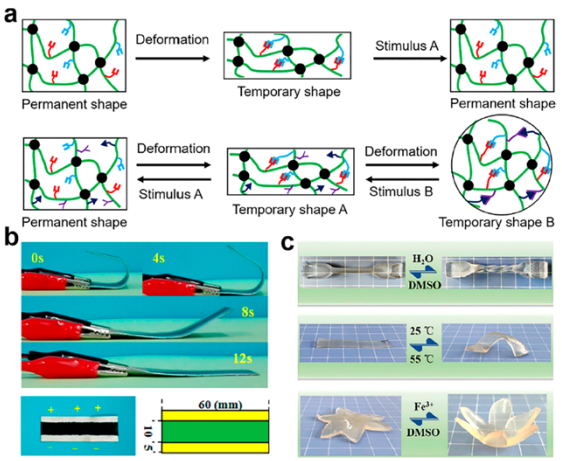

Fu 2020, Functional conductive hydrogels for bioelectronics

Magnetic Hydrogel for Controlled Release

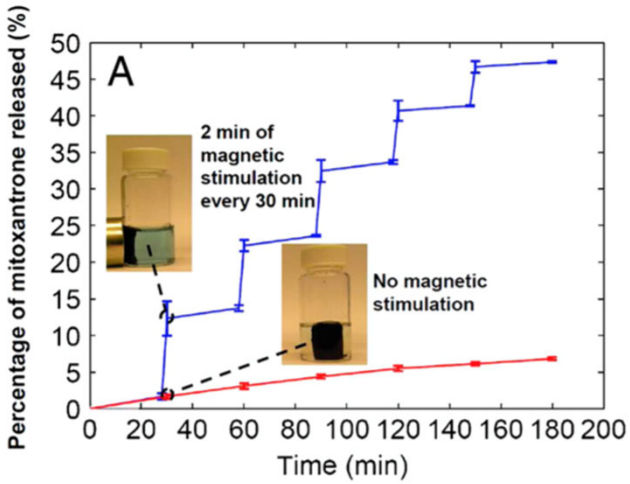

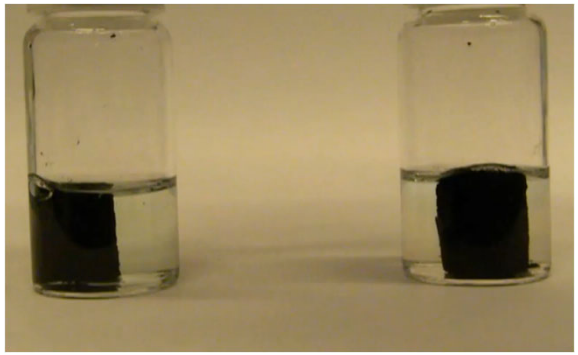

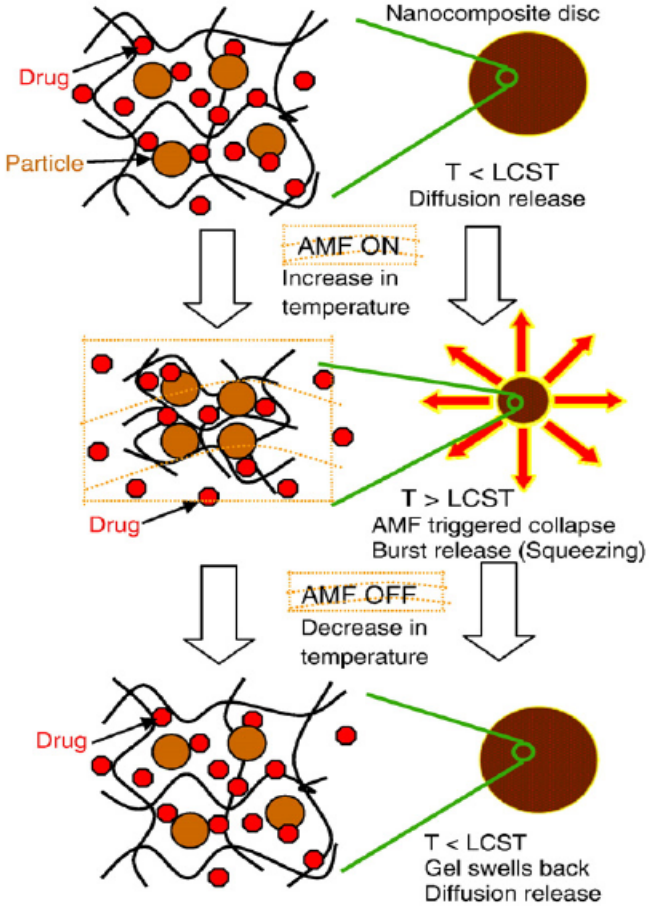

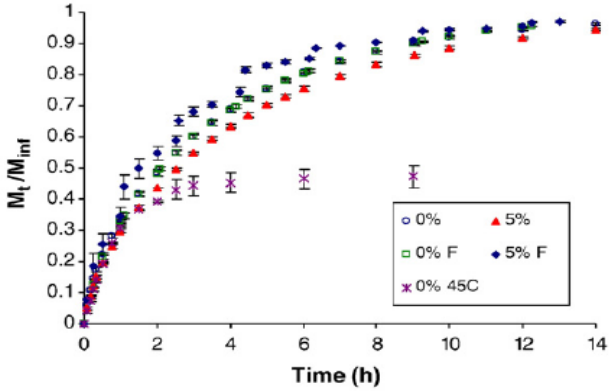

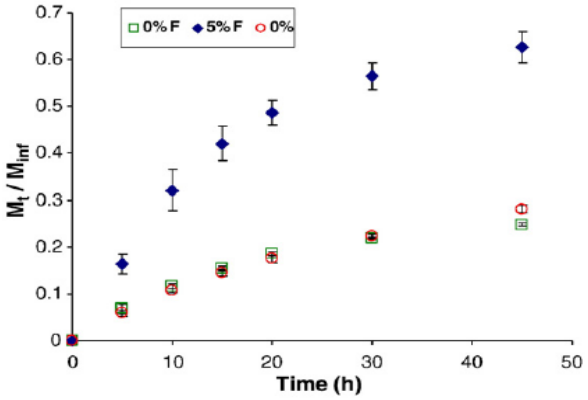

www.pnas.org/cgi/doi/10.1073/pnas.1007862108

Satarkar NS and Hilt JZ. *J Control Release 130: 246,* 2008

Ultrasound-Responsive Hydrogels

ABSTRACT: The development of tunable, ultrasound-responsive hydrogels that can deliver protein payload on-demand when exposed to focused ultrasound is described in this study. Reversible Diels−Alder linkers, which undergo a retro reaction when stimulated with ultrasound, were used to cross-link chitosan hydrogels with entrapped FITC-BSA as a model protein therapeutic payload. Two Diels−Alder linkage compositions with large differences in the reverse reaction energy barriers were compared to explore the influence of linker composition on ultrasound response. Selected physicochemical properties of the hydrogel construct, its basic degradation kinetics, and its cytocompatibility were measured with respect to Diels−Alder linkage composition. Focused ultrasound initiated the retro Diels−Alder reaction, controlling the release of the entrapped payload while also allowing for real-time visualization of the ongoing process. Additionally, increasing the focused ultrasound amplitude and time correlated with an increased rate of protein release, indicating stimuli responsive control.

KEYWORDS: *chitosan, hydrogels, ultrasound, controlled release, click chemistry, Diels−Alder*

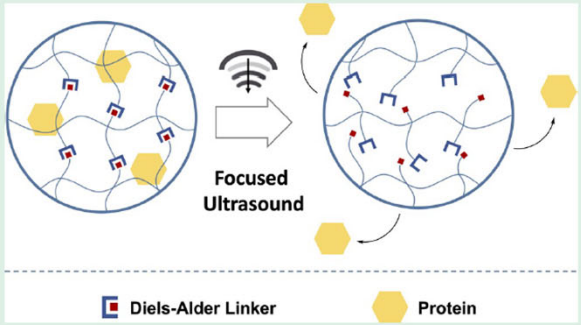

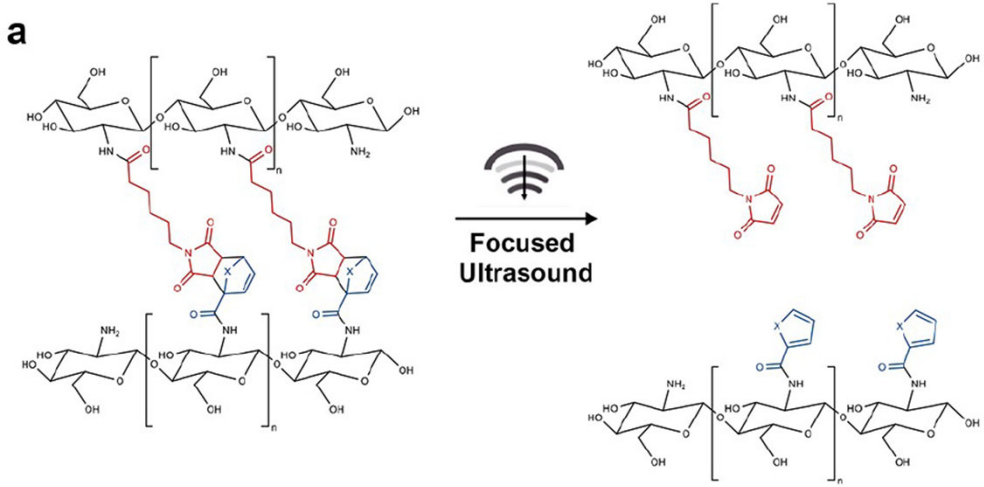

Arrizabalaga 2022, Ultrasound-responsive hydrogels for on-demand protein release

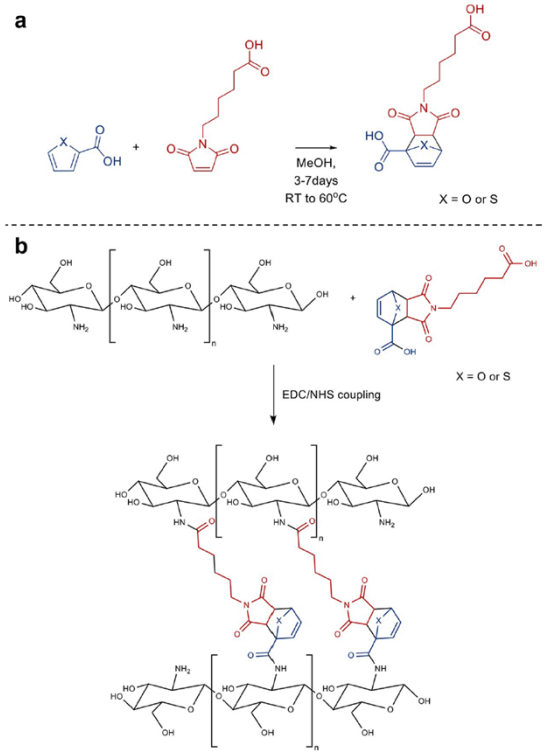

Figure 1. (a) Diels−Alder reaction between 6-maleimidohexanoic acid and a thiophene or furan-based diene. (b) Cross-linking of chitosan with a Diels−Alder linker (FDA or TDA) via EDC/NHS coupling reaction.

Figure 5. Ultrasound-mediated protein release from hydrogels. (a) Retro Diels−Alder reaction prompted by focused ultrasound for chitosan hydrogels cross-linked with either FDA or TDA. (b) Focused ultrasound dependent release of FITC-BSA from Ch-GLU, Ch-FDA, and Ch-TDA hydrogels (n = 3). *Significant difference ($p < 0.05$). (c) Real-time B-mode ultrasound imaging during focused ultrasound (5 min with a positive peak pressure of 37 MPa and peak negative pressure of 16 MPa) treatment of Ch-GLU, Ch-FDA, and Ch-TDA. A diagram and pictures of the setup used for focused ultrasound are available in the Supporting Information (Figures S1 and S2).

Force-Sensitive Polymers

Force-Sensitive Polymers

Exposure to forces causes changes in the position or state of matter. In particular, the conformation, bond angle, and bond length of polymers change upon exposure to an external force, which is the origin of the viscoelastic behavior that is unique to polymeric materials. When the external force is sufficiently high, irreversible destruction of the macromolecule occurs, which enters the field of polymer mechanochemistry.

Depending on the type of mechanophore, a wide variety of functions have been realized, including color change, small-molecule release, metal-catalyst generation, energy dissipation through the stretching of hidden length, accelerated degradation, and mechanical cascade reactions for mechanically induced strengthening. Moreover, research in this area has uncovered that mechanochemical reactions can yield products different from those obtained via thermal reactions.

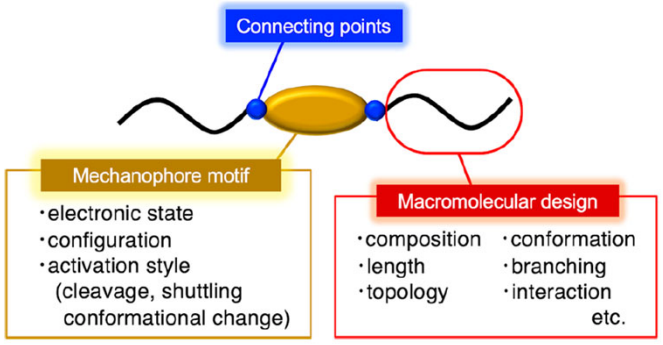

Figure 1. Factors affecting the mechanophore responsivity.

Watabe 2024, Enhancing the reactivity of mechanically responsive units via macromolecular design

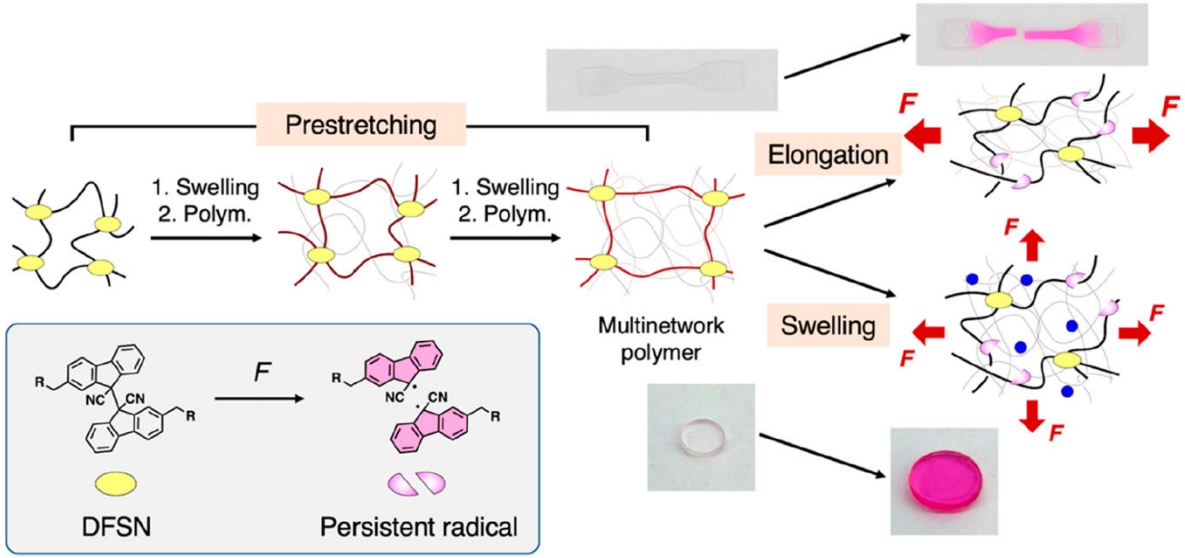

Figure 6. Mechanically sensitive polymer networks based on a multinetwork strategy and a DFSN mechanophore. The multinetwork polymer demonstrates outstanding mechanical response to uniaxial elongation and isotropic expansion during swelling.vc

In cross-linked polymers, the sensitivity of mechanophores has been increased via molecular stretching due to swelling. For example, Qiao et al. have successfully reduced the strain and energy required for mechanochromism under uniaxial elongation by prestretching the molecular chains through a stepwise swelling and cross-linking process, i.e., a multinetwork (MN) strategy.87 The first network doped with SP mechanophores is expanded via monomer swelling, and the isotropically stretched network structure is fixed after the polymerization. By taking advantage of the quantitative feature of the stable radicals generated from a difluorenylsuccinonitrile (DFSN) mechanophore, our group has demonstrated that the MN strategy boosts the amount of mechanically active mechanophores, even though the mechanophore is substantially diluted in the matrix networks

Force-Sensitive Polymers

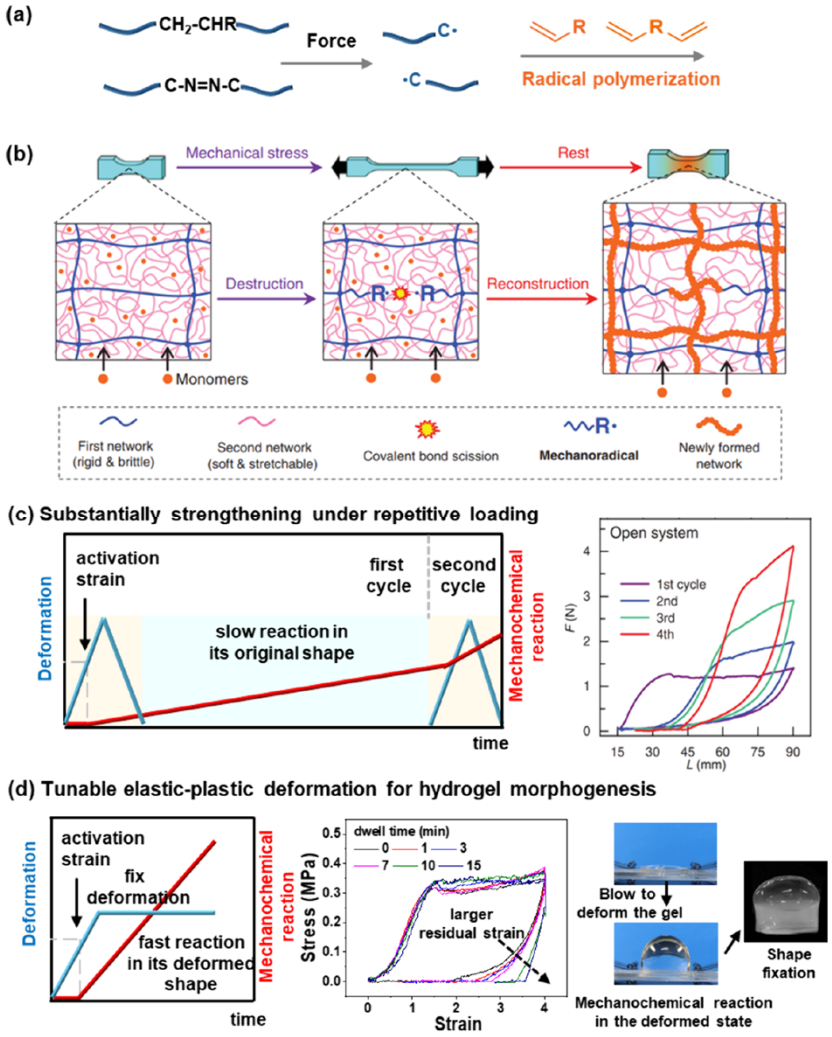

Figure 6. Various mechanoresponsive functions achieved in double network (DN) hydrogels by controlling the kinetics of force-induced chemical reactions and macroscopic material deformation. (a) Illustration of mechanoradical generation from homolytic chain cleavage and azoalkane activation, and its ability to trigger the polymerization of vinyl monomers. (b) Schematic illustration of DN gels undergoing force-induced destruction and reconstruction under external force. (c) Substantial strengthening through repetitive loading, with new network formation in its original shape. (d) Plastic deformation for hydrogel morphogenesis, achieved by controlling the formation of a new network in its deformed state. As the dwell time in the deformed state increased, the sample exhibited a larger residual strain, indicating enhanced plasticity.

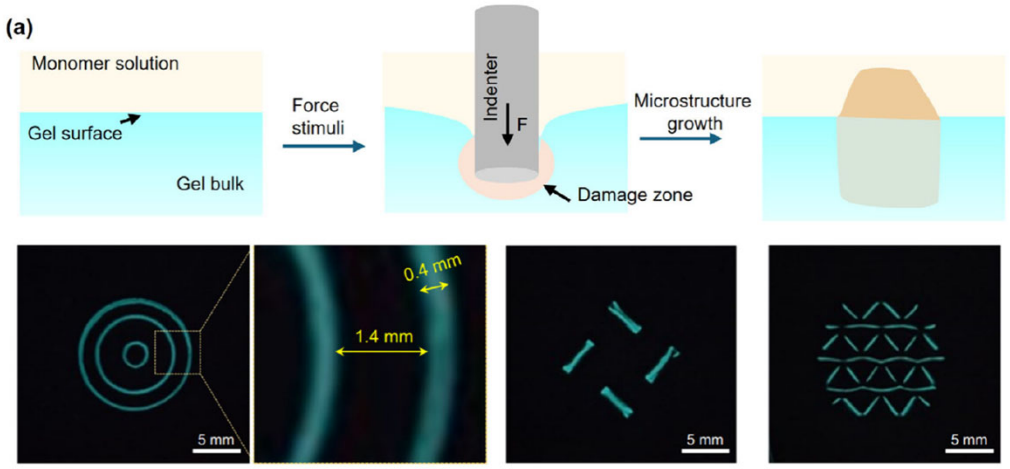

Figure 7. Mechanically induced surface patterning through spatiotemporal control of force. (a) Force-triggered rapid microstructure growth on the DN hydrogel surface.

Wang 2025, Mechanochemistry for on-demand polymer network materials

Force-Sensitive Polymers

The concept of polymer mechanochemistry involves leveraging force to induce chemical reactions within polymer materials, achieving mechanoresponsive functions such as self-reporting of stress, strain, or damage through color changes and force-responsive small molecule release.

To achieve this, researchers have employed mechanoresponsive units, known as mechanophores, to alter the mechanical response of individual polymer chains to external forces, thereby largely changing the network fracture pathways in bulk materials

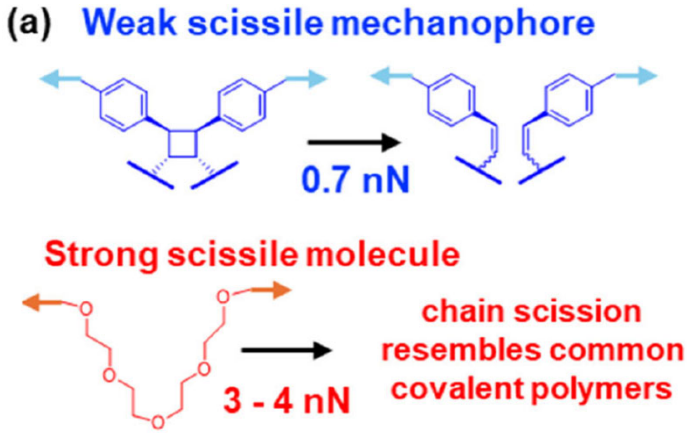

Figure 3. Influence of scissile mechanophore on the mechanical properties of various polymer network materials. (a) Mechanical activation behavior of a weak scissile mechanophore versus a typical strong scissile molecule.

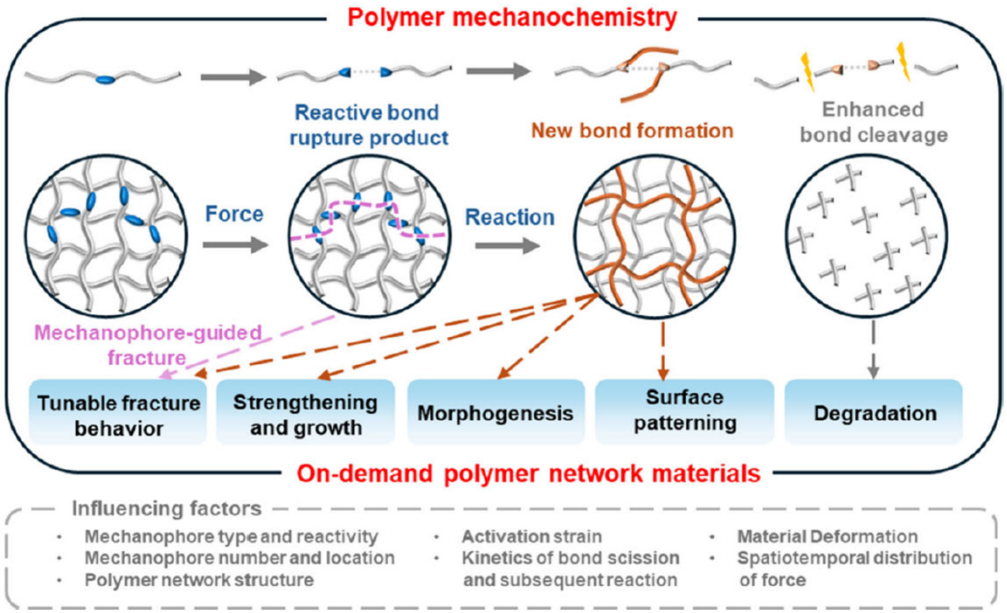

Figure 1. Routes utilizing polymer mechanochemistry to design on-demand polymer network materials and the crucial factors inside. Mechanophores are incorporated into the polymer network to regulate the microscale fracture pathways and resultant macroscale fracture behavior. More importantly, force-induced bond scission can trigger additional chemical reactions to adaptively adjust the polymer structures for on-demand functions.

Wang 2025, Mechanochemistry for on-demand polymer network materials

Pressure-Sensitive Polymers

Baroplastics: Pressure-Induced Miscibility

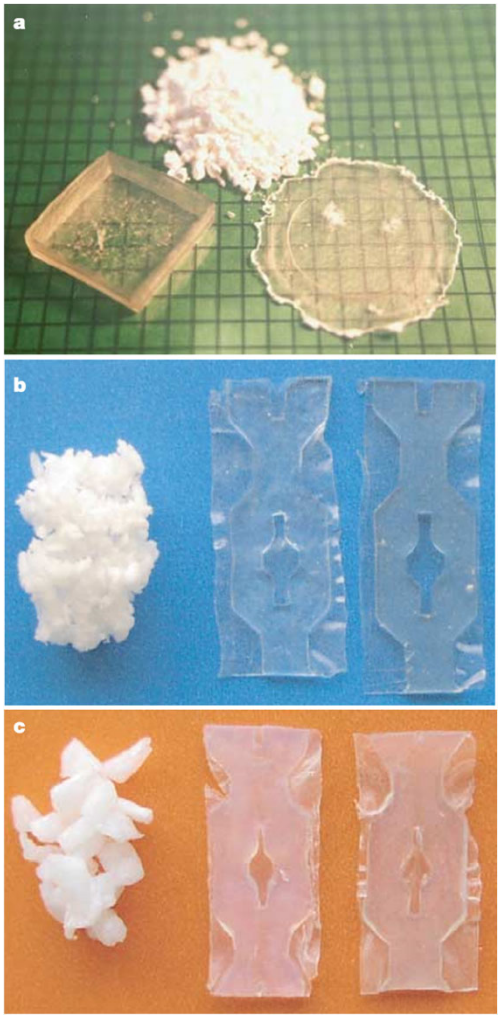

Low-temperature processable polymers

A distinct linkage between packing and energetics, which, for intermediate side chain lengths, is favorable to mixing at low temperatures and leads to a **lower disorder-order transition (LDOT)**.

For copolymers with longer alkyl side chains. On the other hand, the loss of compatibility at low temperatures can be ascribed to a simultaneous increase in unfavorable enthalpic interaction energy and decrease in packing efficiency in the segmentally mixed state.

Processed baroplastics samples.
a) 38,000 g/mol polystyrene-b-poly(n-butyl acrylate), PS-b-PBA, with 45 wt% PBA as obtained from freeze-drying and after processing by compression moulding at 25 °C using a pressure of 34.5 MPa (5,000 p.s.i.).
b) 60,000 g/mol polystyrene-b-poly(2-ethylhexyl acrylate), PS-b-PEHA, with 52 wt% PEHA reprocessed once and ten times at 30 °C under a pressure of 34.5 MPa.
c) PEHA/PS core–shell material with 52 wt% PEHA processed one time and recycled ten times at 25 8C with pressure a pressure of 34.5 MPa.

Gonzalez-Leon 2003, Low-temperature processing of 'baroplastics' by pressure-induced flow

Upon considering the potential uses of such molecularly designed materials, a significant limitation arises from the difficulty to control the bulk thermodynamics of block copolymers, particularly the appearance of order/disorder. Indeed, from an applications standpoint, the strong thermodynamic incompatibility typically found for block copolymers is highly advantageous, as it results in remarkably stable solidlike microphase-separated morphologies. However for processing, where flow is essential, the ability to access the more fluid, segmentally mixed (disordered) state is clearly desirable.[1] In current practice, this is achieved by either heating the material to a sufficiently high temperature in the presence of antioxidants or by adding a common solvent for the different polymer blocks constituting the copolymer. The former approach is generally viable only for rather low molecular weight systems of limited commercial application, unless more complex copolymer architectures such as multiblock are used.[14] The latter is disadvantageous from the standpoint of cost and environmental considerations.

One potential approach to enhanced processability in block copolymer melts might be to exploit the phenomenon of pressure-induced miscibility previously observed for a limited number of polymer pairs. In earlier work, we demonstrated by small-angle neutron scattering that both polystyrene-*block*-poly(*n*-butyl methacrylate), PS-*b*-PBMA, and PS-*b*-poly(hexyl methacrylate), PS-*b*-PHMA, exhibit pressure-induced miscibility,[15,16] although the former undergoes ordering upon heating through a lower disorder−order transition (LDOT),[17,18] while the latter exhibits an upper disorder−order transition (UDOT).[19] For PS-*b*-PBMA, applying 100

Ruzette 2003, Pressure effects on the phase behavior of styrene-n-alkyl methacrylate block copolymers

Baroplastics

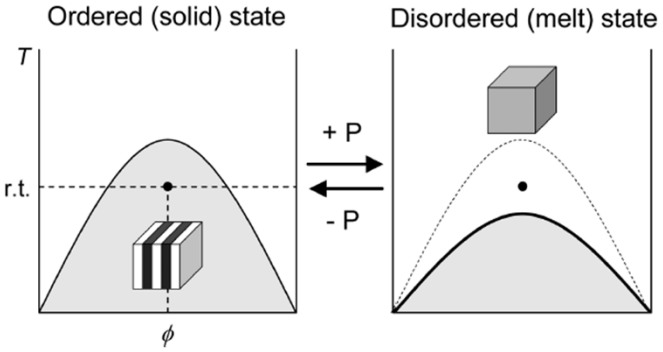

Pressure-induced phase transition of copolymers with an upper disorder-to-order transition (UDOT) phase diagram.

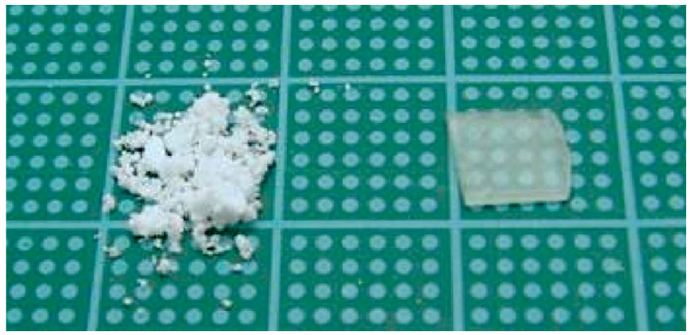

PmCL-b-PLLA (Mw: 60 kDa, LA: 50 wt %) before (left) and after (right) processing under 34.5 MPa for 5 min at 25 °C.

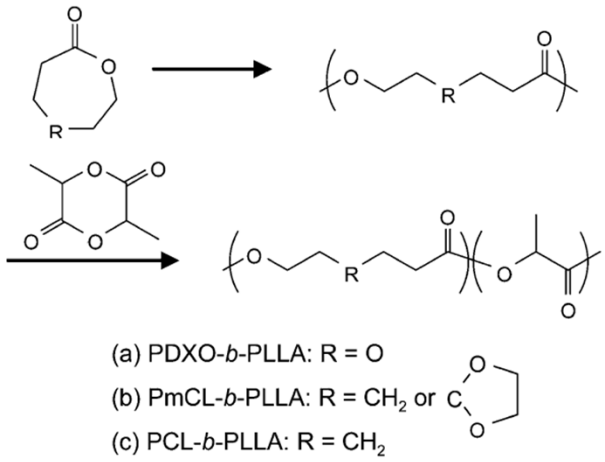

Synthetic Route of Degradable Block Copolyester by Two-Step Ring-Opening Polymerization.

Taniguchi 2012, Low-temperature processable degradable polyesters

In 2012, Taniguchi and Lovell synthesized a series of biodegradable aliphatic polyester block copolymers (BCPs) via 2-step ring-opening polymerization (ROP), which displayed baroplastic behavior under 34.5 MPa of hydraulic pressure at ambient temperature/ The diblock copolymers (DBCPs) were composed of high-T_g PLLA and low-T_g PCL, its derivative poly (caprolactone-*r*-5-ethylene ketal caprolactone) (PmCL), or poly-1,5-dioxepan-2-one (PDXO) (Table 3). Unlike previous BCPs, the high-T_g component, PLLA, was relatively low at around 60 °C, but importantly, PLLA is crystalline with a melting point around 150 °C. Notably, only PLLA was derived from renewable feedstocks, with the remaining polymers were synthesized from petrochemical sources, although a number of routes to PCL from biomass exist. When the PLLA content was between 40 and 60 %, PLLA-*b*-PmCL and PLLA- *b* -PDXO DBCPs could be processed at 25 °C and 34.5 MPa for 5 min to give transparent objects [16]. However, the PLLA-*b*-PCL DBCP required a temperature of 65 °C to be processed, due to the semi-crystalline nature of PCL, which has a melting point at 58 °C. Notably, this temperature also likely surpassed the ≈60 °C T_g of the PLLA hard-block, such that any PLLA chains within amorphous regions may have gained extra mobility, even without a baroplastic mechanism. While the obtained products were initially transparent, they became opaque within a week at 25 °C, or a day at 80 °C, due to the crystallization of PCL.

Despite flying under the radar of most polymer chemists, the field of baroplastics has continuously advanced over the past two decades. Analogous low-temperature processability has been demonstrated in Polymer Blends, BCPs, and CSNPs derived from both petrochemical and sustainable feedstocks. (MacKinnon 2025, Baroplastics: The future of low temperature plastic processing)

Baroplastics

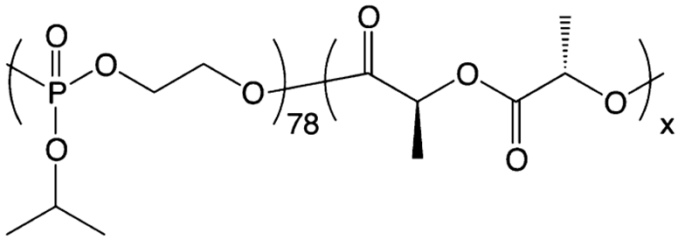

Chemical structure of PIPP78-b-PLLAx.

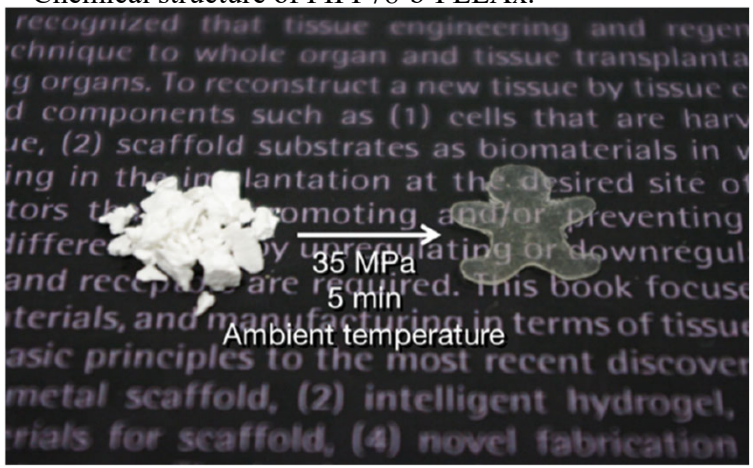

Photograph of the low-temperature processing of $PIPP_{78}$-b-$PLLA_{140}$ under 35 MPa for 5 min at 35 °C.

Iwasaki 2016, Low-temperature processable block copolymers that preserve the function of blended proteins

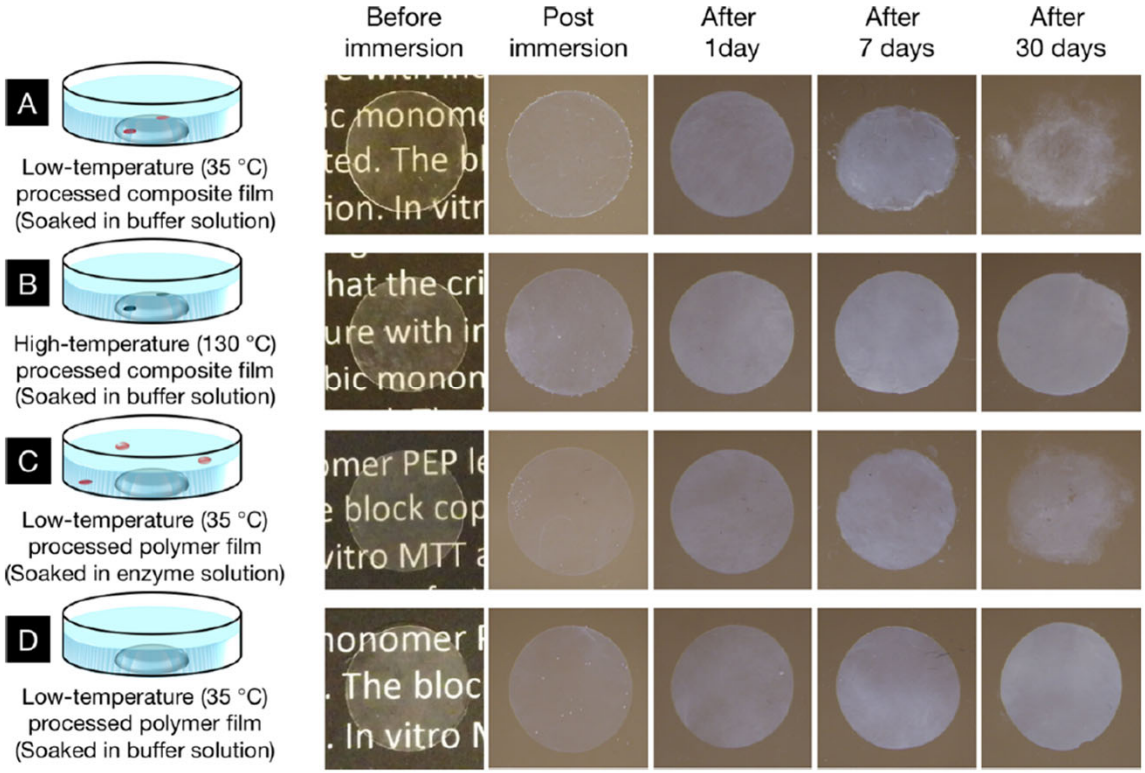

Degradation of polymer films by hydrolysis. (A) Low-temperature (35 °C) processed $PIPP_{78}$-b-$PLLA_{140}$ composite film with proteinase K. The film was soaked in Tris buffer solution. (B) High-temperature (130 °C) processed $PIPP_{78}$-b-$PLLA_{140}$ composite film with proteinase K. The film was soaked in Tris buffer solution. (C) Low-temperature processed $PIPP_{78}$-b-$PLLA_{140}$ film. The film was soaked in Tris buffer solution containing proteinase K. (D) Low-temperature processed $PIPP_{78}$-b-$PLLA_{140}$ film. The film was soaked in Tris buffer solution.

Baroplastics

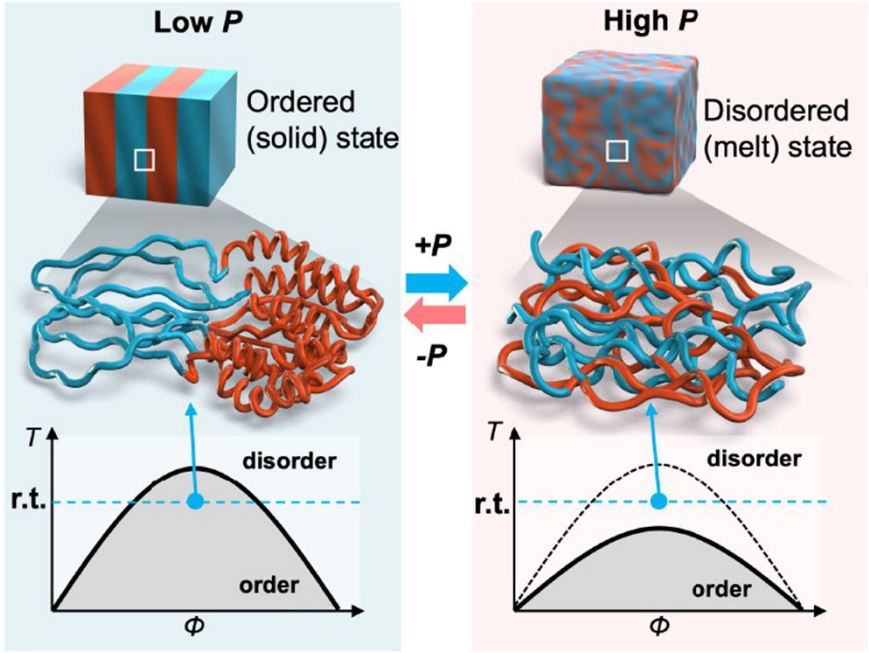

Schematic of pressure-induced order-disorder transition of block copolymers. PS-b-PnBMA: polystyrene-block-poly(n-butyl methacrylate).
From the perspective of pressure-responsive soft materials, polymer mixtures that undergo phase transitions between ordered and disordered states upon compression, called baroplastics, are of great interest. Typical baroplastics are block copolymers comprising soft and hard segments. The soft segment exhibits a low glass transition temperature (T_g) and is rubbery at ambient temperature, whereas the hard segment shows a high T_g and is glassy at ambient temperature. Unlike thermoplastic block copolymers, baroplastic block copolymers undergo an order-disorder transition and flow upon compression at ambient temperatures.

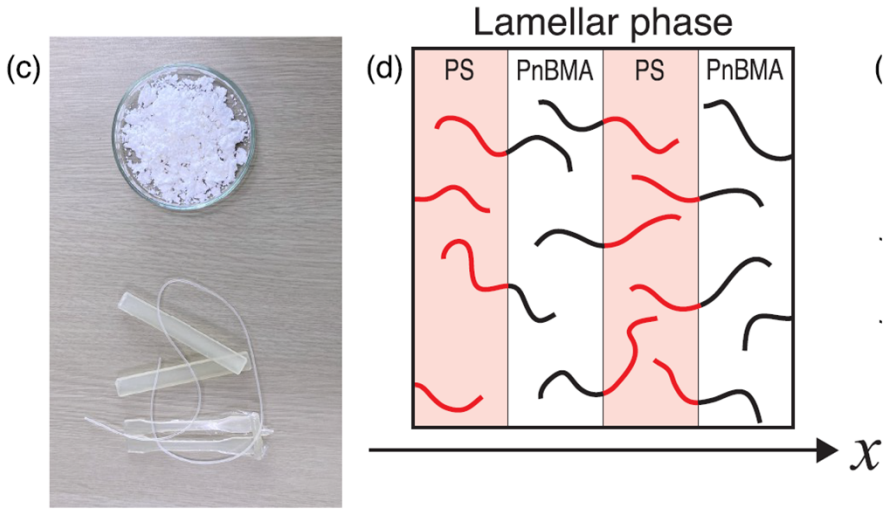

(c) Compression melt molding of degradable baroplastic. Polymer powder (top) was compressed at ambient temperature and 50 MPa to obtain a strand (bottom). Other molded products at the bottom were obtained at 100 °C and 1 MPa.
(d) Changes in the normalized concentration profiles of PS-b-PnBMA upon compression at 443 K in the direction perpendicular to the lamellar interfaces.

Baroplastics have some green advantages over conventional thermoplastics: First, polymers are heated to 200 °C or higher to obtain sufficient fluidity for thermoplastic molding. In contrast, baroplastics require only ambient temperatures (Figure 2c). Low- temperature processing significantly reduces energy consumption and CO_2 emissions in polymer processing. Second, low-temperature polymer processing eliminates the thermal degradation of the polymer during processing. A previous study reported that the mechanical properties of the baroplastic remained unchanged even after 10 cycles of repeated processing. This degradation-free processability significantly improves the polymer lifetime during materials recycling.

Deguchi 2023, Deep-sea-inspired chemistry- A hitchhiker's guide to the bottom of the ocean for chemists

Baroplastics

ABSTRACT: Advancing sustainable plastics is crucial to achieving a circular plastic economy. Baroplastics, block copolymers exhibiting order−disorder transitions under pressure, allow polymer processing at ambient temperatures, reducing energy use and avoiding thermal degradation. Their application, however, has been limited by structural constraints. This study introduces poly(ε-caproclactone-random-5-ethyleneketal ε-caprolactone)-*block*-poly(L-lactide) (PmCL-*b*-PLLA) as a "*baroplasticizer*" for nonbaroplastic PLLA. Blending with the block polymers lowered PLLA's flow temperature by up to 100 °C (160 to 60 °C at 50 MPa) while preserving molecular weight after repeated pressure cycles, ensuring recyclability. The improved formability would arise from a pressure-induced ordered (solid)-to-disordered (melt/solid) phase transition. This work eliminates structural constraints in baroplastics, enabling broader low-temperature processing applications and advancing sustainable polymer technologies.

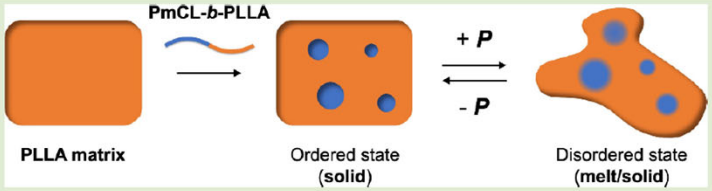

Baroplastics are polymers, often block copolymers, that can be processed (melted, molded, reformed) using pressure instead of high heat, allowing for low-temperature shaping, much faster cycles, and exceptional recyclability without property loss, by temporarily switching from a solid-like state to a liquid-like flow state under compression, then solidifying back. This "baroplastic effect" relies on pressure-induced order-to-disorder transitions (ODT) in their nanostructure, offering a sustainable, energy-efficient alternative to traditional plastics, reducing CO_2 and enabling multiple re-molding cycles.

Baroplastics flow under pressure at low or ambient temperatures, unlike traditional plastics that need heat. They are typically made of block copolymers with hard (high glass transition temp, T_g) and soft (low T_g) segments. Pressure forces the ordered polymer chains to mix (disorder), creating a flowable state; removing pressure restores the solid form.

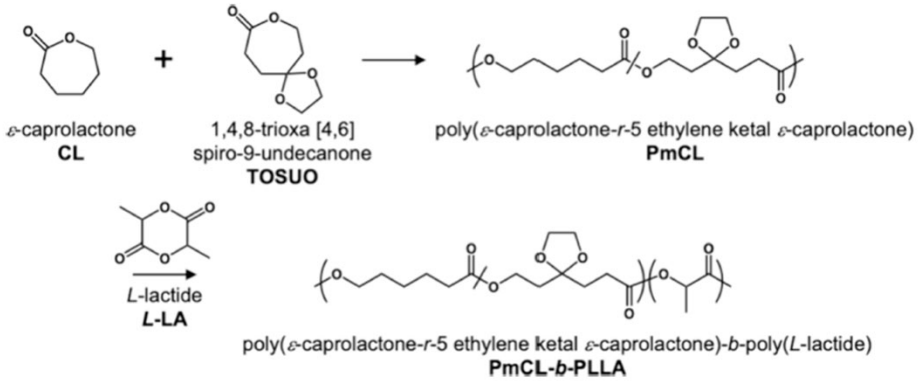

Figure 1. Synthetic scheme of PmCL-*b*-PLLAs by two-step ring-opening polymerization.

Sharma 2025, Baroplastic effect of aliphatic polyester block copolymers for degradation-free multicycle processing of poly(L-lactide)

Baroplastics - The future of low temperature plastic processing

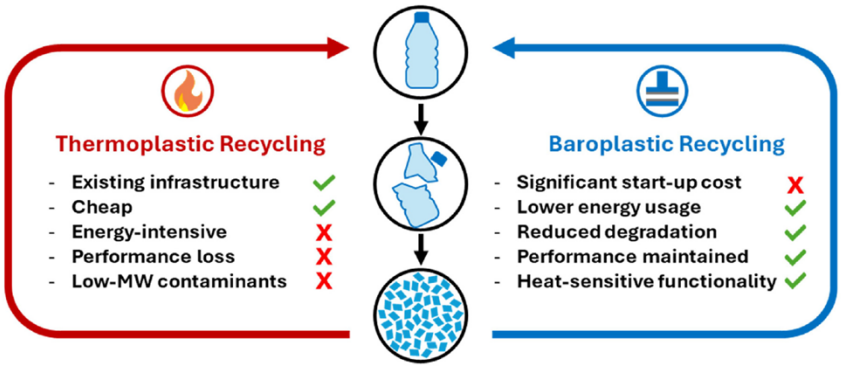

An overview of both conventional thermoplastic and idealized baroplastic processing mechanisms, with some advantages and disadvantages given for each.

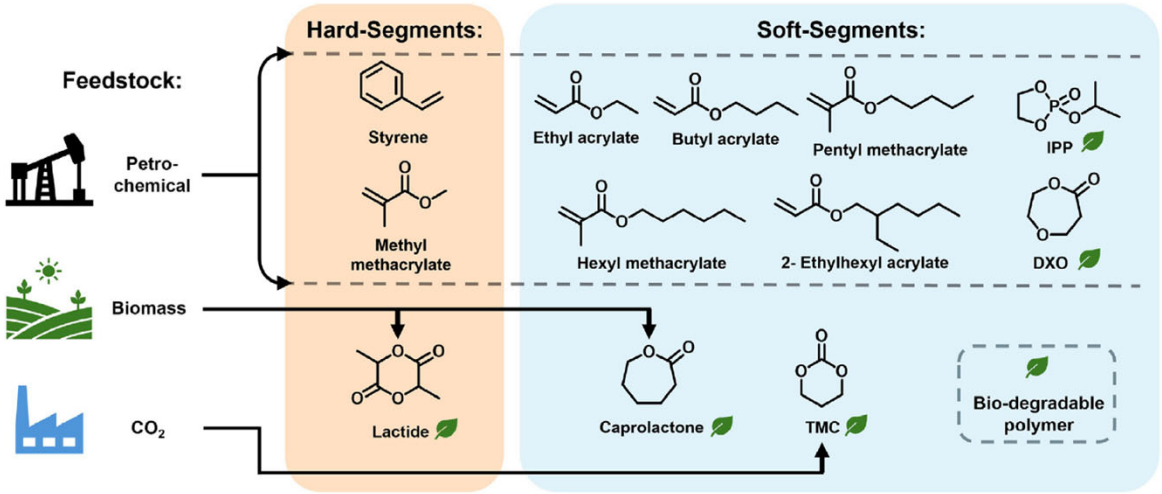

The monomers utilized in low-temperature baroplastics, with their feedstocks and potential for bio-degradability shown.

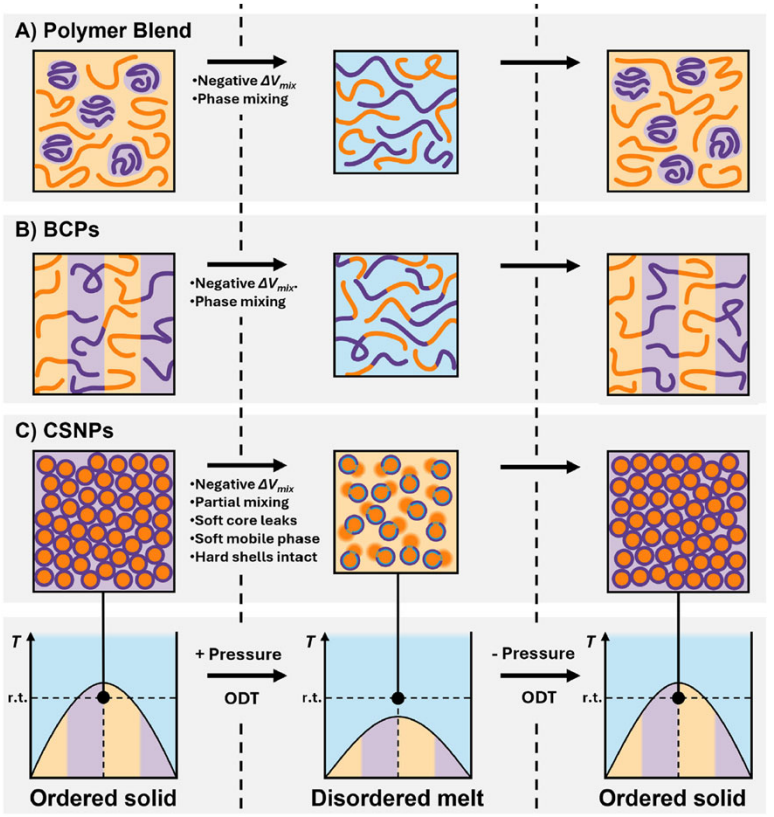

A schematic demonstrating a baroplastic pressure-induced order-disorder transition (ODT) in A) a polymer blend, B) a Block Copolymer (BCP), and C) Core-Shell Nanoparticles (CSNPs), with the ODT spinodal shown to shift downwards under the application of pressure, due to a negative volume change on mixing (Vmix), allowing the polymer to flow at ambient temperature.

MacKinnon 2025, Baroplastics: The future of low temperature plastic processing

Ligand-Sensitive Systems

Glucose Sensitive Systems

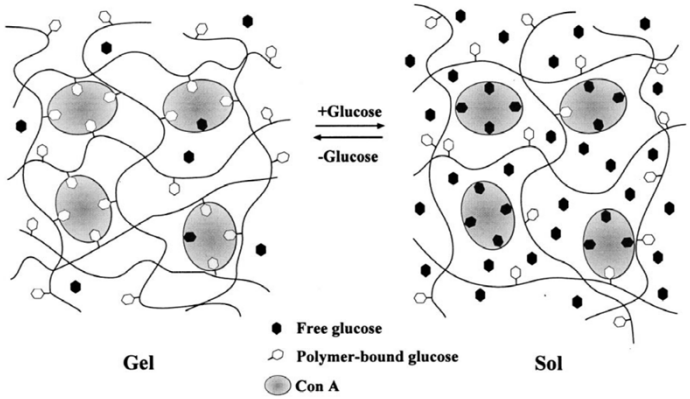

Fig. 6. Sol–gel phase-transition of a glucose-sensitive hydrogel. Large circles represent Con A, a glucose-binding protein. Small open and closed hexagons represent polymer-attached glucose and free glucose, respectively.

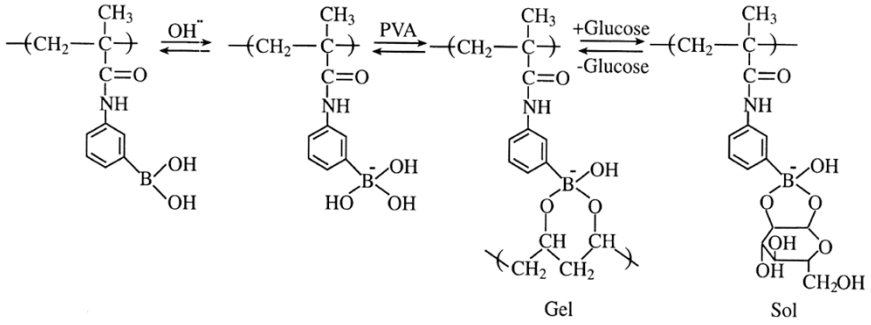

Fig. 7. Sol–gel phase-transition of a phenylborate polymer. At alkaline pH, phenylborate polymer interacts with poly(vinyl alcohol) (PVA) to form a gel. Glucose replaces PVA to induce a transition from the gel to the sol phase.

Qiu 2001, Environment-sensitive hydrogels for drug delivery

The most important properties yet to be achieved:

Kinetics & Reproducibility

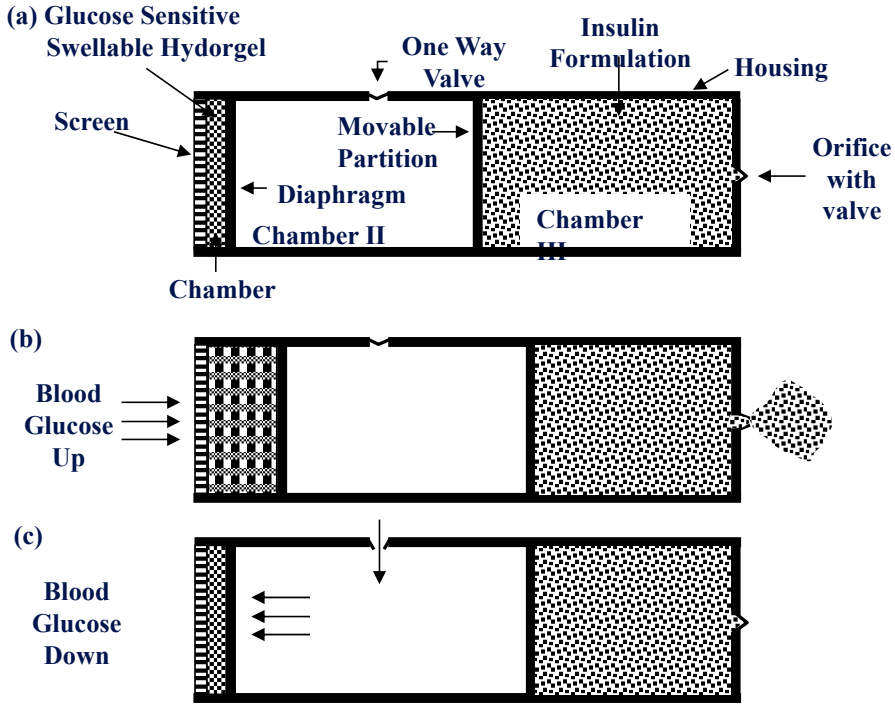

Fig. 7. (a) Schematic of proposed self-regulating mechanochemical insulin pump. (b, c) Expected operation of mechanochemical pump. Arrows indicate water flux. (Siegel 1990, Mechanochemical approaches to self-regulating insulin pump design)

Glucose Sensitive Systems

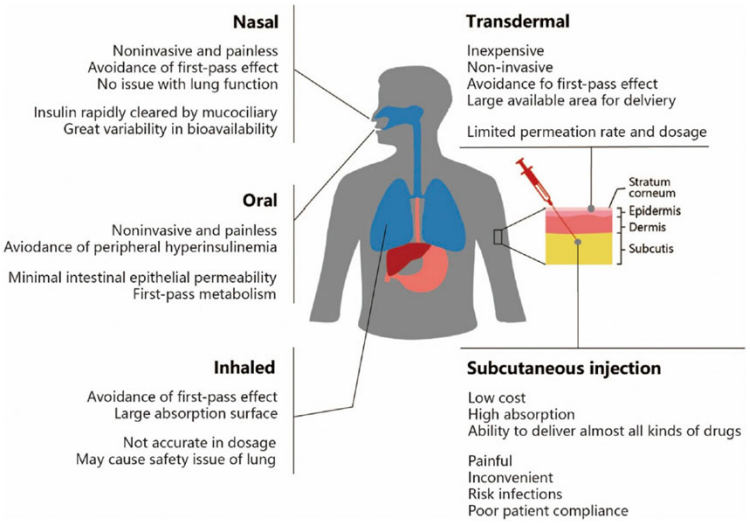

Fig. 3. The advantages and drawbacks of different insulin administrations.

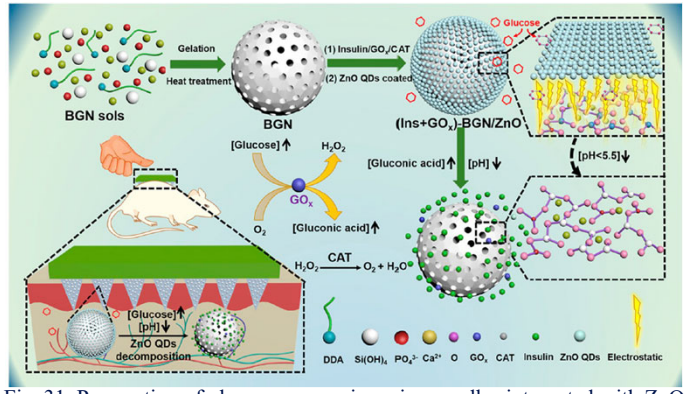

Fig. 31. Preparation of glucose-responsive microneedles integrated with ZnO quantum-dot-capped MBGs for transdermal delivery of insulin.

Shen 2020, Recent progress in design and preparation of glucose-responsive insulin delivery systems

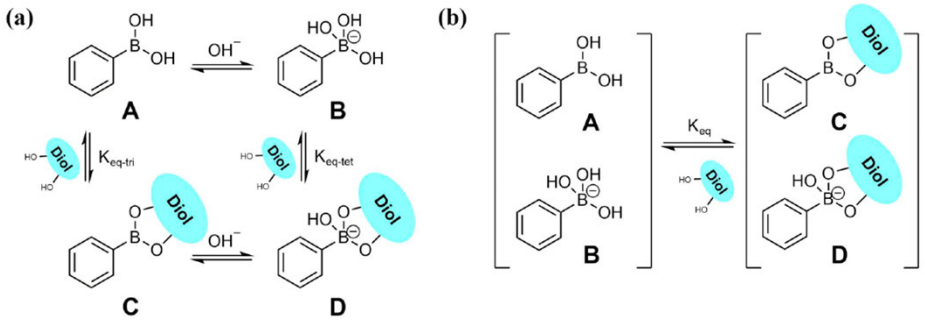

Fig. 4. (a) The equilibrium between charged and uncharged phenylboronic acid and their esters. (b) The equilibrium between phenylboronic acids and their esters. $K_{eq\text{-}tri}$, $K_{eq\text{-}tet}$ and K_{eq} are all equilibrium constants and K_{eq} is named as overall association constant

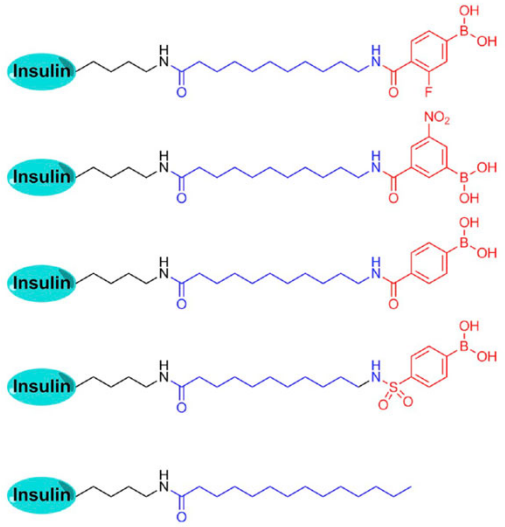

Fig. 17. The structures of aliphatic PBA-modified insulins and the aliphatic insulin [119].

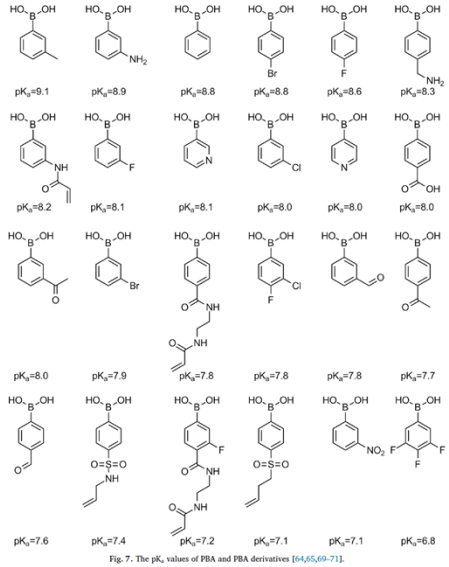

Fig. 7. The pK_a values of PBA and PBA derivatives [64,65,69–71].

Glucose-Responsive Insulin Formulations (GRIF)

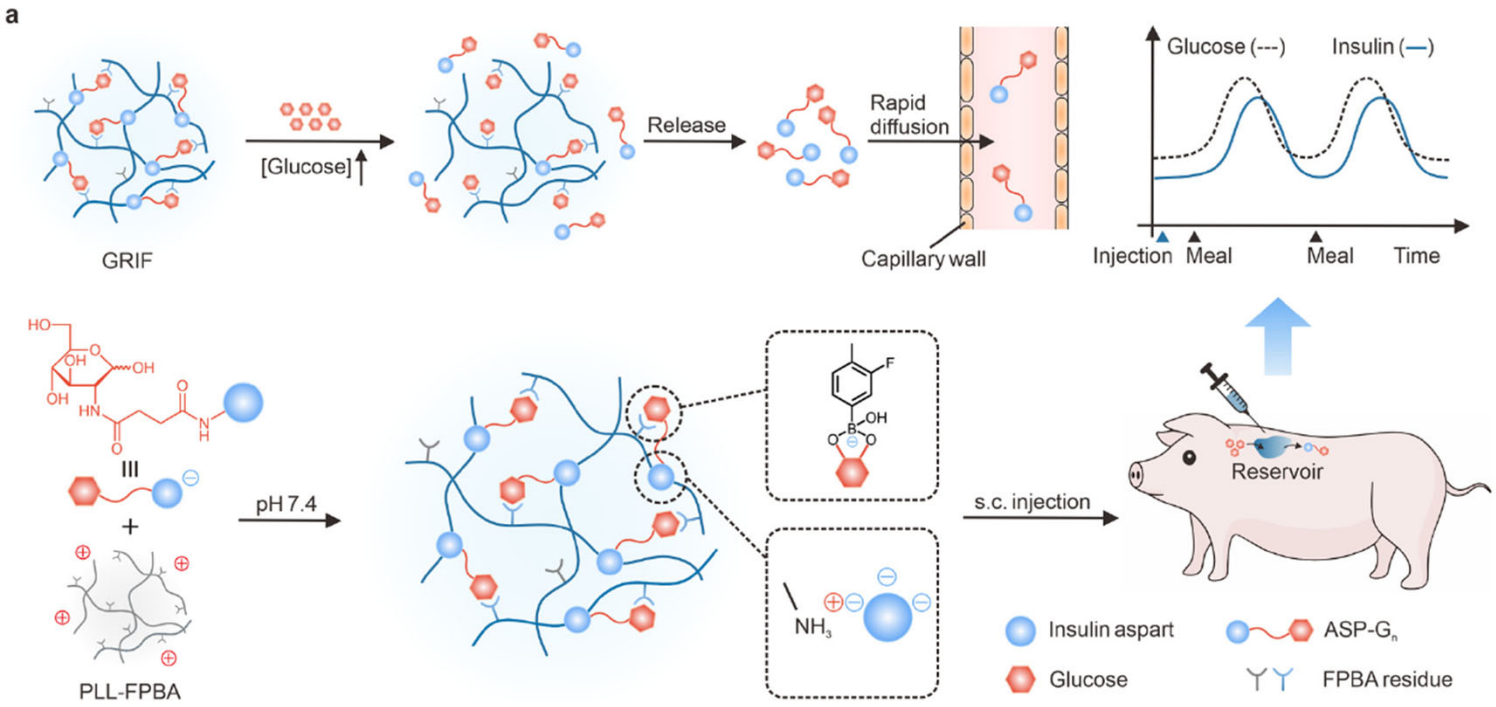

Fig. 1. Dual glucose-responsive insulin formulations (GRIF) for insulin analog delivery. (a) Schematic and glucose-responsive mechanism of the GRIF composed of glucosamine-modified insulin aspart (ASP-Gn) and phenylboronic acid-modified poly-L-lysine (PLL FPBA). The formulations consist of positively charged PLL-FPBA and negatively charged ASP-Gn under a physiological environment (pH = 7.4). The glucosamine moiety in ASP-Gn can form reversible covalent interactions with the cis-diol structure in PLL-FPBA.
In hyperglycemic conditions, free glucose in plasma and tissues competes with FPBA for binding to PLLFPBA, decreasing its positive charge and leading to the dissociation of ASP-Gn and PLL-FPBA. ASP-Gn can rapidly normalize blood glucose (BG) levels.

Liu 2025, Long-acting glucose-responsive insulin with swift onset-of-action

Insulin aspart, an analogue of human insulin approved for use in people with diabetes, is more rapidly absorbed and achieves higher plasma concentrations than human soluble insulin after subcutaneous injection.

Insulin aspart is a rapid-acting human insulin analog created by replacing the amino acid proline with aspartic acid at position B28 of the human insulin B-chain. This specific modification (B28-aspartic acid-human insulin) reduces the insulin's tendency to form dimers and hexamers, enabling faster absorption, a 10-15 minute onset, and shorter duration of action compared to regular human insulin.

Glucose Sensitive Systems

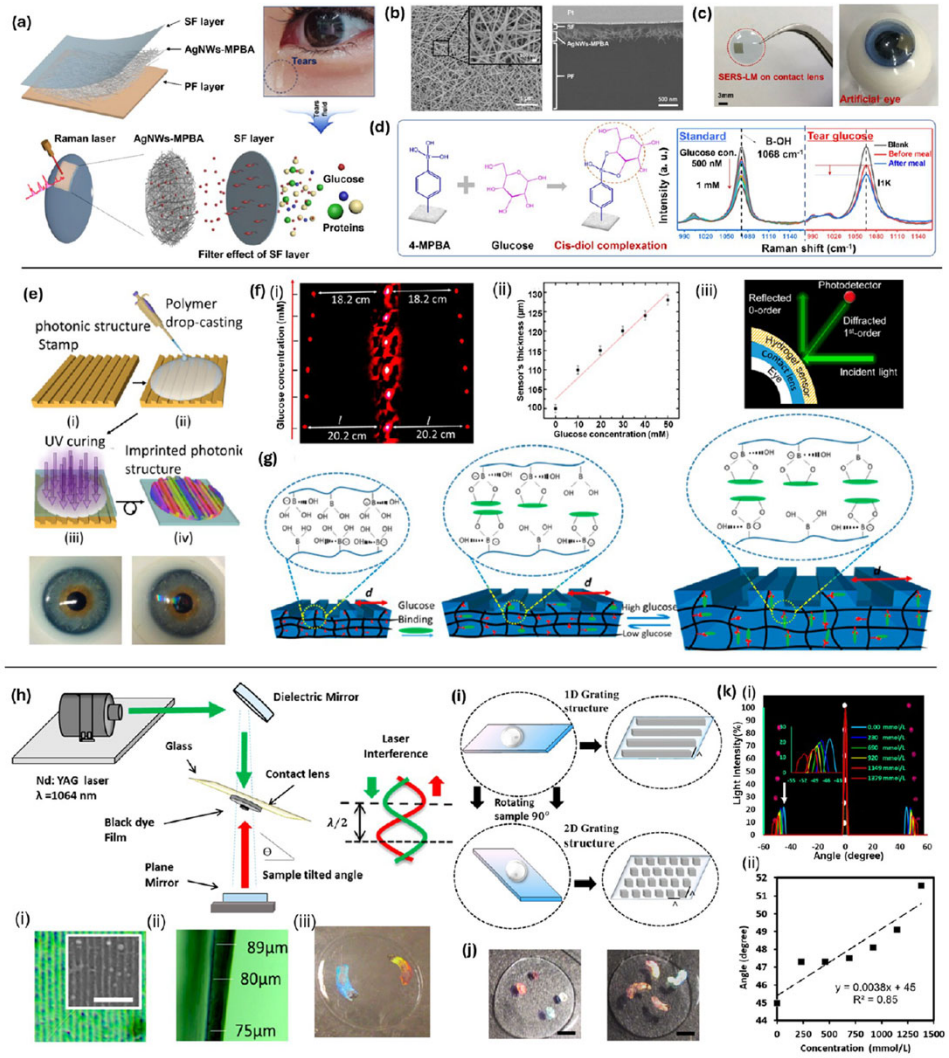

Figure 5. Surface-mounted optical sensors integrated onto the surface of contact lenses.

(a) A combined Surface-Enhanced Raman Scattering-active contact lens materials (SERS-LM) structure integrated with a contact lens for selective glucose detection.

(b) FE-SEM images show silver nanowires (AgNWs) on the silk fibroin (SF) layer, inset high-resolution nanowires, and SERS-LM cross-section after FIB cutting.

(c) A prototype of the SERS-LM integrated into a contact lens.

(d) The chemical selectivity of 4-mercaptophenylboronic acid (4-MPBA) for glucose with Raman spectra changes of the SERS-LM after reacting with varying glucose concentrations.

(e) The fabrication of a hydrogel glucose sensor: i. a photonic structure (PS) master is used as a stamp. ii. PS is coated with monomer solution via drop-casting. iii. UV polymerized monomer on contact lens.

(f) i. Transmitted diffraction patterns of the PS sensor at low glucose concentrations are depicted. ii. The sensor's cross-section changes versus glucose concentration. iii. The setup for projecting diffraction patterns and measurement.

(g) Glucose– phenylboronic acid complexation in the 1D PS sensor.

(h) One-dimensional nanopatterns on contact lenses are fabricated via DLIP with Nd laser (1064 nm, 3.5 ns). i. Optical microscopy of the 1D nanostructure with SEM (scale bar = 5 μm). ii. Lens cross-section in ambient humidity (scale bar = 100 μm). iii. Ink-based holographic nanostructures on lenses (scale bar = 5 mm).

(i) 1D and 2D nanostructures are presented.

(j) Holographic nanostructure designs (rings/patches) on contact lenses.

(k) i. Diffraction measurements on nanopatterned lenses at different Na+ concentrations. ii. Diffraction angle variations corresponding to Na+ concentration changes.

Xia 2025, Optical contact lenses biosensors

Self-Regulated Systems

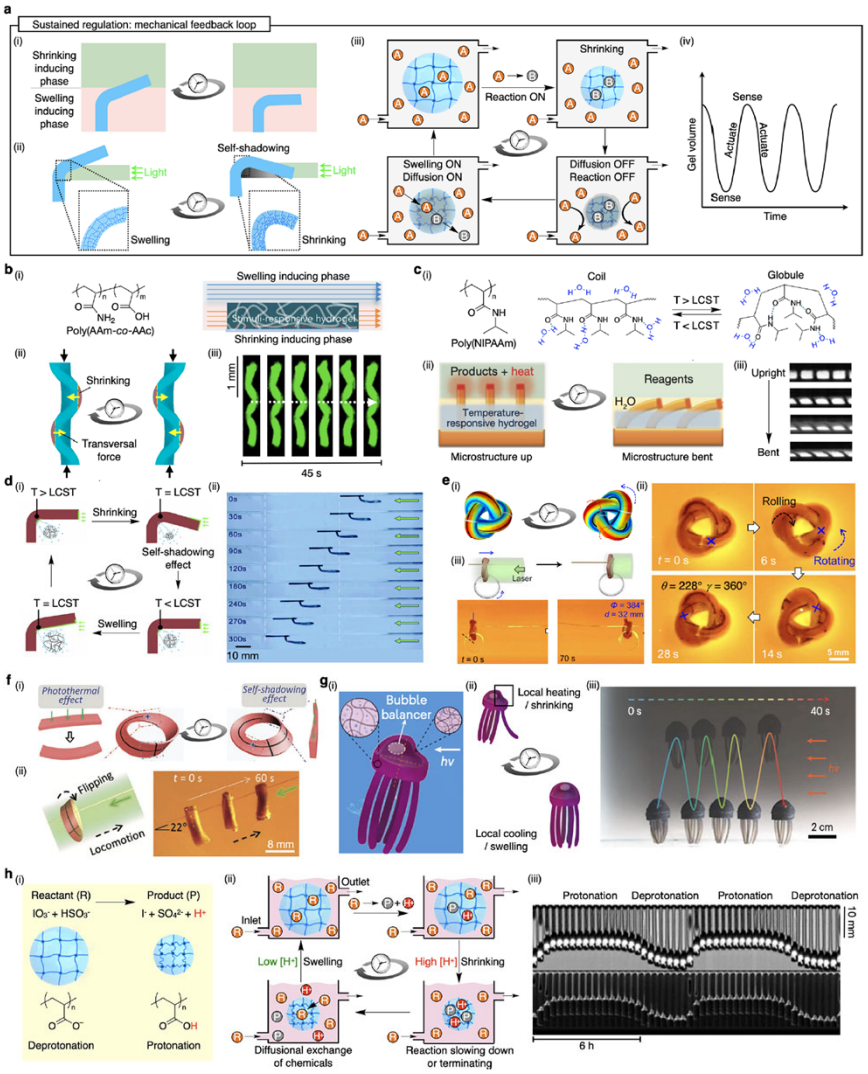

Figure 6. Self-regulating hydrogels with sustained regulation driven by mechanical feedback loop.
(a) (i) Schematics of a chemomechanical feedback loop using a two-phase reactor. One phase induces shrinkage of the gel, while the other phase induces swelling of the gel. (ii) Schematics of a mechanical feedback loop using the self-shadowing effect. The gel shrinks upon light exposure and swells again when the shrunken state blocks the light. (iii) Schematics of a chemomechanical feedback loop using a continuous stirred tank reactor (CSTR). A chemical reaction induces gel shrinkage, which in turn modulates reagent diffusion and triggers reswelling, forming a self-sustained oscillation. (iv) Schematic graph showing time-dependent sustained volume changes of a self-regulating hydrogel driven by a mechanical feedback loop.
(b) (i) Chemical structure of the poly(AAm-co-AAc) hydrogel and schematic of its spatial placement in a two-phase laminar flow system. (ii) Schematics of a mechanical feedback loop based on dynamic buckling. Local swelling and shrinking generate transversal forces that drive snap-through between bistable buckled states, forming a self-regulating cycle. (iii) Time-lapse fluorescence images showing periodic swaying motion of the hydrogel strip under continuous dual-stimuli flow.
(c) (i) Chemical structure of poly(NIPAAm) and schematics of its coil-to-globule transition across the lower critical solution temperature (LCST). (ii) Schematics and time-lapse images of a chemomechanical system integrating a poly(NIPAAm) hydrogel with catalyst-tipped microstructures. (iii) Captured confocal fluorescence images showing microfin configurations during actuation in a bilayer liquid system. The white-colored bottom layer is deionized water labeled with Rhodamine B, while the top layer contains nonfluorescent reagents.
(d) (i) Schematics of a light-fueled mechanical feedback loop in a poly(NIPAAm)−AuNPs hydrogel oscillator. (ii) Time-lapse images showing periodic oscillatory bending of a fishhook-shaped hydrogel under constant light illumination.
(e) (i) Schematics of a topologically constrained trefoil hydrogel knotbot undergoing light-fueled deformation. (ii) Experimental demonstration of directional rolling under localized laser irradiation. (iii) Time-lapse images of the trefoil knotbot under uniform illumination.
(f) (i) Schematics of a twisted hydrogel ribbon undergoing self-sustained deformation under static light. (ii) Time-lapse images showing flipping locomotion of the twisted hydrogel ring on a stretched string under constant illumination.
(g) (i) Schematics of a self-regulating phototactic hydrogel vehicle. Design of the jellyfish-inspired hydrogel robot was composed of poly(NIPAAm) hydrogel embedded with AuNPs and reduced graphene oxide (r-GO). The central air-filled bubble balancer shifts under asymmetric heating. (ii) Schematic cycle of buoyancy- and deformation-mediated feedback loop driving vertical oscillation under constant light illumination. (iii) Time-lapse images of the robot's repeated jumping toward the light under solar simulator illumination.
(h) (i) Reaction scheme of the pH-switch oscillator. (ii) Schematics of a chemomechanical feedback loop coupling hydrogel deformation and proton concentration. (iii) Time-lapse images of a cylindrical hydrogel actuator composed of poly(NIPAAm-co-AAc), suspended in a continuously stirred solution. Light background: shadowscopic image; dark background: directly photographed image. Reaction conditions: KIO3 0.06 M, Na2SO3 0.18 M, H2SO4 0.05 M; flow rate: 240 mL/h.

Chung 2025, Self-regulating hydrogel actuators

Self-Regulated Insulin Systems

Changes in Environmental Factors

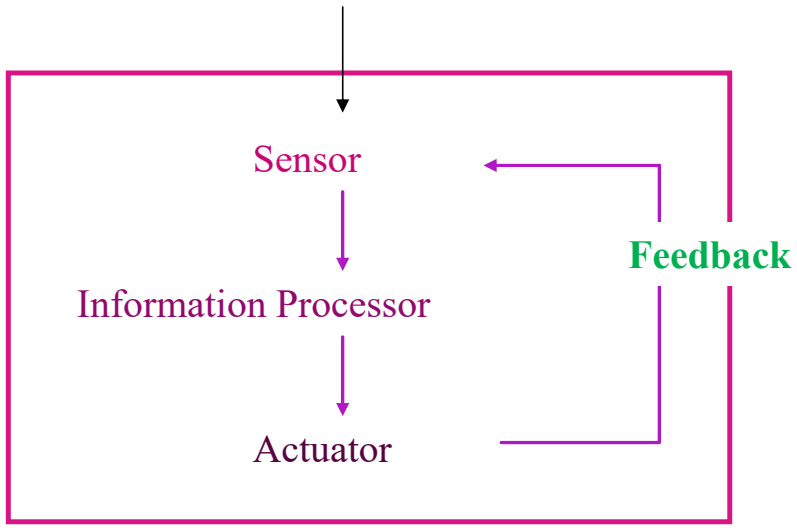

Glucose level changes in blood

Glucose sensor

Determine the amount of insulin to be released

Insulin release

Feedback: Stop insulin release

Specificity, sensitivity
Speed

Accurate dose

Accurate timing

Reversibility
Magnitude
Repeatability

Safety
Biodegradability

Open-loop system

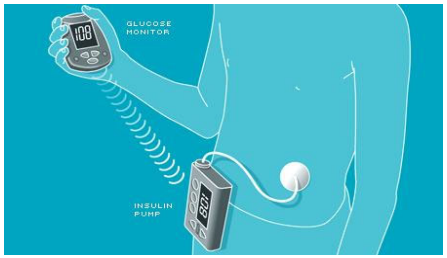

Closed-loop system

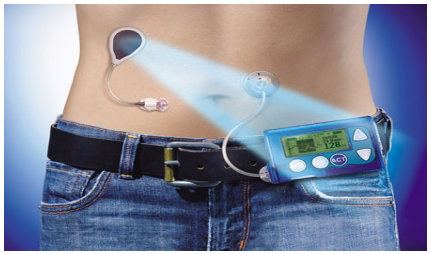

Enzyme-Responsive Systems

Enzyme-Degradable Polypeptide–PolyHIPE

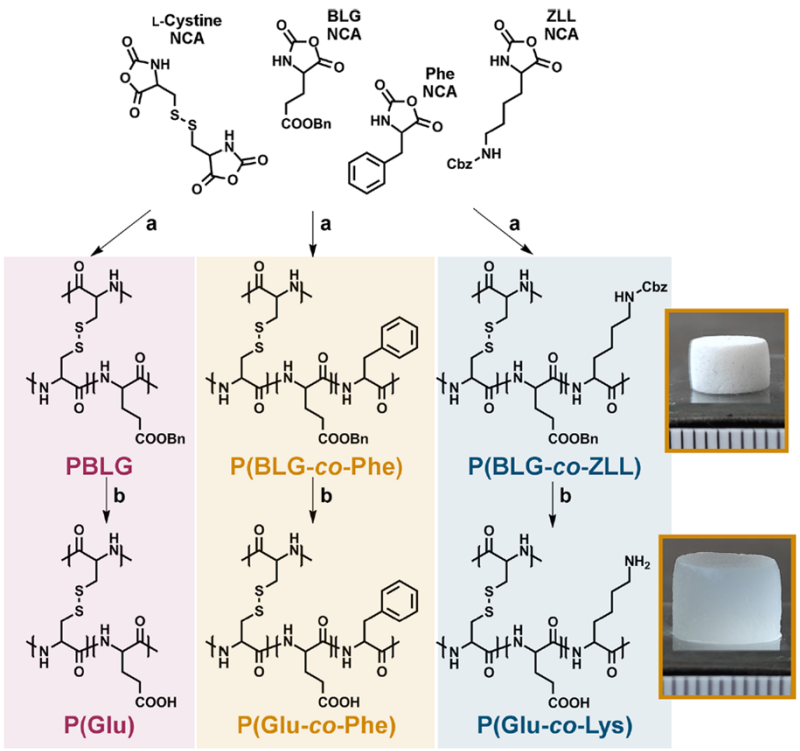

Figure 1. Schematic representation of the preparation of macroporous polypeptide hydrogels by (a) ring-opening polymerization (ROP) of N-carboxyanhydride (NCA) in the continuous phase of high-internal phase emulsions (HIPE), catalyzed with ,N-diisopropylethylamine (DIPEA) and (b) followed by deprotection of the organogels in HBr/TFA. The photographs on the right show dry P(BLG-co-Phe, top) and swollen P(Glu-co-Phe, bottom) at pH 7.5 (scale interval 1 mm).

Onder 2021, Preparation of synthetic polypeptide–polyHIPE hydrogels with stimuli-responsive behavior

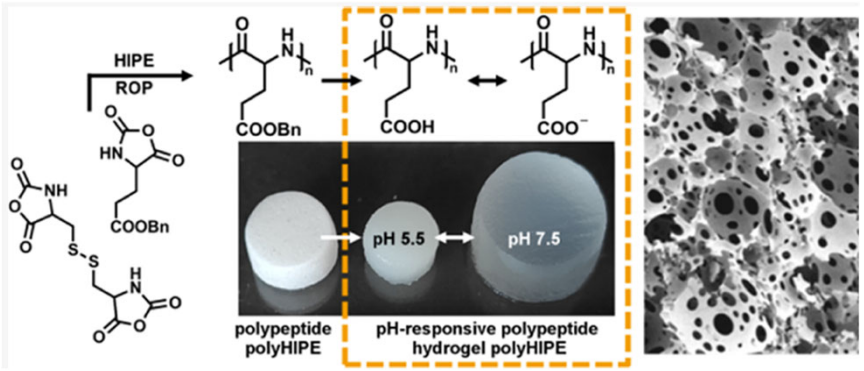

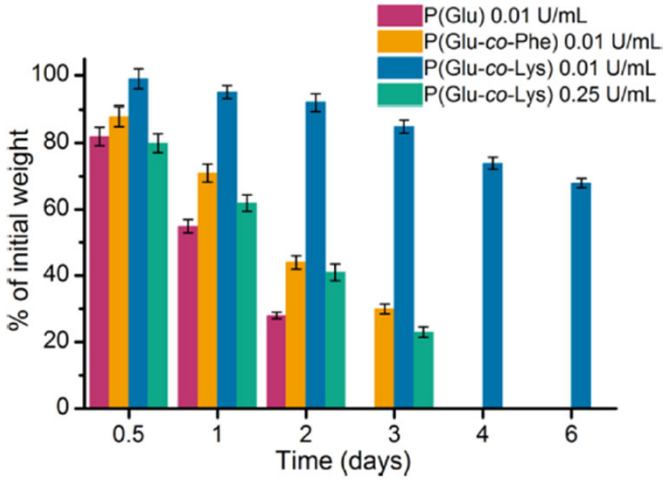

Figure 5. Enzymatic degradation profiles of P(Glu), P(Glu-co-Phe), and P(Glu-co-Lys) hydrogels in 0.01 U/mL protease type XIV solutions at pH 7.5 and 37 °C. P(Glu-co-Lys) hydrogels were also degraded in 0.25 U/mL protease type XIV solution under the same conditions. For each sample, average values of three specimens with standard errors are shown.

Enzyme-responsive Hydrogel Nanoparticles

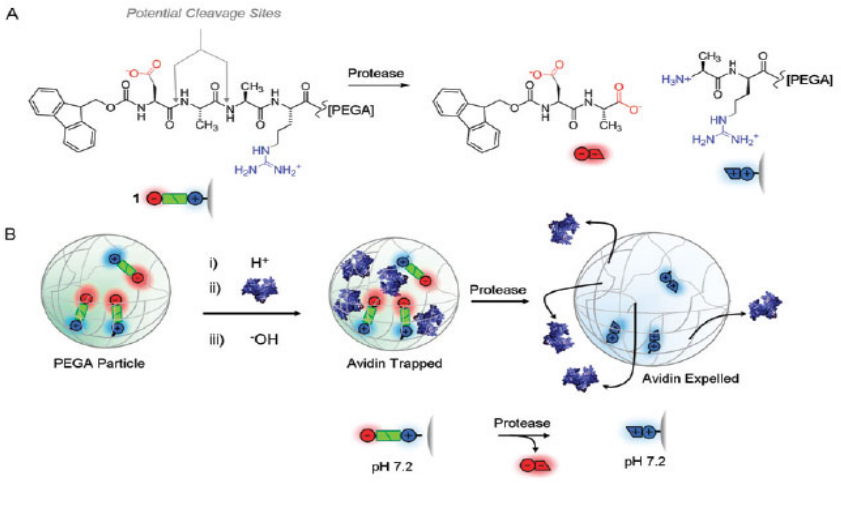

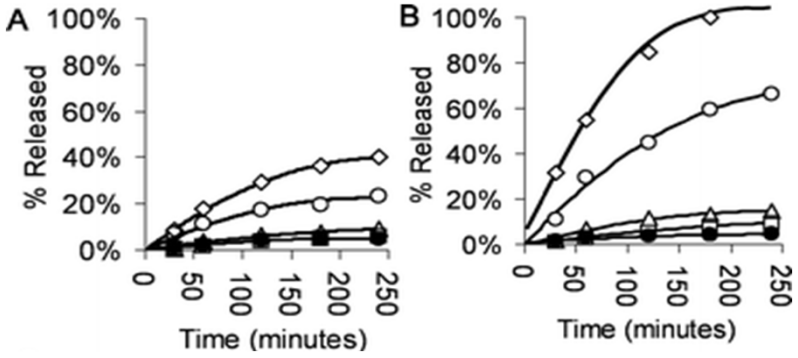

Albumin release

Avidin release

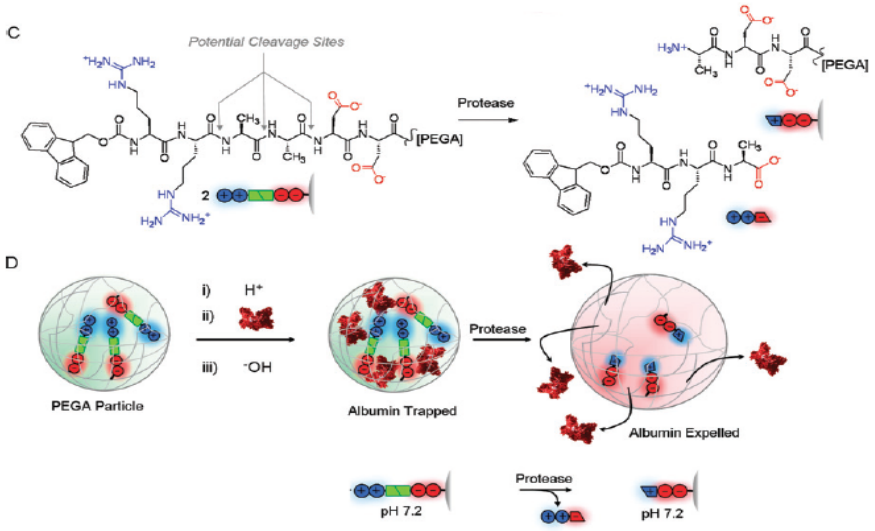

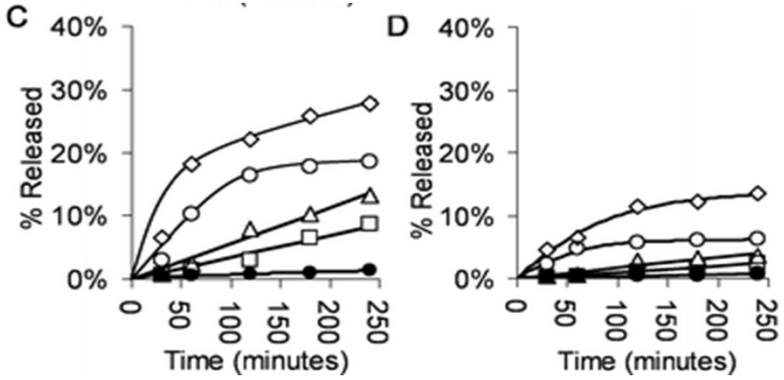

Albumin release

Avidin release

Thornton 2008, Enzyme-responsive hydrogel particles for the controlled release of proteins

Hypoxia-responsive Structures

Hypoxia-Activatable Nanosystems

Hypoxia-activated prodrugs (HAPs), on the other hand, represent a different strategy to deal with the hypoxic tumor microenvironment, turning this problem of hypoxia into a therapeutic target. Now, 11 types of HAPs have entered the clinical trial stage. HAPs are also known as bioreductive prodrugs. Under normoxic conditions, their dormant state will not cause toxic side effects to healthy organs, while in hypoxic regions, HAPs are activated by reductive metabolism and selectively kill hypoxic tumor cells. This is because, in hypoxic tumor cells, the unstable, oxygen-sensitive one-electron reduced HAP intermediates cannot be reversibly oxidized back to parent form as in normoxic conditions. Typical bioreductive drugs include quinones, N-oxides, and nitrocompounds. However, the current mainstream HAPs lack modification sites and do not need extra caging modification. Compared with other types of stimulus-activated prodrugs, the category of HAPs is still on a small scale, and many chemotherapy drugs that have been proven effective have

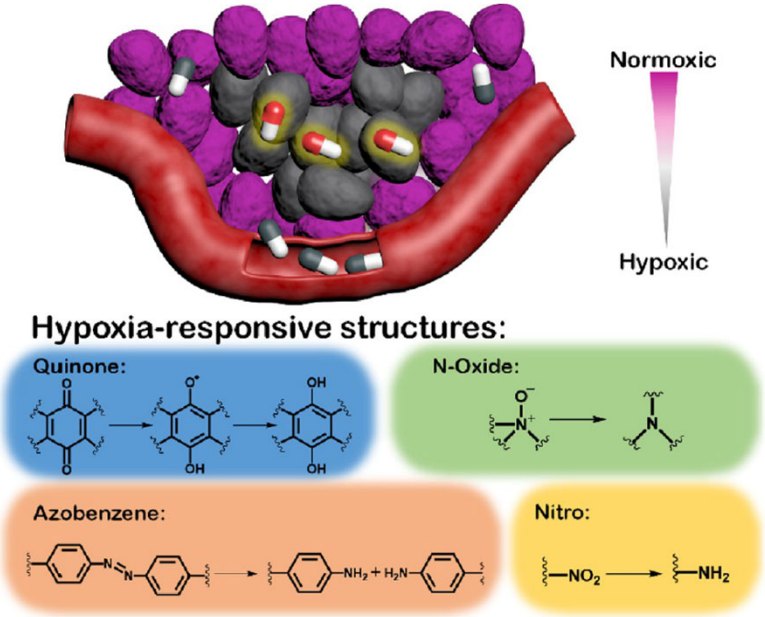

Scheme 4. Schematic illustration of hypoxia responsive prodrugs activated in hypoxic tumor regions and hypoxia-responsive structures for prodrug design.

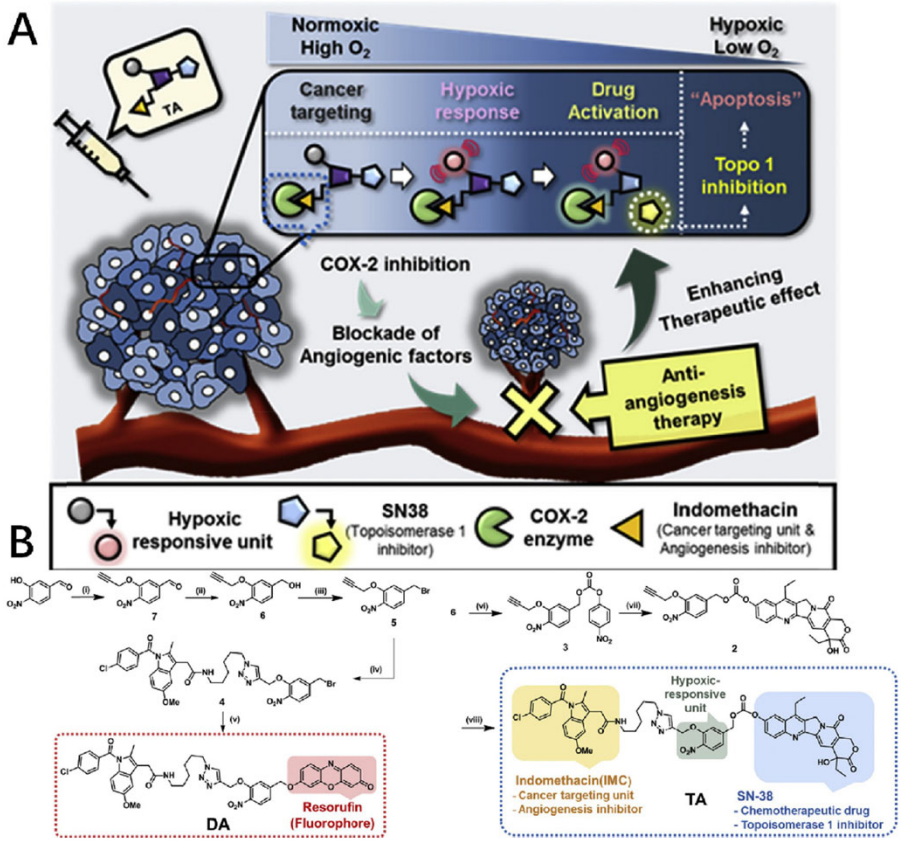

Figure 17. Hypoxia-responsive nitrobenzyl group used for prodrug design: (A) Theranostic prodrug system containing IND as tumor targeting moiety, angiogenesis inhibitor SN-38 as anticancer chemotherapy drug, and resorufin as diagnostic unit was activated in hypoxic tumor microenvironment, which was intensified by suppressing angiogenesis. (B) Synthetic route of nitrobenzyl containing diagnostic unit and therapeutic unit.

Ding 2022, Emerging strategies in stimuli-responsive prodrug nanosystems for cancer therapy

Self-Healing Polymers

Self Healing Plastics

Self-healing refers to the ability of a material to restore functionality after undergoing physical damage.
(Ruiz-Franco 2025, Inducing mechanical self-healing in polymer glasses)

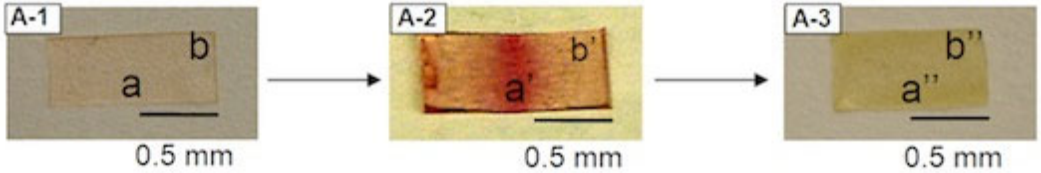

Cell phones, tablets, cars and even weapons systems that can heal themselves when scratched or cracked are no longer confined to science fiction. During the American Chemistry Society's annual conference on Monday, University of Southern Mississippi Professor Marek Urban demonstrated the new material and discussed numerous potential applications. When scratched or cracked, the new plastic responds on a molecular level and regenerates to repair itself without leaving any signs of damage.

Similar developments in the past have made use of embedded capsules with repair material that would fill scratches when a plastic is cracked, but Urban's method repairs broken bonds when an outside stimulus is applied. In the case, sunlight alone can do the trick. "Our new plastic tries to mimic nature, issuing a red signal when damaged and then renewing itself when exposed to visible light, temperature or pH changes,"

Our material is what's called a thermoplastic,"— which means no cross-links are formed during the creation of the plastic. In contrast, plastics that *do* form cross-links are called "thermosets." The key difference between the two, explains Urban, is that once a thermoset cures, its structure is basically set for life, which makes it less-than-optimal for self-healing applications. "Thermoplastics, however, you can heat and reshape however you want," Urban explains.

When we pressed Urban to share more details with us about the bleeding capabilities of his team's latest plastic, he politely declined to go into specifics on the science, explaining that it would have to remain under wraps until a later date.

Nissan recently announced they were creating the world's first self-healing iPhone case that uses their "Scratch Shield" paint originally designed for cars.

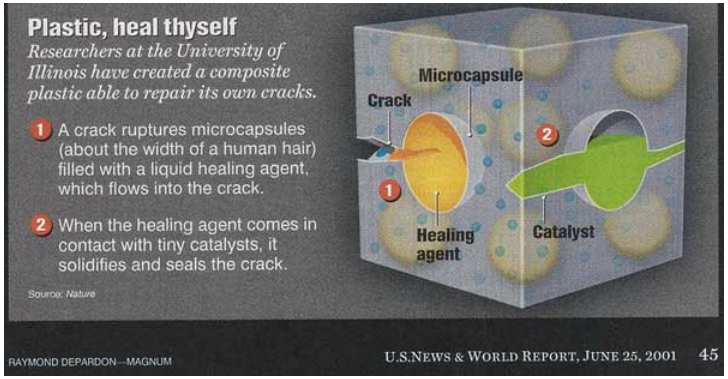

http://www.bgr.com/2012/03/29/scientists-create-self-healing-plastic-the-holy-grail-of-material-science/
http://io9.com/5897475/new-bleeding-healing-plastic-will-be-used-on-airplanes-not-androids

Self Healing Thermosets

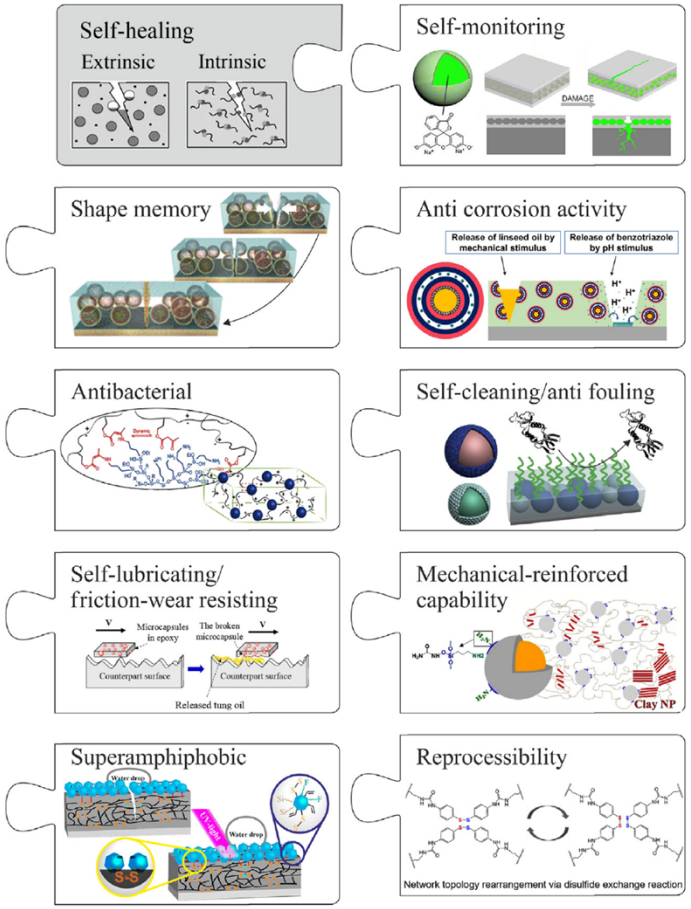

Kutuzova 2022, Self-healing thermosets

FIGURE 22.1 Multifunctional self-healing thermoset systems in composite coating and matrix composite applications [6]: self-healing ability in combination with corrosion protection [40], mechanical reinforcement [50], self-monitoring [51], self-cleaning and superamphiphobic [39,53], self-lubricating [72], antibacterial [73] properties, shape memory [64], and reprocessability [68]. *Modified after Zhang Y, Yuan L, Guan Q, Liang G, Gu A. Developing self-healable and antibacterial polyacrylate coatings with high mechanical strength through crosslinking by multi-amine hyperbranched polysiloxane viadynamic vinylogous urethane. J Mater Chem A 2017;5(32):16889–97. Available from: https://doi.org/10.1039/C7TA04141A; Huang Y, Deng L, Ju P, Huang L, Qian H, Zhang D, et al. Tripleaction self-healing protective coatings based on shape memory polymers containing dual-function microspheres. ACS Appl Mater Interfaces 2018;10 (27):23369–79. Available from: https://doi.org/10.1021/acsami.8b06985; Zhao D, Du Z, Liu S, Wu Y, Guan T, Sun Q, et al. UV light curable self-healing superamphiphobic coatings by photo-promoted disulfide exchange reaction. ACS Appl Polym Mater 2019;1(11):2951–60. Available from: https://doi.org/10.1021/acsapm.9b00656; Chen J-H, Hu D-D, Li Y-D, Meng F, Zhu J, Zeng J-B. Castor oil derived poly(urethane urea) networks with reprocessibility and enhanced mechanical properties. Polymer 2018;143:79–86. Available from: https://doi.org/10.1016/j.polymer.2018.04.013 [68].*

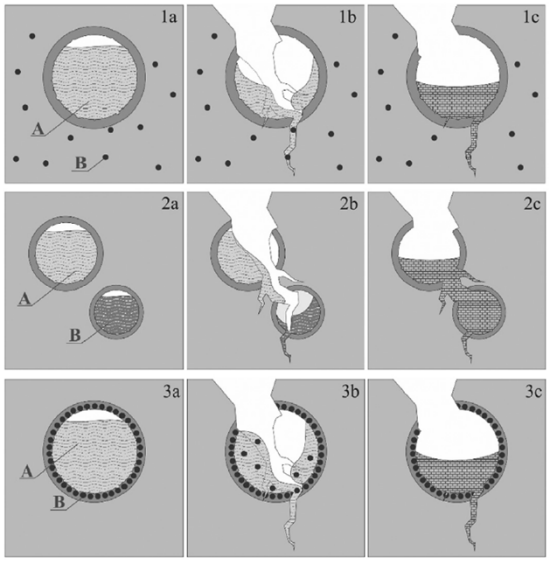

FIGURE 22.19 Self-healing approach based on rupture-release microcapsules: (1) monocapsule or capsule-catalyst systems; (2) dual-capsule system; (3) all-in-one capsule system.

A fundamental problem in the use of materials in general is the loss of their functionality during practical application. This loss of functionality may be due to continuous wear and tear of the materials during their use or to abrupt damage caused by the sudden impact of harmful events such as impact, shock, or pull. This material failure leads to an undesirable collapse in mechanical strength and can cause further consequential damage. An essential strategy to improve the long-term stability of materials under application conditions is the implementation of self-healing properties in the material.

Self Healing Polymers

Self-healing materials open new prospects for more sustainable technologies with improved material performance and devices' longevity.

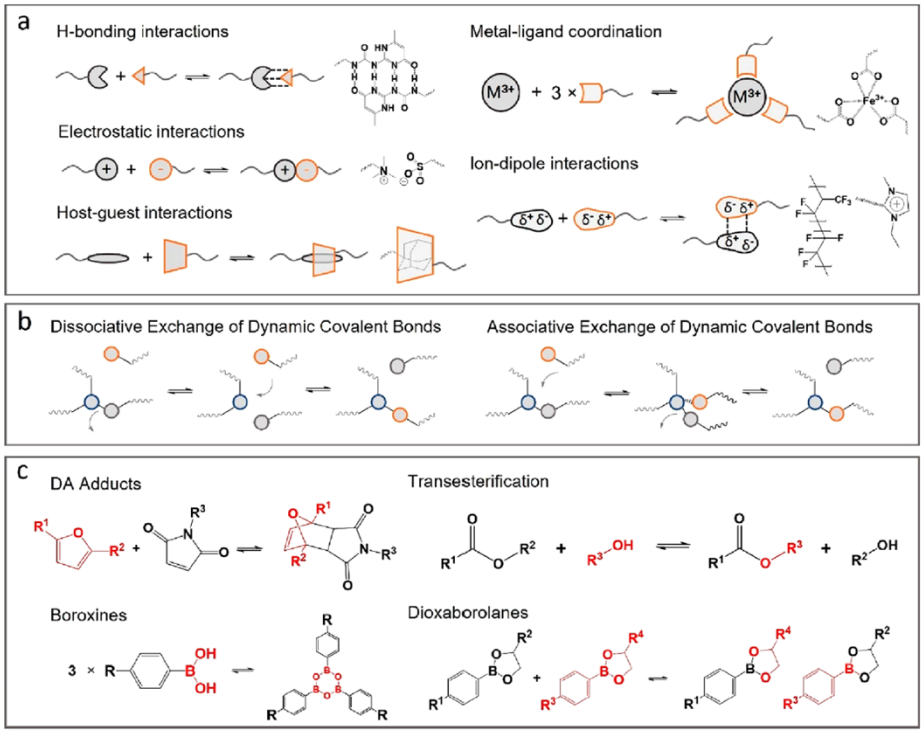

Figure 3. Illustrations of the different dynamic bonds. (a) noncovalent bonds; (b,c) dynamic covalent bonds

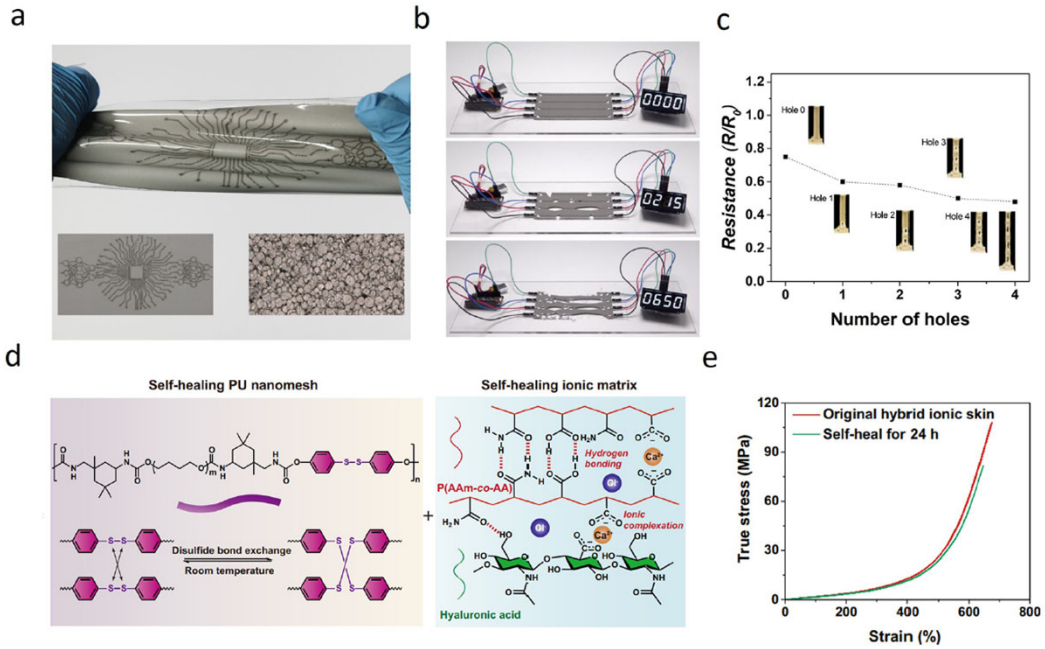

Figure 20. Self-healing polymer for strechable electronics applications. (a) Liquid metal elastomer composite being stretched and twisted with an intricate design of electrically conductive traces. (b) Example of the reconfigurable material (ϕ = 50%) transmitting dc power after severe damage was induced. (c) Photos of hole-punch test during tension; no loss in electrical conductivity was observed after stretch. (d) Schematic illustrations of the hybrid structure and respective self-healing mechanisms of PU nanomesh scaffold and ionic matrix. (e) True stress− strain curves of the original and self-healed hybrid ionic skins.

Li 2022, Intrinsically self-healing polymers- From mechanistic insight to current challenges

Self-Healing at Low/Room Temperature

The strategy for producing materials capable of healing at low temperatures relies on dynamic supramolecular interactions within the polymer matrix, such as **ionic interactions, metal−ligand coordination, and hydrogen bonding, or on the presence of reversible covalent bonds**. In addition, the high mobility of polymer chains in hydrogels and certain elastomers is favorable for imparting self-healing properties at room temperature.

Self-healing in polymers can be broadly categorized into diffusion/mobility-controlled healing and reaction/bond exchange-controlled limited healing.

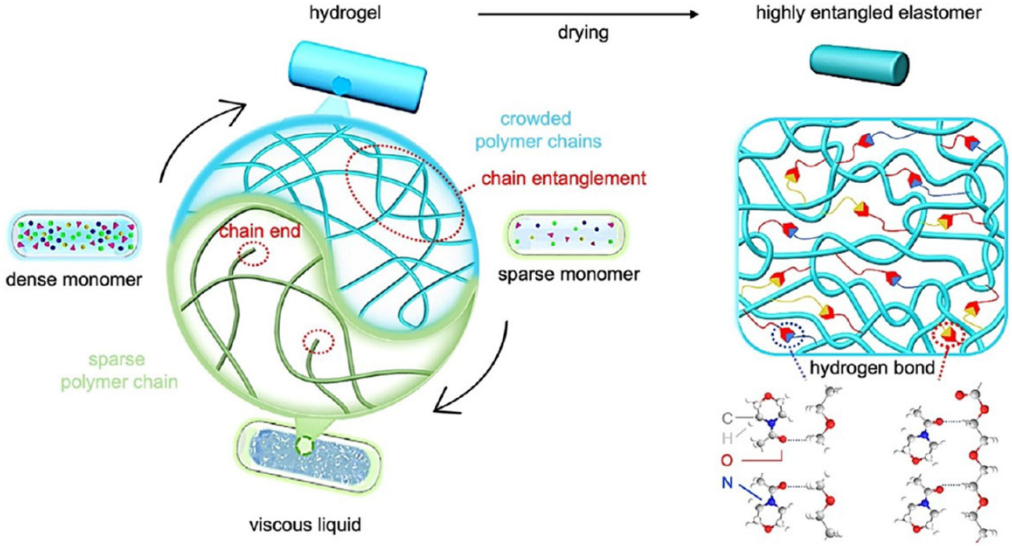

Figure 6. Schematic illustration of the fabrication process of a highly entangled poly((ethylene glycol) methyl ether acrylate-co-acryloylmorpholine) network with densely interlaced polymer chains. (Li, Y.; Feng, X.; Sui, C.; Xu, J.; Zhao, W.; Yan, S. Highly entangled elastomer with ultra-fast self-healing capability and high mechanical strength. Chem. Eng. J. 2024, 479, No. 147689.)

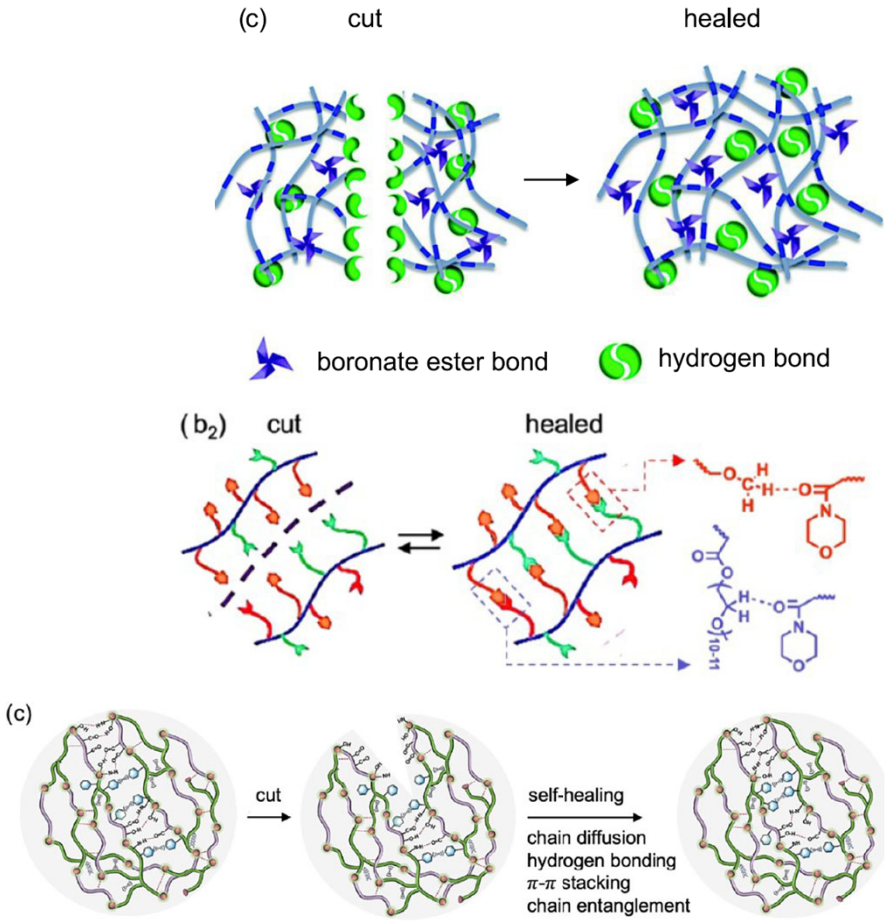

Mantala 2025, Requirements for achieving self-healing at low orroom temperature in polymers

Self-Healing Hydrogels

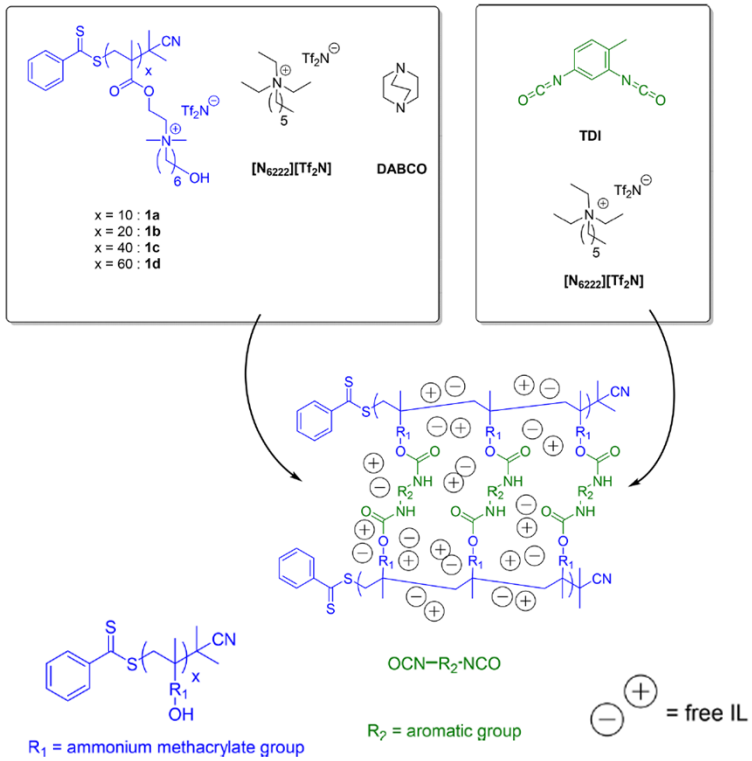

Scheme 1. Structures of curable coating components and resulting cross-linked polyurethane network composite coatings.

ABSTRACT: A peelable gel coating based on a curable ammonium-alcohol ionic liquid (IL) prepolymer has been developed for the decontamination of toxic industrial chemicals (TICs) from porous substrates. The physical properties of these coatings can be tuned by controlling the prepolymer molecular weight (prepared by RAFT polymerization) and by altering the formulation of the initial coating mixture. The initially applied (uncured) solutions can be applied onto porous wood and ceramic substrates with minimal soak-in, and these films cure quickly in situ under ambient conditions. These coatings were tested in a series of assays meant to demonstrate their effectiveness as TIC vapor barriers and materials that absorb liquid TICs from the aforementioned substrates. The coatings were found to suppress ~80% of the vapor released by a TIC simulant (odichlorobenzene) from these substrates and to extract up to 85% of the mass of the originally applied simulant that soaked into these substrates.

Mori 2018, Curable ionic liquid prepolymer-based ion gel coating system

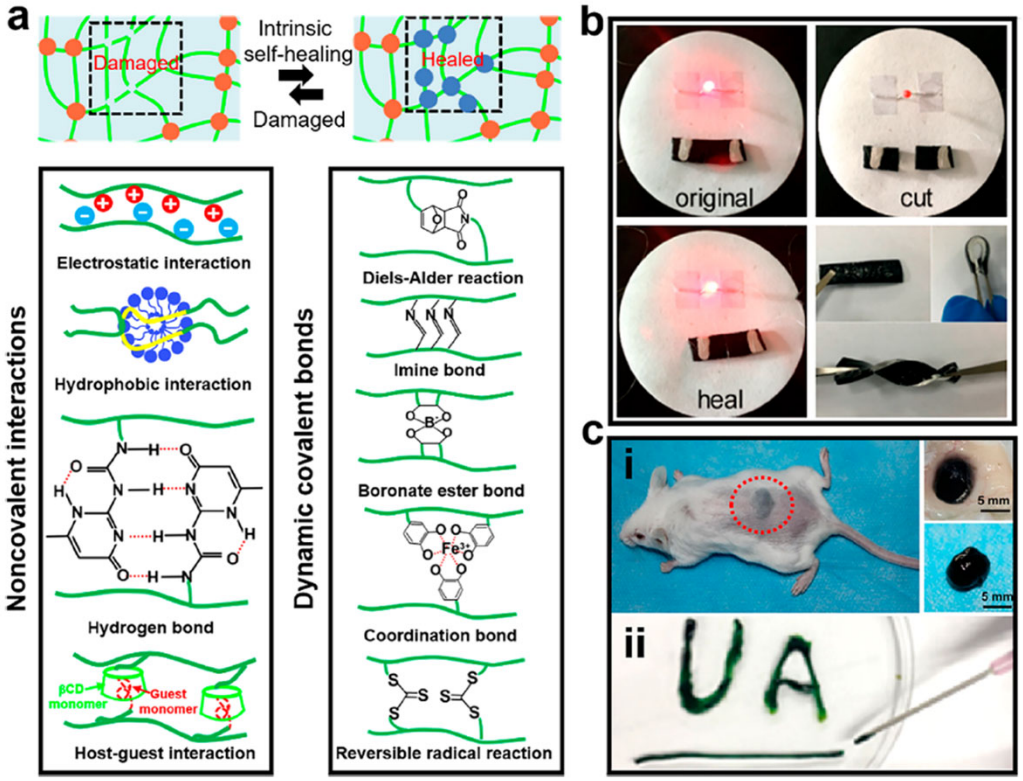

Figure 4. Self-healing and injectable conductive hydrogels. (a) Schematic illustration and mechanism diagram of fabricating intrinsic self-healing conductive hydrogels. (b) Self-healing conductive hydrogel based on transferring CNT film into a repairable carrageenan/PAAm hydrogel. (c) Injectable self-healing conductive hydrogels. The upper panel (i) shows the subcutaneous injection of a Dex-AT/CECS conductive hydrogel. The lower panel (ii) shows an injectable PANI/PSS-UPy conductive hydrogel that can pass through a needle and be molded into different shapes.

Fu 2020, Functional conductive hydrogels for bioelectronics

Self-Healing Hydrogels

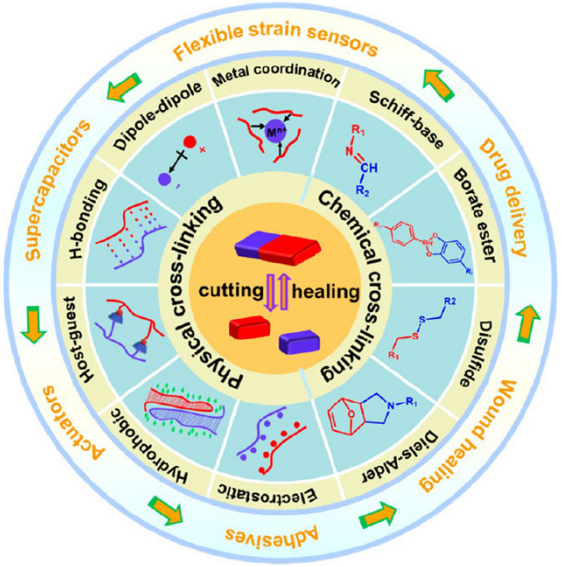

Figure 1. Synthesis and applications of self-healing hydrogels.

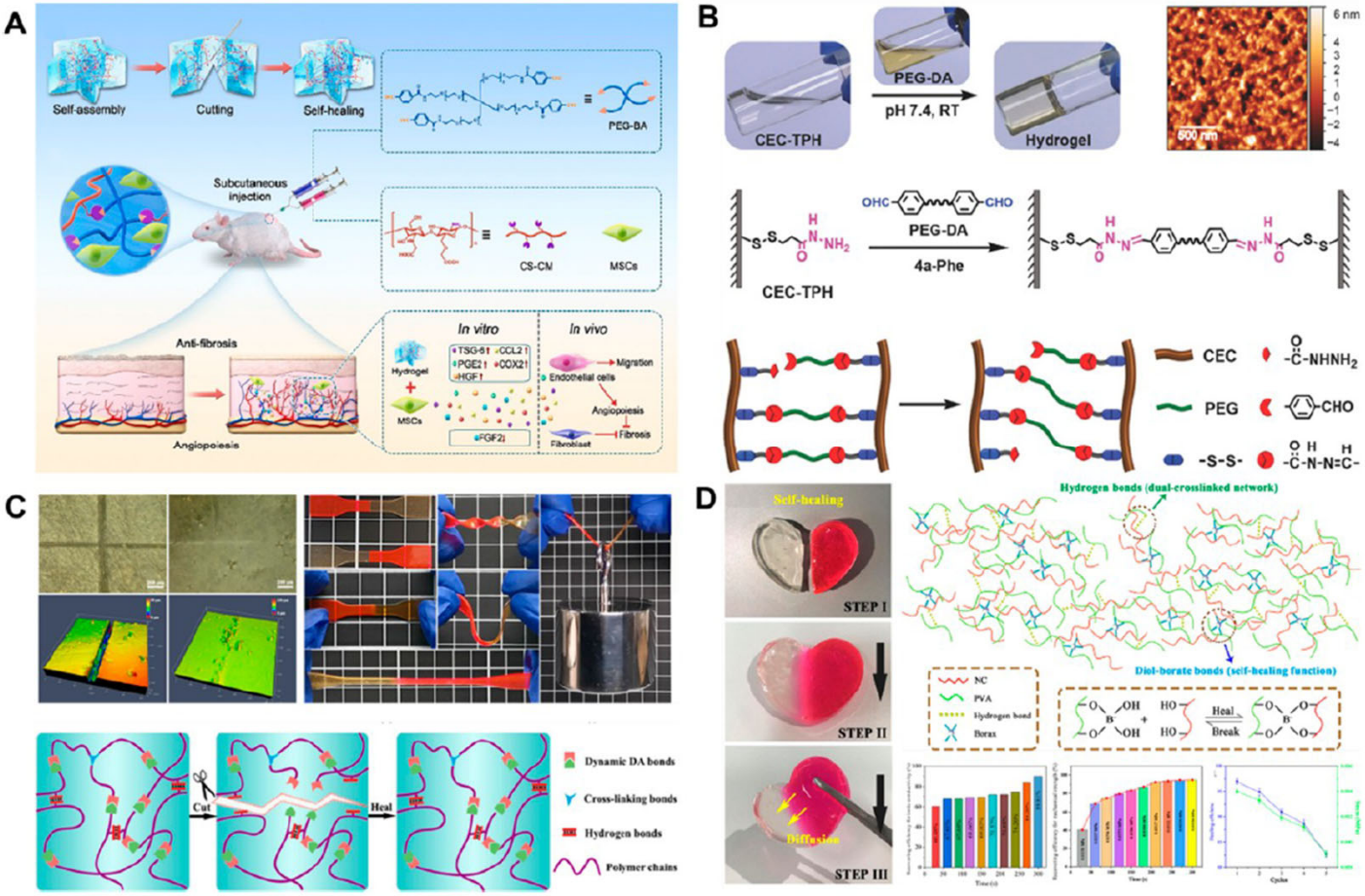

Yin 2023, Self-healing hydrogels- From synthesis to multiple applications

Figure 3. Schematic diagrams of self-healing hydrogels: (A) Obtained from Schiff base bonds. (B) Obtained from acylhydrazone bonds. (C) Obtained from Diels−Alder bonds. (D) Obtained from borate ester bonds.

PVA-Boric Acid Gel

Scheme 1. Reactions of BDBA with Hydroxyl Groups on *x*PVAc Form Mono- (Yellow) and Diesterified (Red) Boronate Species, of which Only the Diesterified Species Lead to Intra- and Interchain Crosslinks between Polymer Chains (Blue)

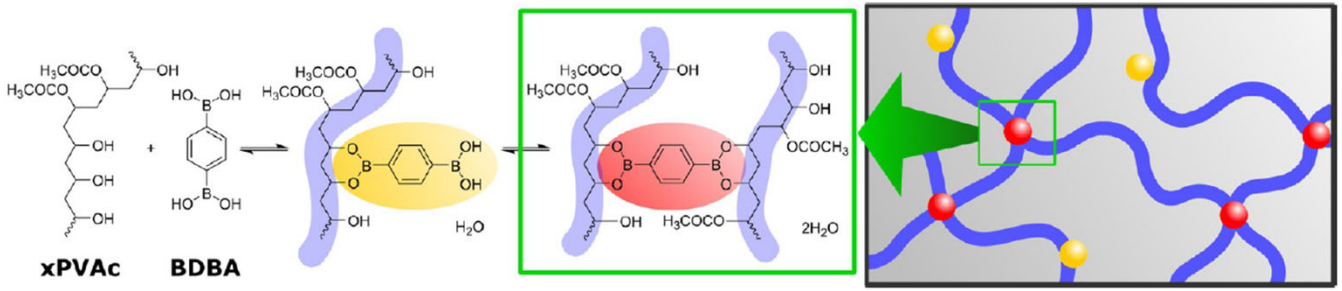

Soft, peelable organogels from 40% hydrolyzed poly(vinyl acetate) (40PVAc) and benzene-1,4-diboronic acid (BDBA).

Figure 1. Gels of 6 wt % 40PVAc/0.3 wt % BDBA in methanol, DMSO, and THF (left to right) 7 days after preparation.

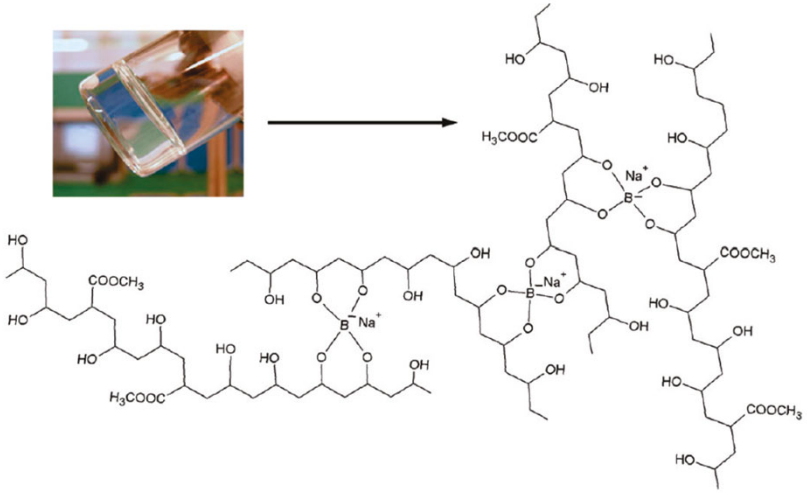

Scheme 1. Representation of the structure of the PVAc network induced by borate cross-links and (top left) an example of a cross-linked aqueous dispersion.

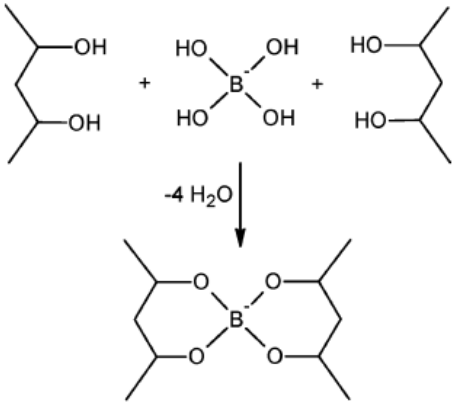

"Peelable" Gels. Hydrogels employing two component gellants, poly(vinyl alcohol) and borate as a crosslinker (PVA-B) have been investigated extensively. The ester cross-links are reversible, so a steady-state concentration of them is established. Initially formed gels "age", allowing conformations of the polymer chains and locations of cross-links to change. Depending upon the length (i.e., average molecular weight) of the PVA chains, the concentrations of PVA and borate ion, temperature, and pH of the aqueous part, the gels can be very stiff or quite malleable.

Duncan 2017, Soft, peelable organogels from partially hydrolyzed poly(vinyl acetate
Natali 2011, Structural and mechanical properties of "peelable" organoaqueous dispersion
Carretti 2009, New frontiers in materials science for art conservation: Responsive gels and beyond.

Vitrimers

A vitrimer is a unique class of polymers that combines the permanent, cross-linked network of thermosets with the thermoplastic-like recyclability and processability of thermoplastics. Vitrimers achieve this through **dynamic covalent bonds** that can exchange and reconfigure at elevated temperatures, allowing the material to be reshaped and reprocessed without losing its network integrity or material properties. This unique behavior makes them highly versatile for applications like self-healing materials, recyclable composites, and advanced 3D printing.

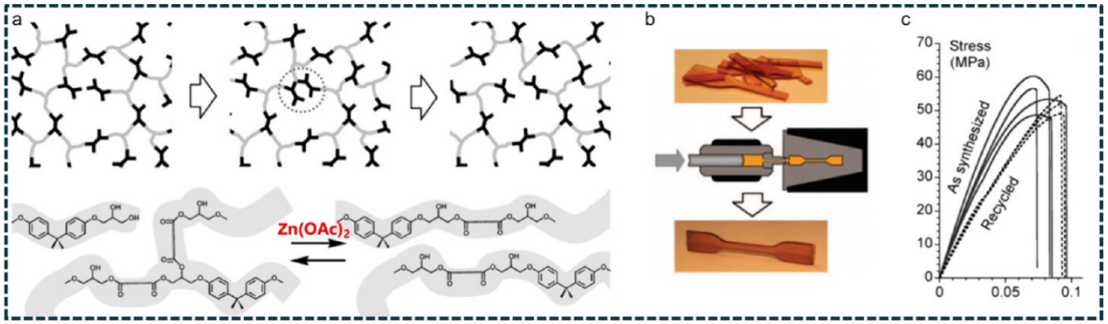

Figure 5. (a) Schematic diagram of the topological rearrangement of the epoxy/carboxylic acid system catalyzed by zinc acetate; (b) Recovery of waste vitrimer by hot pressing; (c) stress−strain curve of the vitrimer before and after recycling.[6] Reproduced or adapted with permission from ref 6. Copyright (2011) The American Association for the Advancement of Science.

The concept of vitrimers emerged from the need to overcome the fundamental limitations of traditional polymers, specifically the permanent cross-linking in thermosets that prevented remelting, reprocessing, or dissolution, as well as the inadequate long-term stability and durability often associated with thermoplastics. The concept of a vitrimer was first proposed in 2011 by Ludwik Leibler and colleagues. It was demonstrated through the introduction of zinc acetate or zinc acetylacetonate catalysts into a bisphenol A glycidyl ether (DGEBA)/carboxylic acid system.6

(6) Montarnal, D.; Capelot, M.; Tournilhac, F.; Leibler, L. Silica-like malleable materials from permanent organic networks. Science 2011, 334, 965−968.

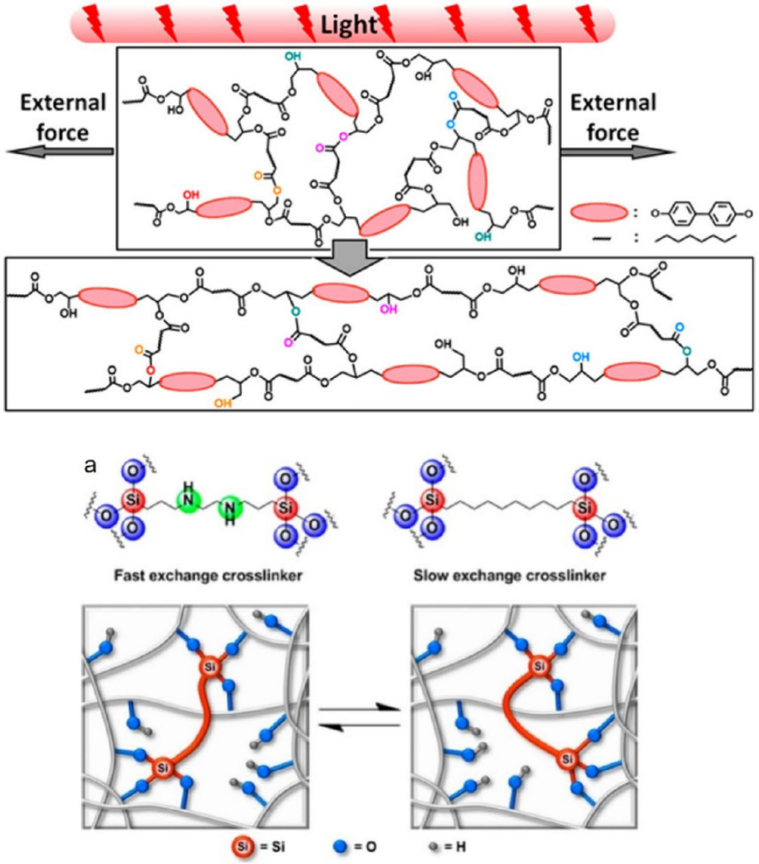

Ye 2025, Vitrimer as a sustainable alternative to traditional thermoset- recent progress and future prospective

Vitrimers

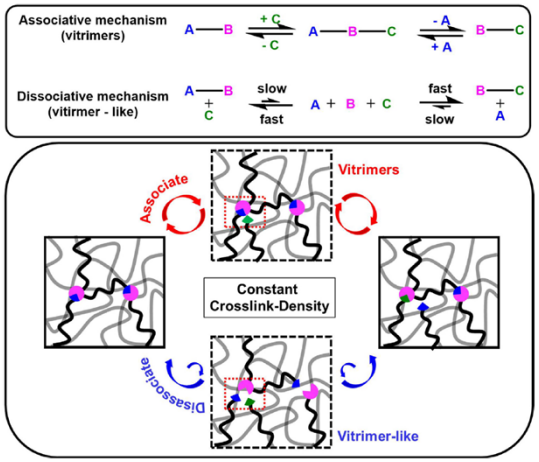

Scheme and image illustration of vitrimers and vitrimer-like materials. The crosslink density of these materials is almost constant at different temperature

Covalent Adaptable Networks (CANs) are polymeric materials with covalent crosslinks which become reversibly dynamic when a specific stimuli such as heat, catalyst, light, or pH is applied. In the absence of the corresponding stimuli, their cross-linked structure can impart to them thermoset-like properties such as increased strength and durability.

Vitrimers are a new class of CANs. In contrast to CANs, the crosslinks of these vitrimers are associative in nature, with **their crosslinks being broken only when new bonds are formed**. As a result, the crosslink density of associative CANs can be considered almost constant regardless of external stimuli.

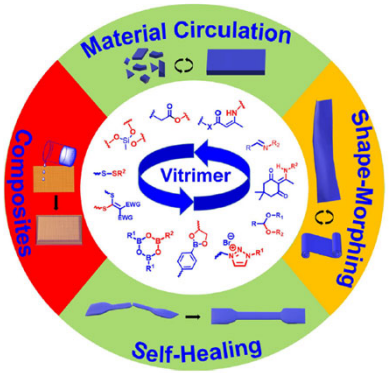

Schematic illustration of dynamic covalent bonds used in vitrimeric materials and their applications.

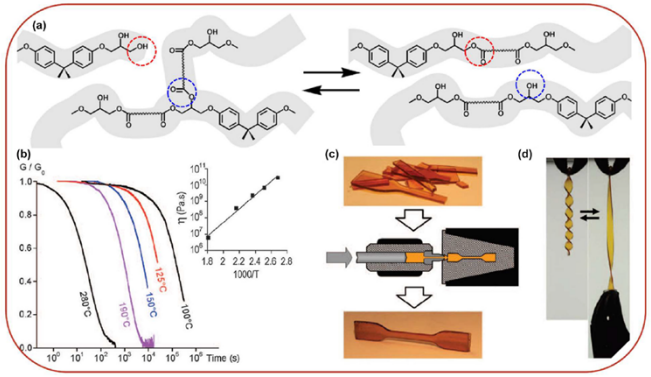

(a) Illustration of transesterification in hydroxyl-ester networks. (b) Normalized stress relaxation at different temperatures. The inset shows the temperature variation of zero-shear viscosity. (c) Reprocessing the broken pieces in an injection machine to recover its initial aspect and properties. (d) Reshaping the sample into a fusilli-shape.

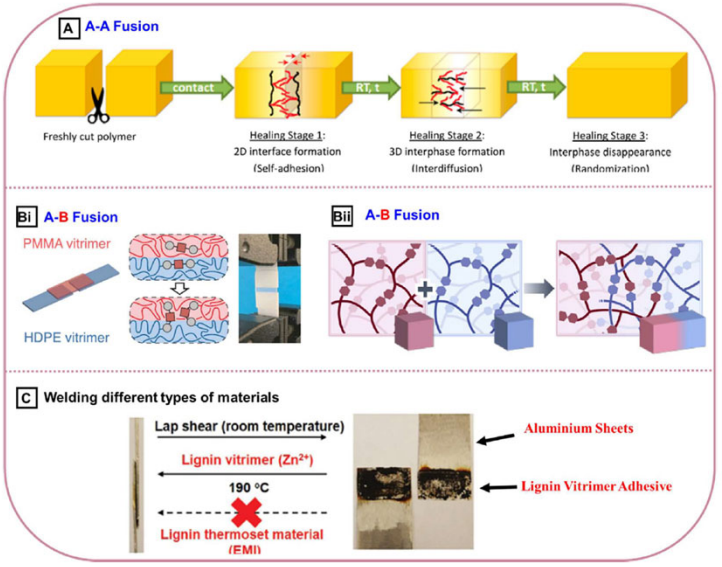

Schematic illustration of (a) A–A fusion, (b) A–B fusion, and (c) welding different types of materials using vitrimers.

Zheng 2021, Vitrimers- Current research trends andtheir emerging applications

Vitrimers

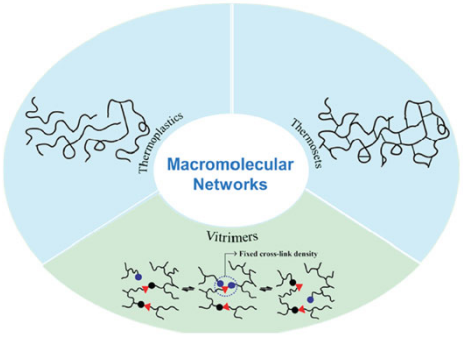

Figure 1. The macromolecular networks of thermoplastics, thermosets and vitrimers. Zhang 2022, Recycling strategies for vitrimers

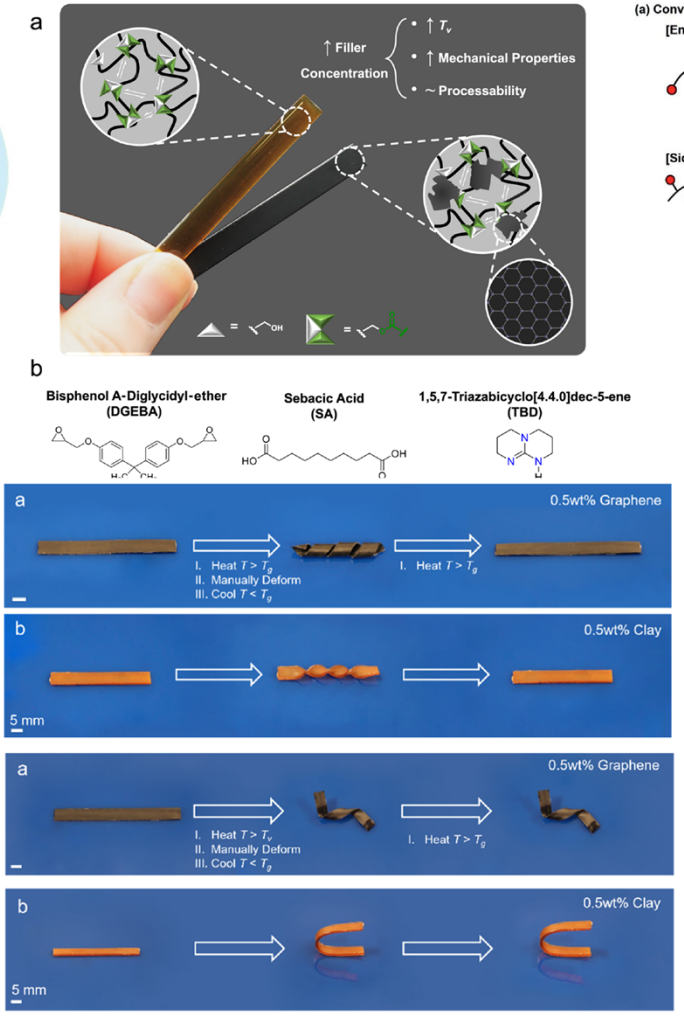

Hubbard 2022, Vitrimer vomposites- Understanding the role of filler in vitrimer applicability

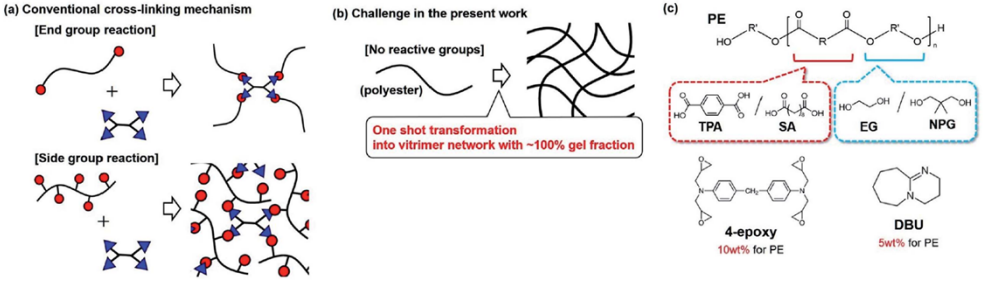

Fig. 1 Schematic representation of (a) conventional cross-linking mechanisms, (b) the challenge in the present work, and (c) components of the present vitrimer preparation.

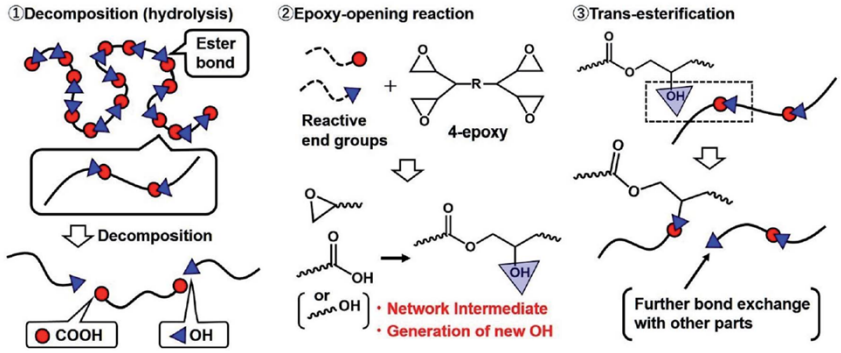

Fig. 3 Probable cross-linking mechanism derived from the experimental results.

Kimura 2022, One-shot transformation of ordinary polyesters into vitrimers- decomposition triggered cross-linking and assistance of dynamic covalent bonds

Vitrimers

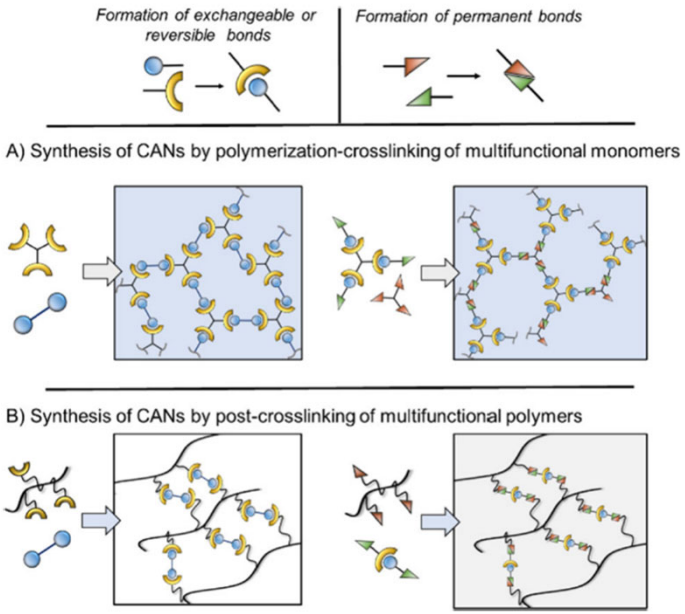

Figure 1. Synthetic strategies for the preparation of CANs A) by polymerization/cross-linking of multifunctional monomers and B) by cross-linking of functional polymer backbone.

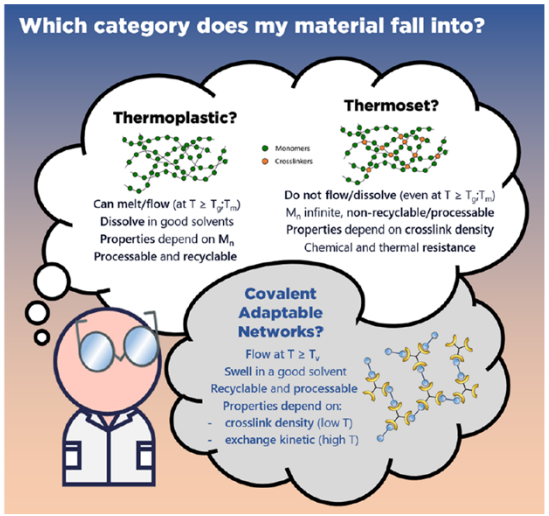

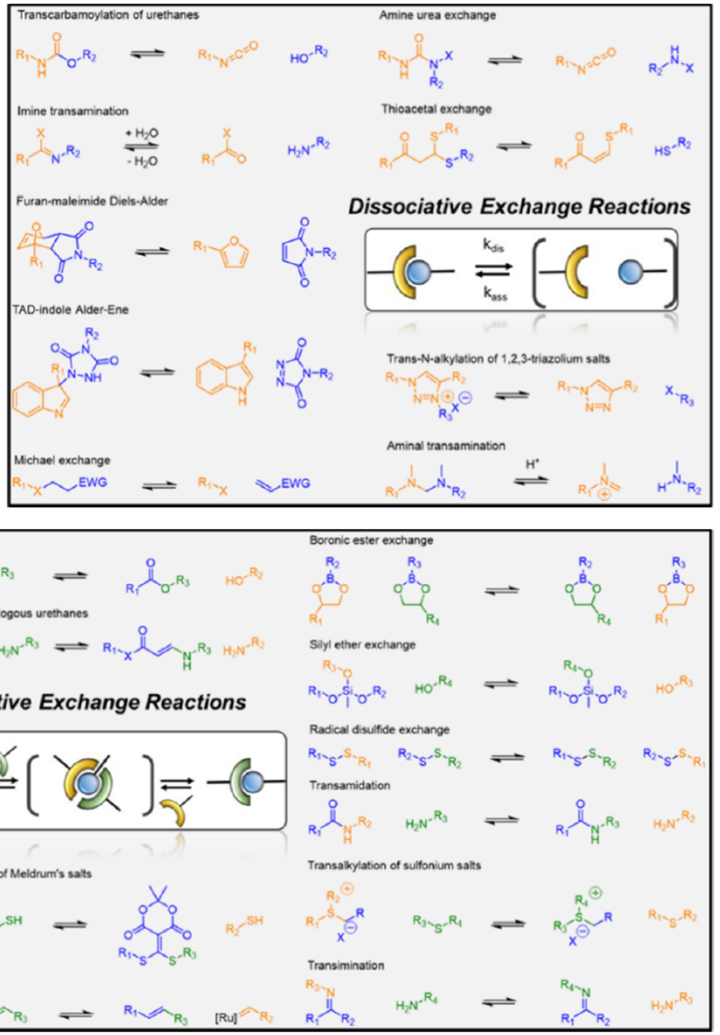

Figure 2. Typical covalent exchange reactions used in the Covalent Adaptable Network design.

Berne 2025, How to characterize covalent adaptable networks

Vitrimers

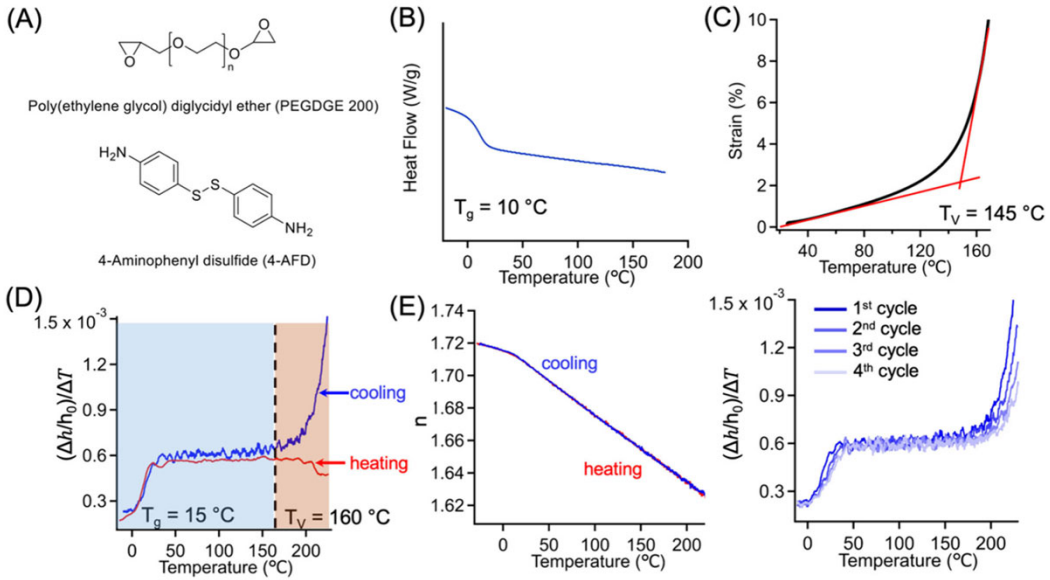

Figure 1. (A) Chemical structure of PEGDGE and 4-aminophenyl disulfide for preparing catalyst-free vitrimers. (B) DSC results (obtained from the 2nd heating cycle) for bulk vitrimer samples. (C) Non-isothermal creep measurement for disulfide-based vitrimer with an applied stress of 5 kPa. (D) Plot of $\frac{\Delta h / h_0}{\Delta T}$ vs temperature for disulfide-based vitrimer films obtained during cooling (blue) and heating (red) cycles. The change from light blue region to orange region represents the transition at T_v. (E) Refractive index (n) as a function of temperature for disulfide-based vitrimer films derived obtained during cooling (blue) and heating (red) cycle. (F) Plot of $\frac{\Delta h / h_0}{\Delta T}$ vs temperature for disulfide-based vitrimer films as a function of cycle number. The vitrimer film thickness was approximately 200 nm.

Figure 1. Synthetic strategies for the preparation of CANs A) by polymerization/cross-linking of multifunctional monomers and B) by cross-linking of functional polymer backbone.

Wang 2025, Ellipsometric characterization of network topology transition in vitrimers

Vitrimers are an emerging class of covalent adaptable networks, which can be reprocessed at elevated temperatures while preserving crosslinking density. In these systems, the onset temperature of bond exchange is often dubbed "topology freezing transition temperature (T_v)" and is characterized by a sharp reduction in material viscosity. Here, we provide a universal and external stress-free method to determine T_v in submicrometer ($<\mu$m) supported films, by measuring their thickness change as a function of temperature by ellipsometry. This study investigated a range of vitrimer systems, including catalyst-free, externally catalyzed, and internally catalyzed networks, to confirm the general applicability of our approach. We demonstrate the high sensitivity of ellipsometry in detecting changes in the apparent thermal expansion behaviors of vitrimer films, specifically linked to the onset of bond exchange in vitrimers, which is distinguished from most other methods that primarily capture macroscopic thermomechanical behaviors. Our results also suggest that the mechanism by which ellipsometry reveals the T_v in vitrimers is governed by their change in relaxation dynamics, which are fundamentally distinct from the thermodynamically driven glass transition observed in conventional polymers. We believe the ellipsometric method can not only streamline the characterization of T_v in vitrimers but also provide deeper insights into their dynamic exchange mechanisms by distinguishing between their microscopic and macroscopic properties.

Vitrimers

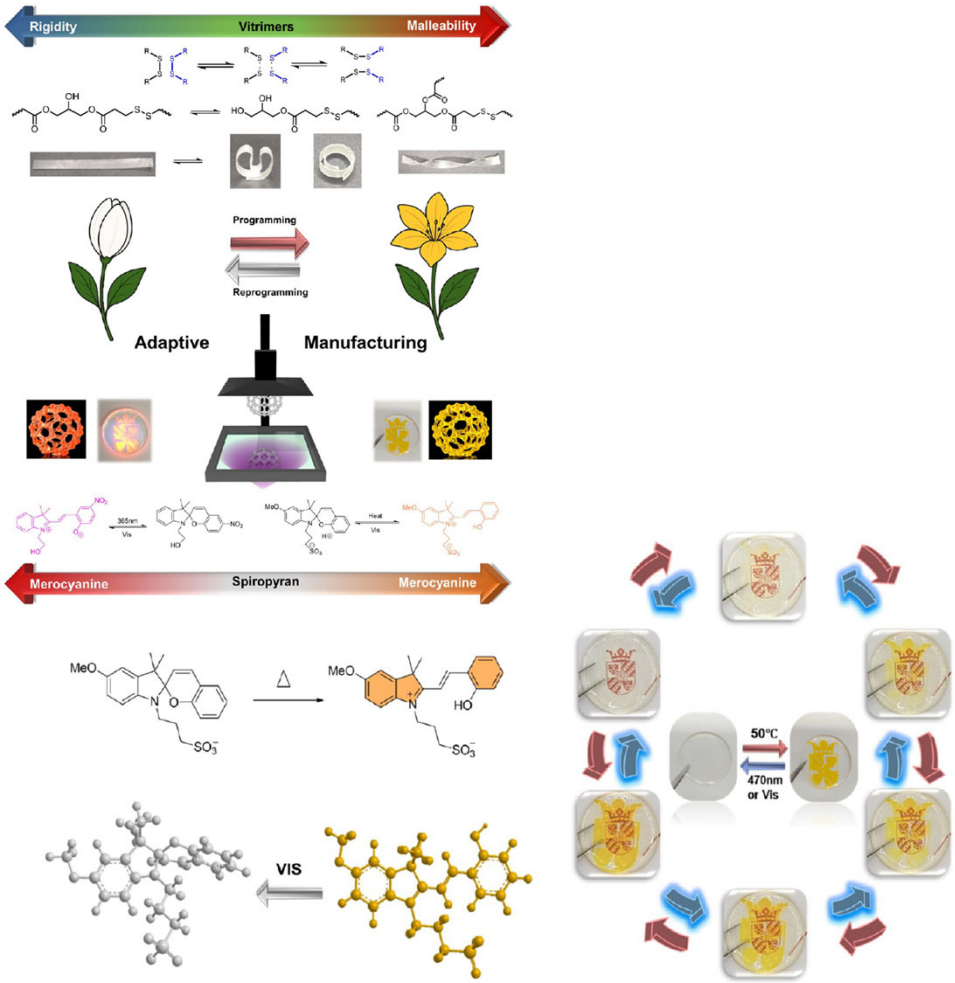

Figure 5. (a) Thermal isomerization from SP2 to its more thermodynamically stable open protonated merocyanine form. (b) Thermal response color change cycle for the university logo, diameter: 25 mm.

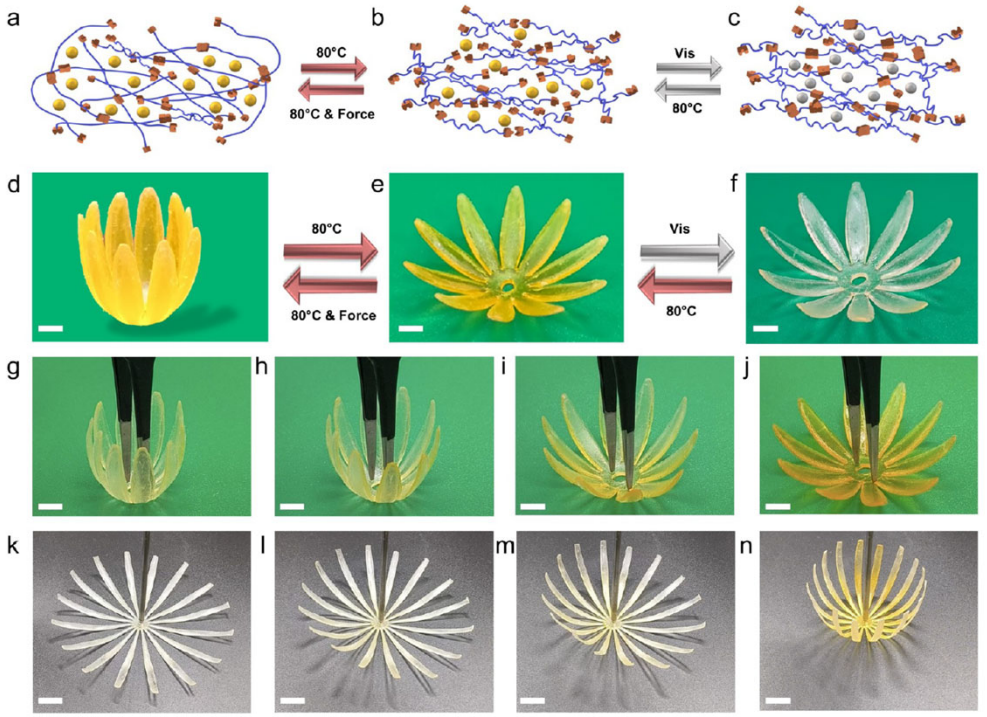

Figure 6. (a–c) Schematic representation of network topological isomerization and thermochromic transition within the 3D printed structures. Blue lines indicate polymer chains, yellow dots represent SP2 molecular switches, and squares (either attached or detached) represent dynamic covalent bonds (DCBs) in the polymer network. (d–f) Overview of the transition from open to closed and from colorless to yellow; scale bar, 5 mm. (g–j). Printed flower bloom at 80 °Cand color transition process; scale bar, 5 mm. (k-n) Printed flower bloom at 80 °C and color transition process; scale bar, 6 mm.

Zhang 2025, 3D-printed dual photo- and thermally responsive materials for smart adaptability

Smarter but Not Smart Enough

Getting Smarter

- Smarter materials:
  - proteins, peptides, DNAs, hybrid materials, affordable degradable materials
- Smarter response:
  - multiple stimuli-sensitivity, new stimuli, fast-responsive
- Smarter function:
  - cell-free enzyme synthesis, microfabrication, extracellular matrix, bioseparation, actuation, sensor

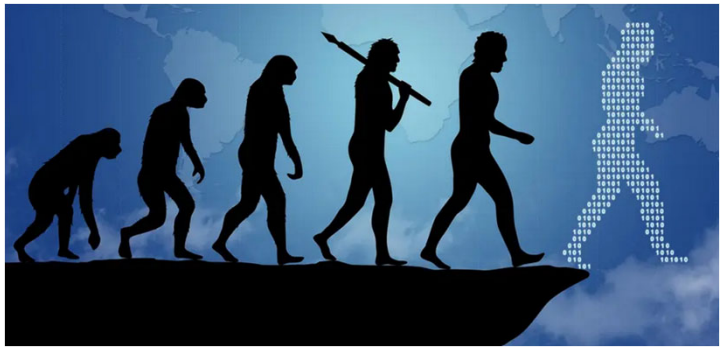

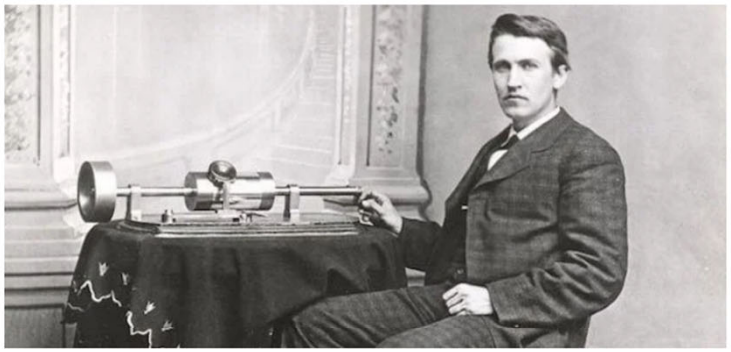

National Park Service, Thomas Edison National Historical Park

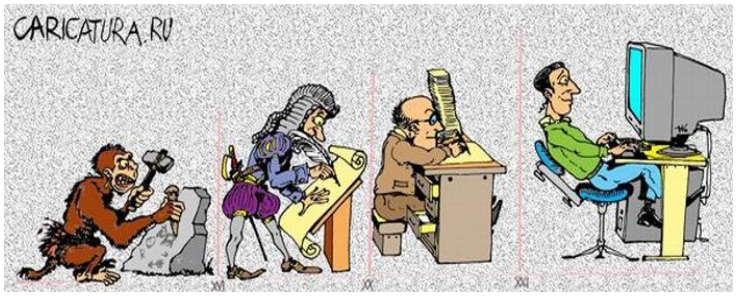

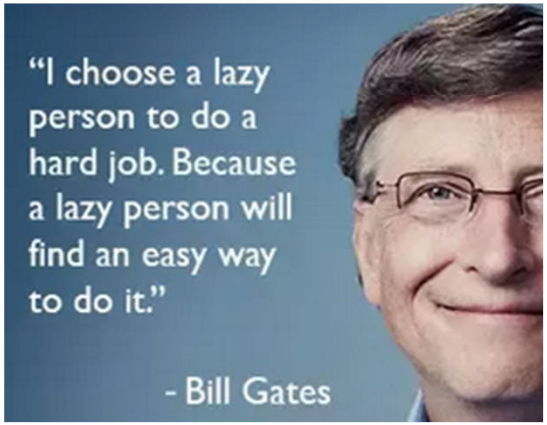

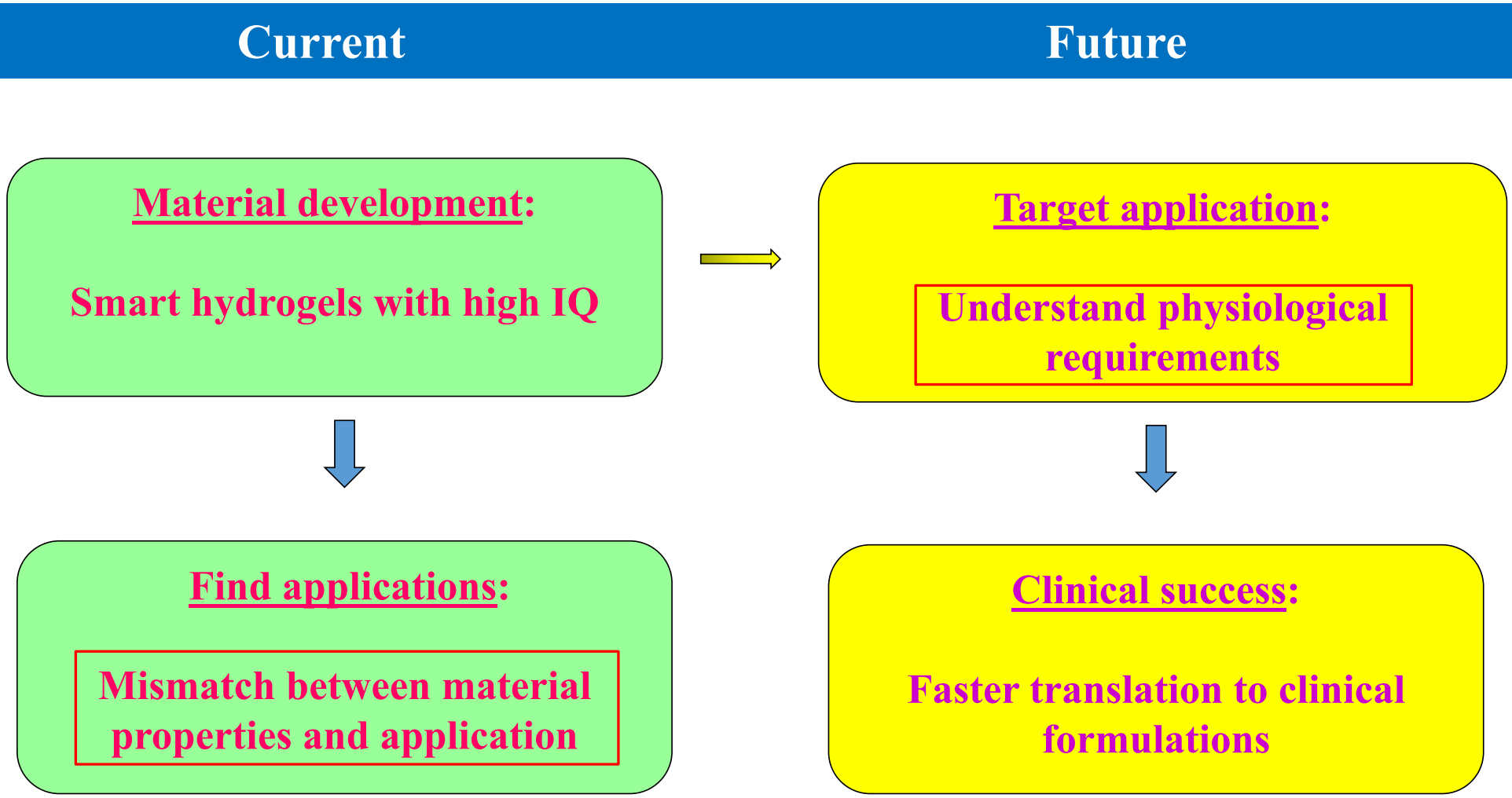
Current
Future
Material development:
Smart hydrogels with high IQ
Target application:
Understand physiological requirements
Find applications:
Mismatch between material properties and application
Clinical success:
Faster translation to clinical formulations

Getting Smarter

REVIEW ARTICLE OPEN

Smart nanoparticles for cancer therapy

Leming Sun[1,2], Hongmei Liu[1], Yanqi Ye[3], Yang Lei[2], Rehmat Islam[2], Sumin Tan[1], Rongsheng Tong[1], Yang-Bao Miao[4]✉ and Lulu Cai[1]✉

Smart nanoparticles, which can respond to biological cues or be guided by them, are emerging as a promising drug delivery platform for precise cancer treatment. The field of oncology, nanotechnology, and biomedicine has witnessed rapid progress, leading to innovative developments in smart nanoparticles for safer and more effective cancer therapy. In this review, we will highlight recent advancements in smart nanoparticles, including polymeric nanoparticles, dendrimers, micelles, liposomes, protein nanoparticles, cell membrane nanoparticles, mesoporous silica nanoparticles, gold nanoparticles, iron oxide nanoparticles, quantum dots, carbon nanotubes, black phosphorus, MOF nanoparticles, and others. We will focus on their classification, structures, synthesis, and intelligent features. These smart nanoparticles possess the ability to respond to various external and internal stimuli, such as enzymes, pH, temperature, optics, and magnetism, making them intelligent systems. Additionally, this review will explore the latest studies on tumor targeting by functionalizing the surfaces of smart nanoparticles with tumor-specific ligands like antibodies, peptides, transferrin, and folic acid. We will also summarize different types of drug delivery options, including small molecules, peptides, proteins, nucleic acids, and even living cells, for their potential use in cancer therapy. While the potential of smart nanoparticles is promising, we will also acknowledge the challenges and clinical prospects associated with their use. Finally, we will propose a blueprint that involves the use of artificial intelligence-powered nanoparticles in cancer treatment applications. By harnessing the potential of smart nanoparticles, this review aims to usher in a new era of precise and personalized cancer therapy, providing patients with individualized treatment options.

Signal Transduction and Targeted Therapy (2023)8:418 ; https://doi.org/10.1038/s41392-023-01642-x

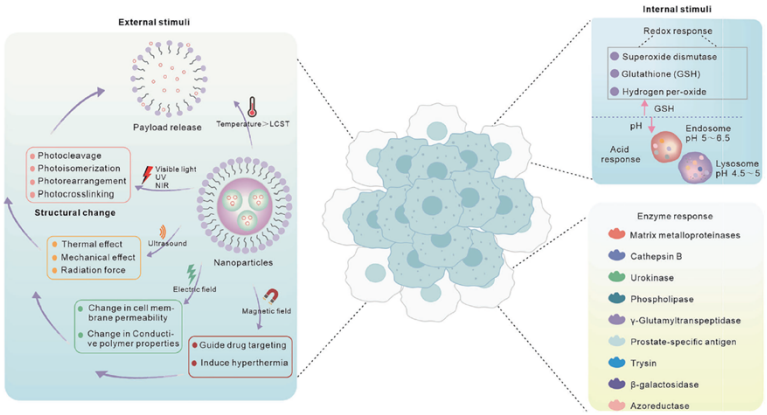

Sun 2023, Smart nanoparticles for cancer therapy

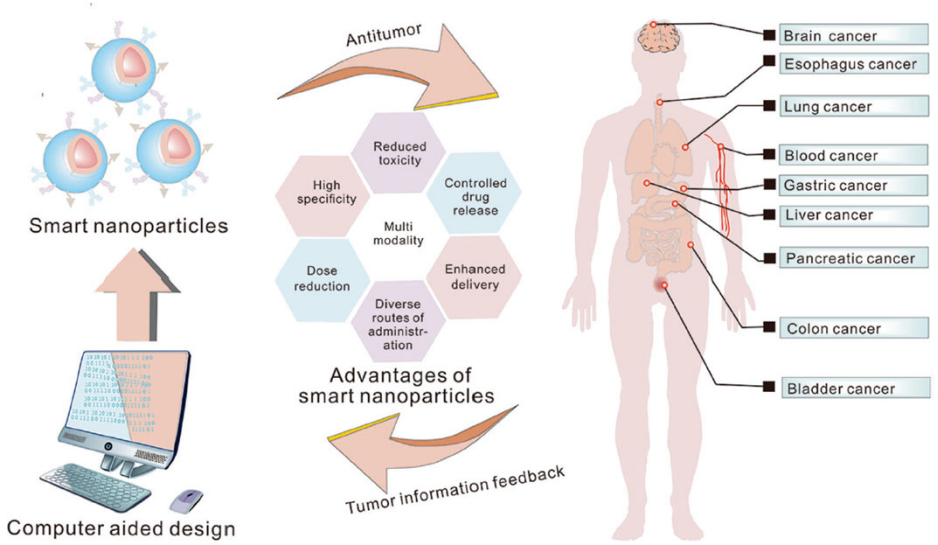

Fig. 1 Schematic illustration of smart nanoparticles for cancer treatment

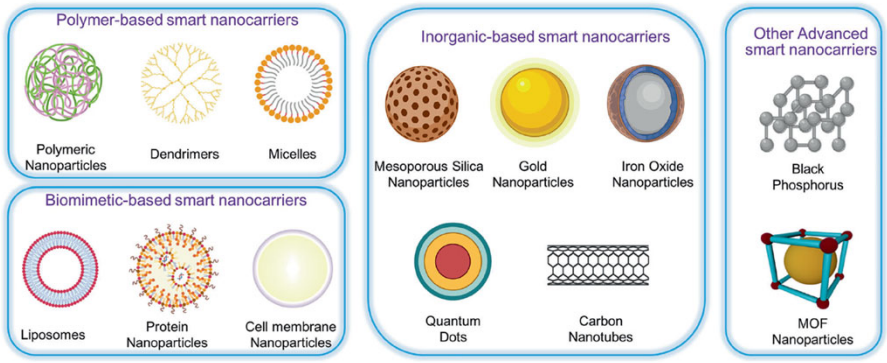

Fig. 2 Nanocarriers for smart nanoparticles

Mimicking Biosystems

Biomimetics

"Study of Materials, Structures, and Processes designed through eons of evolution of life to inspire and improve the engineering & design of artificial materials, man-made structures & processes." (Marc J. Madou, *Fundamentals of Microfabrication. The science of Miniaturization*. 2nd Edition. CRC Press. 2002).

Artificial materials that function as biological entities do.

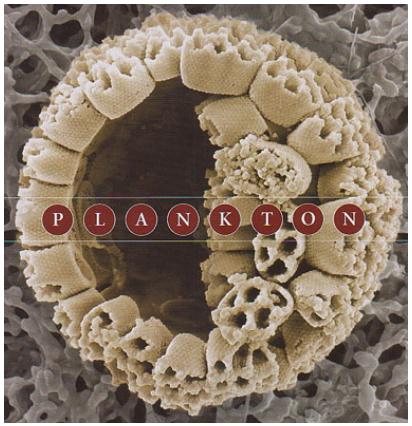

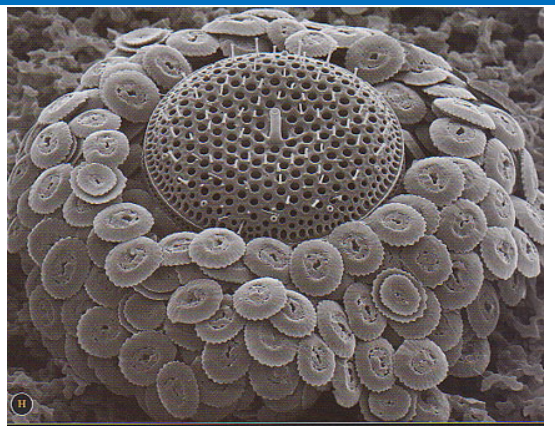

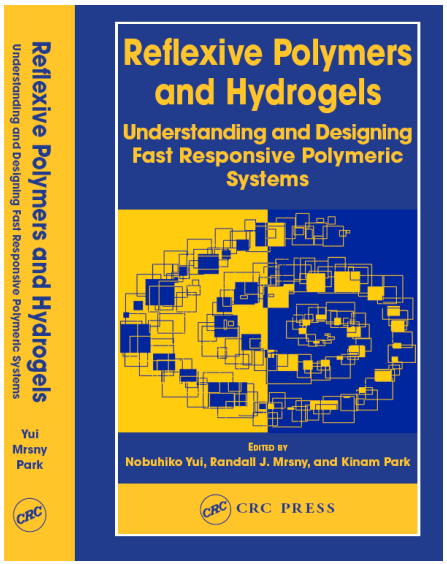

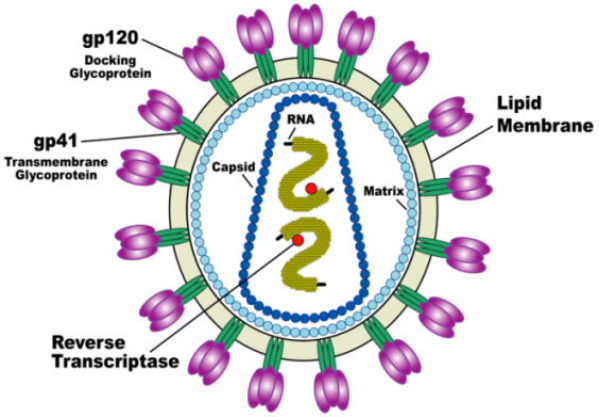

Natural Systems	Synthetic Systems
Efficacy, Simplicity (Bottom-up)	Diffusion, Selectivity (Top-down)
⇩	⇩
Survival	Miniaturization
⇩	⇩
Biological Need	Clinical Efficacy

The Invisible Gorilla Experiment

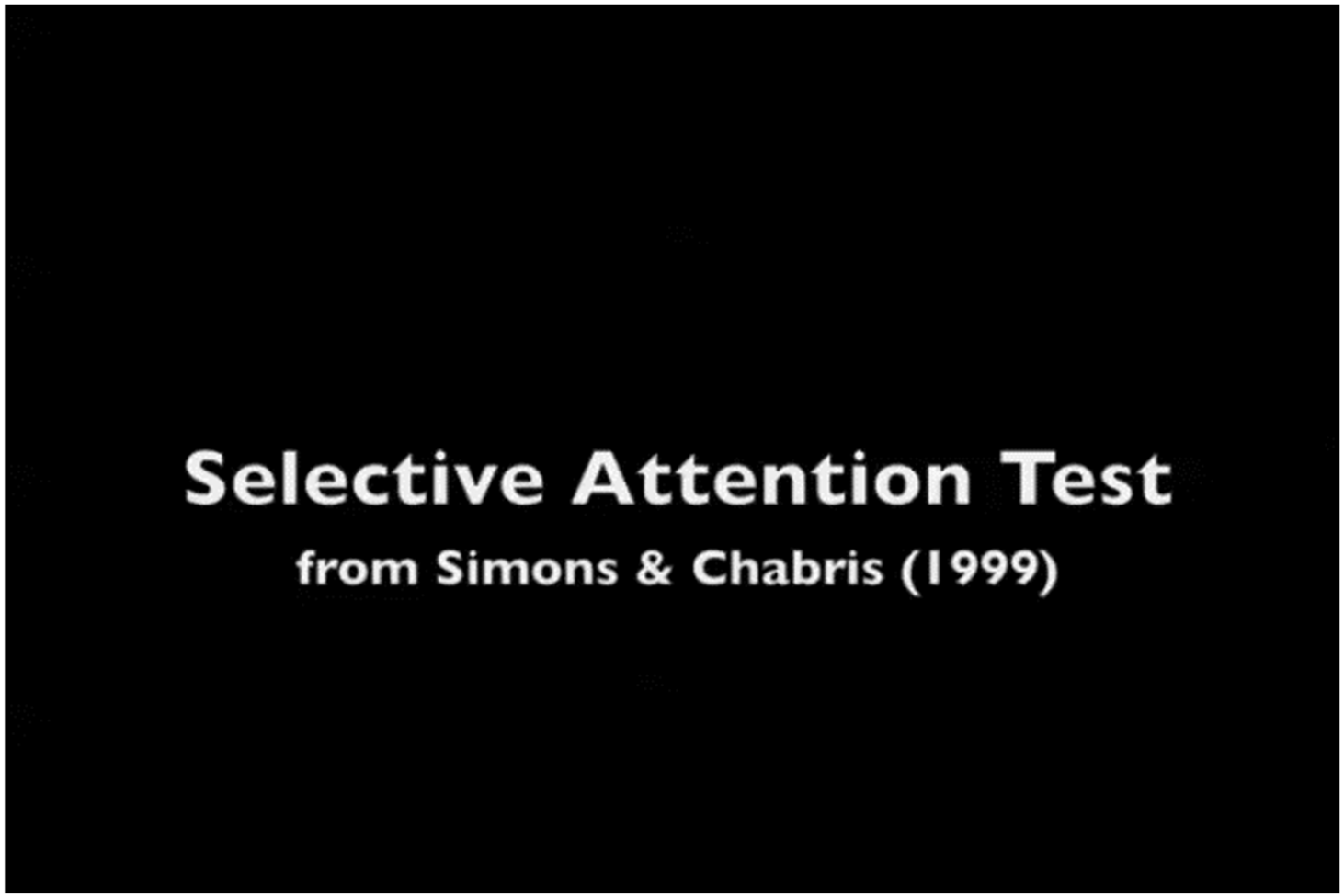

https://www.youtube.com/watch?v=vJG698U2Mvo

The Monkey Business Illusion

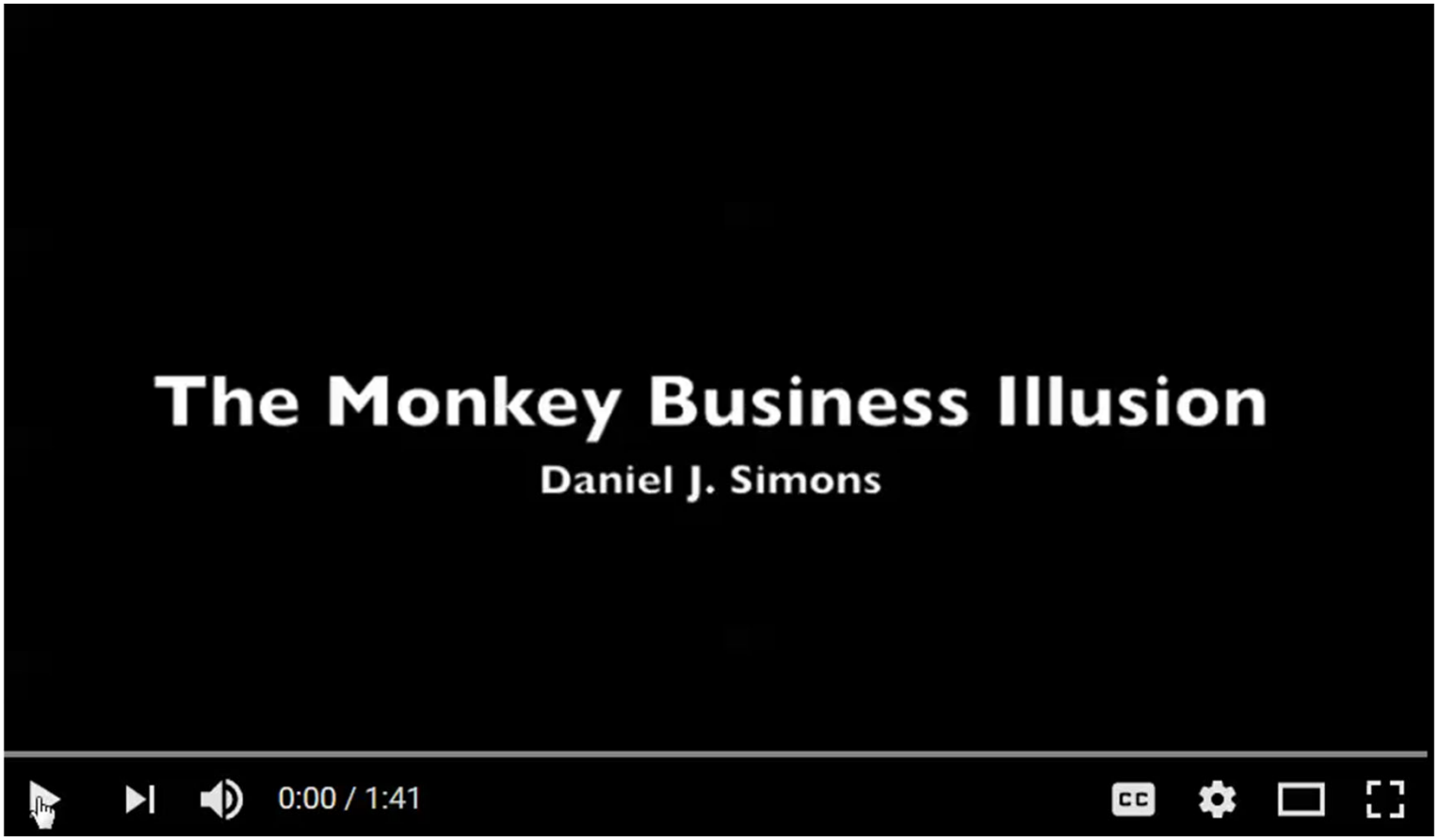

Theinvisiblegorilla.com